

**DOCKETED**

<b>Docket Number:</b>	21-AFC-02
<b>Project Title:</b>	Willow Rock Energy Storage Center
<b>TN #:</b>	265108
<b>Document Title:</b>	Willow Rock CURE Data Request 2 Response, Attachment DR136-1_Part 1
<b>Description:</b>	Resubmission of files previously submitted through Kiteworks
<b>Filer:</b>	Kathryn Stevens
<b>Organization:</b>	WSP USA Inc.
<b>Submitter Role:</b>	Applicant Consultant
<b>Submission Date:</b>	7/29/2025 8:34:58 PM
<b>Docketed Date:</b>	7/30/2025

# GEOTECHNICAL CHARACTERIZATION REPORT FOR THE WILLOW ROCK PROJECT SITE

*Prepared for:*

Hydrostor Inc.  
333 Bay Street, Suite 520  
Toronto, ON M5H 2V1, Canada

December 18, 2024

*Prepared by:*



**LANE**  
POWER & ENERGY SOLUTIONS, INC.

**LANE**  
2900 North Loop West  
Suite 1210  
Houston, TX 77092



**AGAPITO ASSOCIATES, INC.**  
715 Horizon Drive, Suite 340  
Grand Junction, CO 81506  
1536 Cole Blvd. Bldg. 4, Suite 310  
Lakewood, CO 80401

# GEOTECHNICAL CHARACTERIZATION REPORT FOR THE WILLOW ROCK PROJECT SITE

## TABLE OF CONTENTS

		<u>Page</u>
<b>1</b>	<b>Introduction.....</b>	<b>1-1</b>
<b>2</b>	<b>Geological Setting.....</b>	<b>2-1</b>
	2.1 Records Search.....	2-1
	2.2 Regional and Local Geology .....	2-1
<b>3</b>	<b>Site Specific Geotechnical Conditions.....</b>	<b>3-1</b>
	3.1 Surficial Geotechnical Investigation.....	3-1
	3.2 Subsurface Geotechnical Investigation.....	3-3
	3.2.1 Core Hole Lithology .....	3-3
	3.2.2 Rock Quality .....	3-14
	3.2.3 Packer Testing.....	3-18
	3.2.4 Falling Head Testing.....	3-21
	3.2.5 Rising Head Testing.....	3-21
	3.2.6 Geophysical Logging.....	3-22
	3.2.7 Structural Defects.....	3-22
<b>4</b>	<b>Geotechnical Characterization .....</b>	<b>4-1</b>
	4.1 Geomechanical Properties of the Intact Rock.....	4-1
	4.1.1 Unit Weight.....	4-1
	4.1.2 Uniaxial Compressive Strength .....	4-1
	4.1.3 Triaxial Compressive Strength .....	4-5
	4.1.4 Elastic Properties .....	4-5
	4.1.5 Slake Durability .....	4-5
	4.1.6 Petrographic Analysis .....	4-9
	4.1.7 CERCHAR Abrasivity.....	4-9
	4.2 Rock Mass Classification.....	4-14
	4.2.1 Rock Mass Rating .....	4-14
	4.2.2 NGI Q-system .....	4-17
	4.3 In Situ Stress Conditions.....	4-21
	4.3.1 Regional Stress.....	4-21
	4.3.2 Borehole Breakout .....	4-21
	4.3.3 Sigma Overcore .....	4-23
	4.4 Seismic Risk.....	4-24
	4.5 Rock Mass Strength and Deformation Properties.....	4-25
	4.5.1 Geological Strength Index .....	4-25
	4.5.2 Hoek-Brown Criterion .....	4-30
	4.5.3 Mohr-Coulomb Criterion .....	4-34
	4.5.4 Rock Mass Elastic Modulus.....	4-35
	4.5.5 Joint Stiffness.....	4-36
	4.5.6 Rock Mass Dilation.....	4-37

**5 Conclusions..... 5-1**  
**6 References..... 6-2**

Appendix A Geotechnical Logs ..... A-1  
 Appendix B Acoustic Televiewer Logs ..... B-1  
 Appendix C Laboratory Testing Reports ..... C-1  
 Appendix D Rock Mass Ratings ..... D-1  
 Appendix E IST2D Stress Measurements..... E-1

LIST OF TABLES

	Page
Table 3-1. Laboratory UCS Test Results from the Surface Geotechnical Investigation Program.....	3-1
Table 3-2. Summary of Lithology in the Subsurface Core Holes .....	3-5
Table 3-2. Summary of Lithology in the Subsurface Core Holes ( <i>continued</i> ).....	3-6
Table 3-2. Summary of Lithology in the Subsurface Core Holes ( <i>continued</i> ).....	3-7
Table 3-2. Summary of Lithology in the Subsurface Core Holes ( <i>continued</i> ).....	3-8
Table 3-3. Effect of Alteration on Fresh Rock.....	3-11
Table 3-4. RQD Classification System .....	3-15
Table 3-5. Condition of Rock Mass Discontinuities Associated with Different Hydraulic Conductivities .....	3-21
Table 3-6. Falling Head Test Summary for Core Hole ZEV-CH-05-24.....	3-21
Table 3-7. Summary of Structure Orientation and Dip in the Investigation Horizon .....	3-25
Table 3-8. Discontinuity Spacing Classification.....	3-26
Table 4-1. Summary of Laboratory Rock Mechanics Testing Results from the Exploration Core Holes .....	4-1
Table 4-2. Summary of Triaxial Test Results from the Exploration Core Holes.....	4-5
Table 4-3. Summary of Petrographic Analysis from Core Holes ZEV-CH-05-24 and ZEV-CH-06-24 .....	4-10
Table 4-3. Summary of Petrographic Analysis from Core Holes ZEV-CH-05-24 and ZEV-CH-06-24 ( <i>continued</i> ).....	4-11
Table 4-4. Summary of CERCHAR Abrasivity Test Results from Core Holes ZEV-CH-05-24 and ZEV-CH-06-24 .....	4-12
Table 4-4. Summary of CERCHAR Abrasivity Test Results from Core Holes ZEV-CH-05-24 and ZEV-CH-06-24 ( <i>continued</i> ).....	4-13
Table 4-5. Summary of IST2D Stress Testing in Core Hole ZEV-CH-03-23 .....	4-23
Table 4-6. Hoek-Brown Parameters.....	4-33
Table 4-7. Global Rock Mass Strength for Various Rock Conditions.....	4-33
Table 4-8. Intact Mohr-Coulomb Properties for Various Stresses.....	4-35
Table 4-9. Rock Mass Mohr-Coulomb Properties for Various Stresses .....	4-35
Table 4-10. Rock Mass Modulus .....	4-36
Table 4-11. Summary of Joint Normal Stiffness and Joint Shear Stiffness .....	4-36

## LIST OF FIGURES

Figure 1-1.	Location of the Willow Rock Project Site .....	1-2
Figure 2-1.	Geologic Map of the Antelope Valley in the Western Mojave Desert Showing the Location of the Project Site.....	2-3
Figure 2-2.	15-Minute Rosamond Quadrangle Geologic Map Showing the Location of the Project Site .....	2-4
Figure 2-3.	15-Minute Rosamond Quadrangle Geologic Map Showing the Project Site and the Mapped and Inferred Location of the Northwest-Southeast Trending Normal Fault .....	2-5
Figure 2-4.	Satellite Image Showing the Project Site and the Surface Exposure of the Northwest-Southeast Trending Normal Fault.....	2-6
Figure 2-5.	Cross-Section Showing the Bedrock Geology around the Project Site .....	2-7
Figure 3-1.	Logged and Inferred Subsurface Geotechnical Conditions at the Project Site ....	3-2
Figure 3-2.	Location of Deep Subsurface Investigation Core Holes at the Project Site .....	3-4
Figure 3-3.	Degree of Alteration Logged in Core Hole ZEV-CH-01-23 .....	3-11
Figure 3-4.	Degree of Alteration Logged in Core Hole ZEV-CH-02-23 .....	3-12
Figure 3-5.	Degree of Alteration Logged in Core Hole ZEV-CH-03-23 .....	3-12
Figure 3-6.	Degree of Alteration Logged in Core Hole ZEV-CH-04-24 .....	3-13
Figure 3-7.	Degree of Alteration Logged in Core Hole ZEV-CH-05-24 .....	3-13
Figure 3-8.	Degree of Alteration Logged in Core Hole ZEV-CH-06-24 .....	3-14
Figure 3-9.	Rock Quality Logged in Core Hole ZEV-CH-01-23 .....	3-15
Figure 3-10.	Rock Quality Logged in Core Hole ZEV-CH-02-23 .....	3-16
Figure 3-11.	Rock Quality Logged in Core Hole ZEV-CH-03-23 .....	3-16
Figure 3-12.	Rock Quality Logged in Core Hole ZEV-CH-04-24 .....	3-17
Figure 3-13.	Rock Quality Logged in Core Hole ZEV-CH-05-24 .....	3-17
Figure 3-14.	Rock Quality Logged in Core Hole ZEV-CH-06-24 .....	3-18
Figure 3-15.	Flow Rate and Permeability Recorded in Core Hole ZEV-CH-01-23 .....	3-19
Figure 3-16.	Flow Rate and Permeability Recorded in Core Hole ZEV-CH-02-23 .....	3-19
Figure 3-17.	Flow Rate and Permeability Recorded in Core Hole ZEV-CH-03-23 .....	3-19
Figure 3-18.	Flow Rate and Permeability Recorded in Core Hole ZEV-CH-04-24 .....	3-20
Figure 3-19.	Flow Rate and Permeability Recorded in Core Hole ZEV-CH-05-24 .....	3-20
Figure 3-20.	Flow Rate and Permeability Recorded in Core Hole ZEV-CH-06-24 .....	3-20
Figure 3-21.	Stereonet and Rosette Diagram of the Joints between the Elevations of 560 and 60 ft above MSL for ZEV-CH-01-23.....	3-22
Figure 3-22.	Stereonet and Rosette Diagram of the Joints between the Elevations of 560 and 60 ft above MSL for ZEV-CH-02-23.....	3-23
Figure 3-23.	Stereonet and Rosette Diagram of the Joints between the Elevations of 560 and 60 ft above MSL for ZEV-CH-03-23.....	3-23
Figure 3-24.	Stereonet and Rosette Diagram of the Joints between the Elevations of 560 and 60 ft above MSL for ZEV-CH-04-24.....	3-24
Figure 3-25.	Stereonet and Rosette Diagram of the Joints between the Elevations of 560 and 60 ft above MSL ZEV-CH-05-24 .....	3-24
Figure 3-26.	Stereonet and Rosette Diagram of the Joints between the Elevations of 560 and 60 ft above MSL ZEV-CH-06-24 .....	3-25
Figure 3-27.	Histogram Showing the Distribution of Discontinuity Spacing for All Joints in the Investigation Horizon.....	3-27

Figure 3-28. Histogram Showing the Distribution of Discontinuity Spacing for the Primary Joint Set in the Investigation Horizon..... 3-27

Figure 3-29. Histogram Showing the Distribution of Discontinuity Spacing for the Secondary Set in the Investigation Horizon..... 3-28

Figure 4-1. Intact Rock Strength Recorded in Core Hole ZEV-CH-01-23 ..... 4-2

Figure 4-2. Intact Rock Strength Recorded in Core Hole ZEV-CH-02-23 ..... 4-2

Figure 4-3. Intact Rock Strength Recorded in Core Hole ZEV-CH-03-23 ..... 4-3

Figure 4-4. Intact Rock Strength Recorded in Core Hole ZEV-CH-04-24 ..... 4-3

Figure 4-5. Intact Rock Strength Recorded in Core Hole ZEV-CH-05-24 ..... 4-4

Figure 4-6. Intact Rock Strength Recorded in Core Hole ZEV-CH-06-24 ..... 4-4

Figure 4-7. Slake Durability Index Recorded in Core Hole ZEV-CH-01-23..... 4-6

Figure 4-8. Slake Durability Index Recorded in Core Hole ZEV-CH-02-23..... 4-6

Figure 4-9. Slake Durability Index Recorded in Core Hole ZEV-CH-03-23..... 4-7

Figure 4-10. Slake Durability Index Recorded in Core Hole ZEV-CH-04-24..... 4-7

Figure 4-11. Slake Durability Index Recorded in Core Hole ZEV-CH-05-24..... 4-8

Figure 4-12. Slake Durability Index Recorded in Core Hole ZEV-CH-06-24..... 4-8

Figure 4-13. Rock Mass Rating for Core Hole ZEV-CH-01-23 ..... 4-14

Figure 4-14. Rock Mass Rating for Core Hole ZEV-CH-02-23 ..... 4-15

Figure 4-15. Rock Mass Rating for Core Hole ZEV-CH-03-23 ..... 4-15

Figure 4-16. Rock Mass Rating for Core Hole ZEV-CH-04-24 ..... 4-16

Figure 4-17. Rock Mass Rating for Core Hole ZEV-CH-05-24 ..... 4-16

Figure 4-18. Rock Mass Rating for Core Hole ZEV-CH-06-24 ..... 4-17

Figure 4-19. Q Ratings for Core Hole ZEV-CH-01-23 ..... 4-18

Figure 4-20. Q Ratings for Core Hole ZEV-CH-02-23 ..... 4-18

Figure 4-21. Q Ratings for Core Hole ZEV-CH-03-23 ..... 4-19

Figure 4-22. Q Ratings for Core Hole ZEV-CH-04-24 ..... 4-19

Figure 4-23. Q Ratings for Core Hole ZEV-CH-05-24 ..... 4-20

Figure 4-24. Q Ratings for Core Hole ZEV-CH-06-24 ..... 4-20

Figure 4-25. Map Showing the Measured Orientation of the In Situ Horizontal Stresses in the Antelope Valley ..... 4-21

Figure 4-26. Theoretical Borehole Cross-Section, Showing the Relationship between the Major Principal Horizontal Stress, the Minor Principal Horizontal Stress for Borehole Breakout, and Tensile Fracture ..... 4-22

Figure 4-27. Acoustic Televiewer Logs Showing Borehole Breakout in the Amplitude Logs for Core Holes ZEV-CH-01-23 and ZEV-CH-02-23 ..... 4-22

Figure 4-28. Map Showing the Chance of any Level of Damaging Earthquake Shaking in 100 years from the 2023 50-State National Seismic Hazard Model..... 4-25

Figure 4-29. GSI Ratings for Core Hole ZEV-CH-01-23 ..... 4-27

Figure 4-30. GSI Ratings for Core Hole ZEV-CH-02-23 ..... 4-27

Figure 4-31. GSI Ratings for Core Hole ZEV-CH-03-23 ..... 4-28

Figure 4-32. GSI Ratings for Core Hole ZEV-CH-04-24 ..... 4-28

Figure 4-33. GSI Ratings for Core Hole ZEV-CH-05-24 ..... 4-29

Figure 4-34. GSI Ratings for Core Hole ZEV-CH-06-24 ..... 4-29

Figure 4-35. Linear Regression Analysis for the Input and Derivation of  $m_i$  Constant ..... 4-31

Figure 4-36. Guidelines for Estimating Disturbance Factor..... 4-32

***DISCLAIMER:*** *This report contains professional opinions based on information provided by the Owner. Agapito Associates, Inc. makes no warranties, either expressed or implied, as to the accuracy or completeness of the information herein. Opinions are based on subjective interpretations of geotechnical data; other equally valid interpretations may exist. Identification and control of hazardous conditions are the responsibilities of the Owner.*

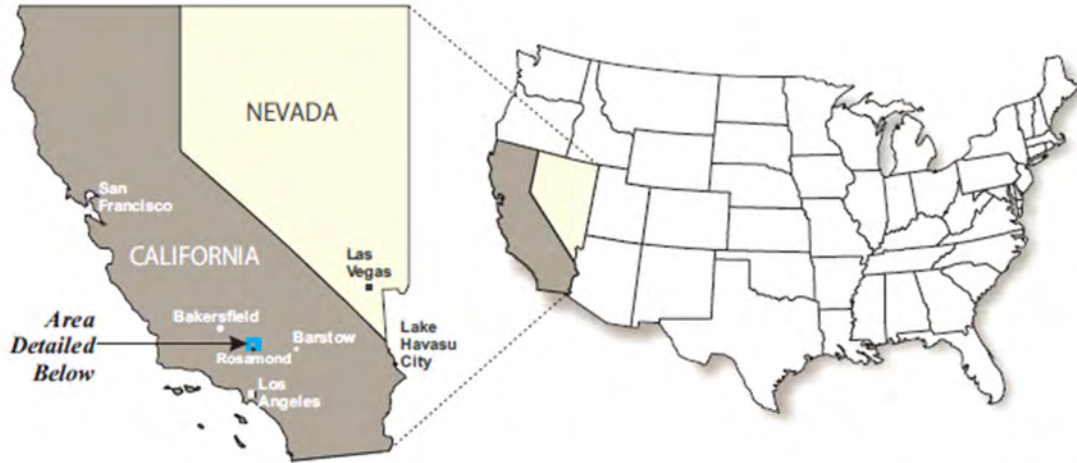
## 1 INTRODUCTION

The Willow Rock Project site (Project site) is located approximately 2 miles north of Rosamond, California in the Mojave Desert (Figure 1-1). The site is bounded by the Antelope Valley Freeway to the west and the Sierra Highway to the east. Drilling records from the site indicate the existing ground surface is approximately located between 2,540 and 2,580 feet (ft) above mean sea level (MSL).

The site has been selected for investigation into the feasibility for the construction of an Advanced Compressed Air Energy Storage (A-CAES) cavern. Hydrostor's target depth for cavern construction is between the intervals of 2,000 and 2,500 ft below ground surface (bgs). Since depth is a function of surface elevation, this investigation will refer to subsurface elevations to maintain constant vertical measurements. Therefore, the "target cavern horizon" equates to an elevation of 560 to 60 ft above MSL.

The geotechnical characterization in this report is largely constrained to the anticipated ground conditions within the target cavern horizon. Accepting that the characterization of the overlying ground conditions for vertical shaft construction will require further analysis of core hole data, some initial broad comments on shaft constructability can be made. The main purpose of this report, however, is to summarize our analysis of the data collected from six (6) deep subsurface investigation core holes and provide geotechnical design parameters for both empirical and numerical assessment methodologies for cavern construction.





951-20 Lane Hydrostor Zevsar[California-Nevada-Lane\_Willow Rock.cdr](12-10-2024)

**Figure 1-1. Location of the Willow Rock Project Site**

## **2 GEOLOGICAL SETTING**

### **2.1 Records Search**

To obtain existing information on the geological and hydrological settings of the Willow Rock Project site, a literature search was performed, of which the following sources are referenced:

- Geology of the Willow Springs and Rosamond Quadrangles California (Dibblee 1963)
- Areal Geology of the Western Mojave Desert California (Dibblee 1967)
- Willow Springs and Rosamond 15-minute quadrangle USGS maps (2008)
- Geotechnical Data Report – Zevsar Energy Storage Project (Yeh and Associates, Inc 2023)

The information from Dibblee (1963) was collected during the U.S. Geological Survey’s study of the areal geology of the western Mojave Desert. The main aim of the study was to determine whether formations of Tertiary and Quaternary age might contain hidden saline deposits of economic value. A secondary aim was to determine the general character of the pre-Tertiary crystalline bedrock complex within the two mapped quadrangles and investigate its relations to the depositional history and structure of the Cenozoic formations.

The information from Dibblee (1967) was part of a geologic investigation carried out by the U.S. Geological Survey of the known and potential deposits of borate minerals in the southern California desert regions.

The information from the geotechnical data report, which was provided by Hydrostor, summarizes the results of a shallow subsurface geotechnical site investigation carried out by Yeh and Associates, Inc. in 2023.

### **2.2 Regional and Local Geology**

The Willow Rock Project site is located in the Antelope Valley in the Western Mojave Desert in California (Figure 2-1). Antelope Valley is a structural basin filled with Cenozoic alluvial sedimentary deposits a hundred- to several thousand-feet in thickness (Dibblee 1963). The valley is bounded by the Garlock fault to the northwest and the San Andreas fault to the southwest, forming the “Mojave block” (Dibblee 1967). The Project site, shown in Figure 2-2 within the 15-minute Rosamond quadrangle (USGS 2008), is situated on the remnants of an isolated low hill which is comprised of exposed quartz monzonite.

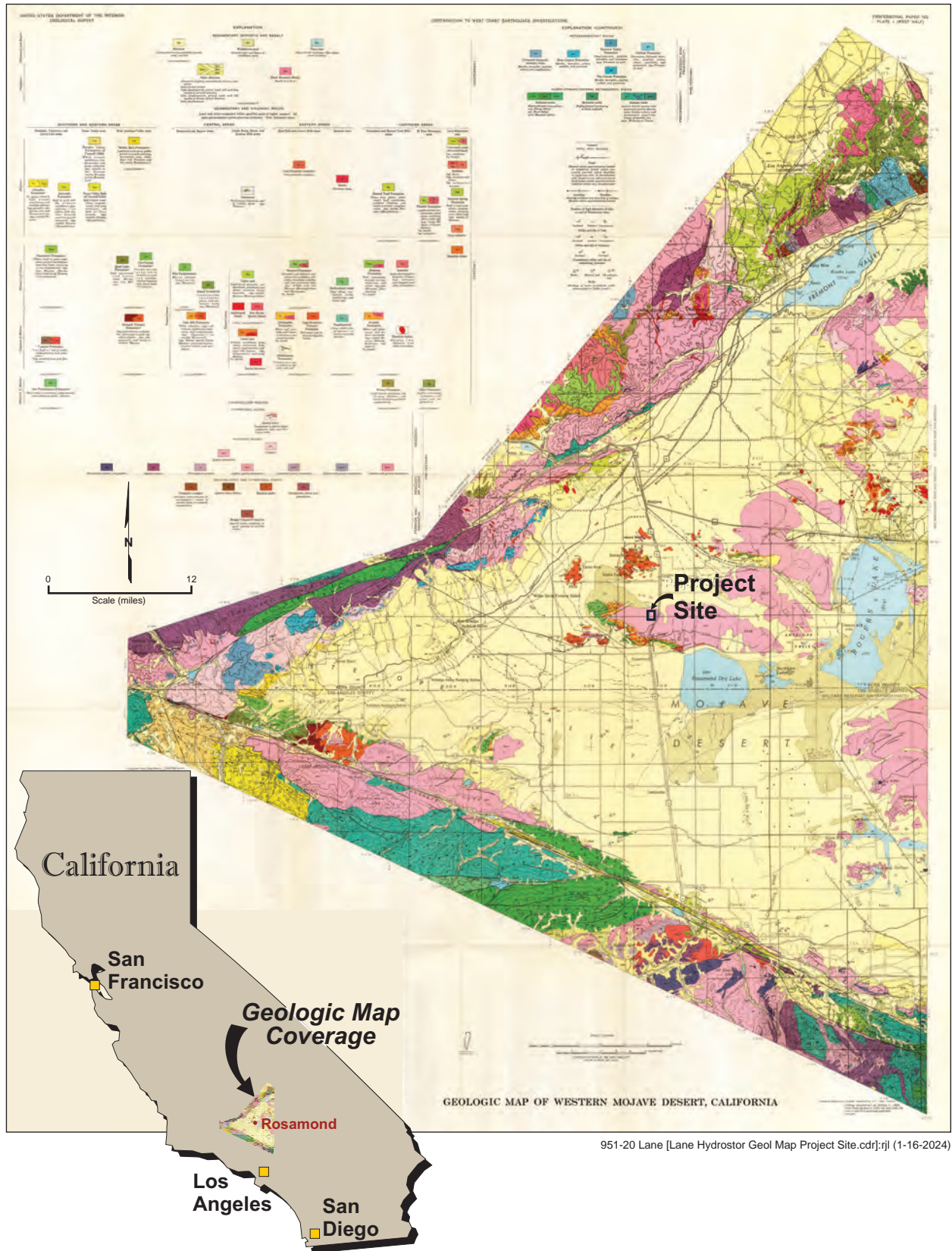
The quartz monzonite is a plutonic rock that is probably Mesozoic, possibly Cretaceous in age (Dibblee 1963). It is by far the most extensive plutonic rock in the area and is the main rock type of the granitic batholith that underlies the Mojave Desert. Dibblee (1963) describes the quartz monzonite as a medium to coarse-grained holocrystalline granitic rock, gray-white when fresh but commonly buff white on weathering. It is composed of more or less equal percentages of quartz, potassium feldspar, and plagioclase, a small percentage of biotite, and locally small amounts of hornblende.

Near the Project site, the quartz monzonite is locally cut by dike swarms of pegmatite and aplite of the same mineralogic composition of almost entirely quartz and feldspar. The dikes range from less than an inch to about 6 ft in width and are traceable from a few feet to half a mile (Dibblee

1963). They are typically parallel, trending to the northwest, and are vertical or steeply inclined to the southwest.

The Project site is situated along the northeastern side of the Rosamond Hills area (Figure 2-2). The Rosamond Hills consist of a large eastward-trending uplifted area, possibly an upwarp, of quartz monzonite (Dibblee 1963). The hills are cut by many minor high-angle normal faults that trend either west-northwest or east-northeast. The largest fault within the Rosamond Hills is located immediately northeast of the Project site (Figure 2-3). The fault trends northwest within the quartz monzonite for approximately 5 miles and appears to extend another mile northwestward through the recent alluvium. As shown in Figure 2-4, surface exposures of the fault are marked by a zone of pulverized quartz monzonite covered by a white caliche-like crust. This fault, nor any of the other faults within Rosamond Hills show evidence of recent activity (Dibblee 1963).

The 15-minute Rosamond quadrangle map indicates the Project site is underlain by a continuous massive unit of quartz monzonite (Figure 2-5). The quartz monzonite forms the crystalline bedrock basement complex upon which assemblages of Cenozoic age rest unconformably (Dibblee 1963). Seismic reflection profiling of the western Mojave Desert indicates the basement rocks are between 15 and 20 miles thick (Cheadle et al. 1986).



951-20 Lane [Lane Hydrostor Geol Map Project Site.cdr]:rjl (1-16-2024)

**Figure 2-1. Geologic Map of the Antelope Valley in the Western Mojave Desert Showing the Location of the Project Site**

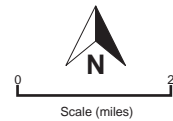
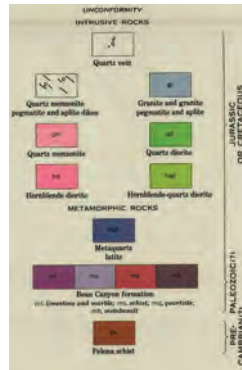
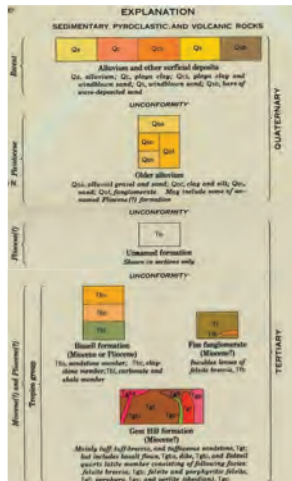
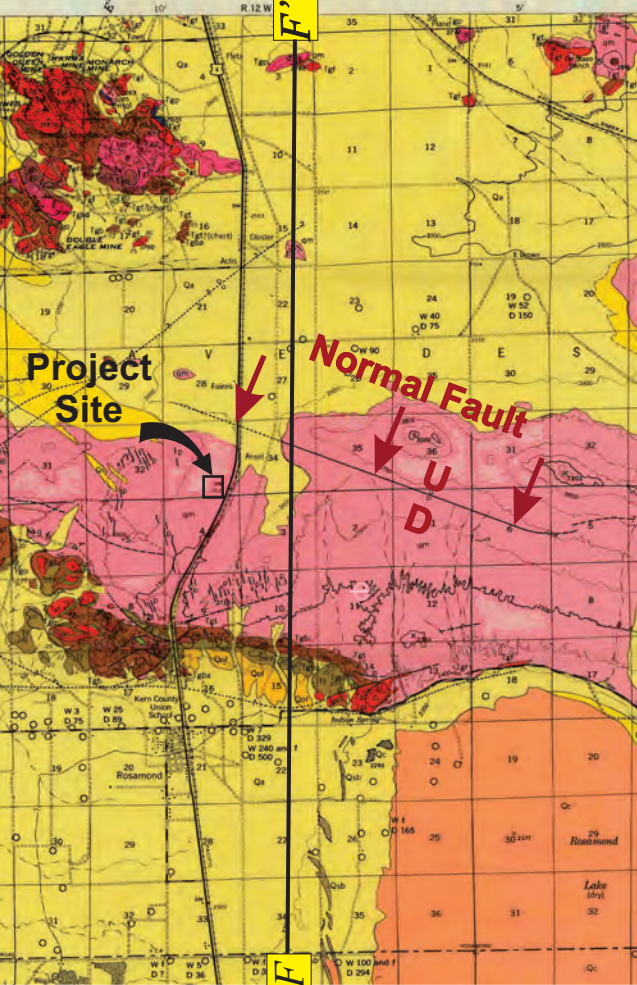


Figure 2-2. 15-Minute Rosamond Quadrangle Geologic Map Showing the Location of the Project Site

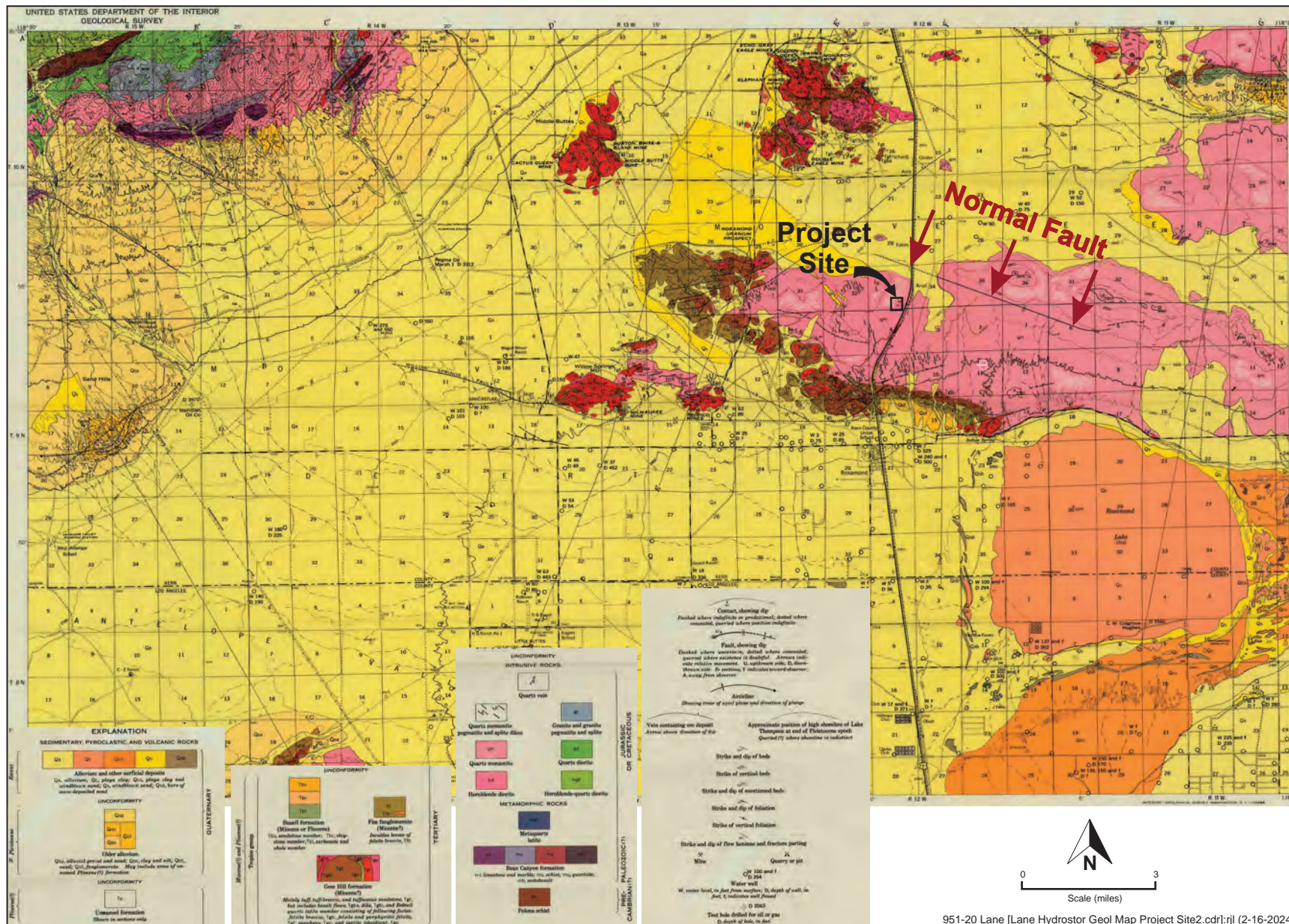


Figure 2-3. 15-Minute Rosamond Quadrangle Geologic Map Showing the Project Site and the Mapped and Inferred Location of the Northwest-Southeast Trending Normal Fault

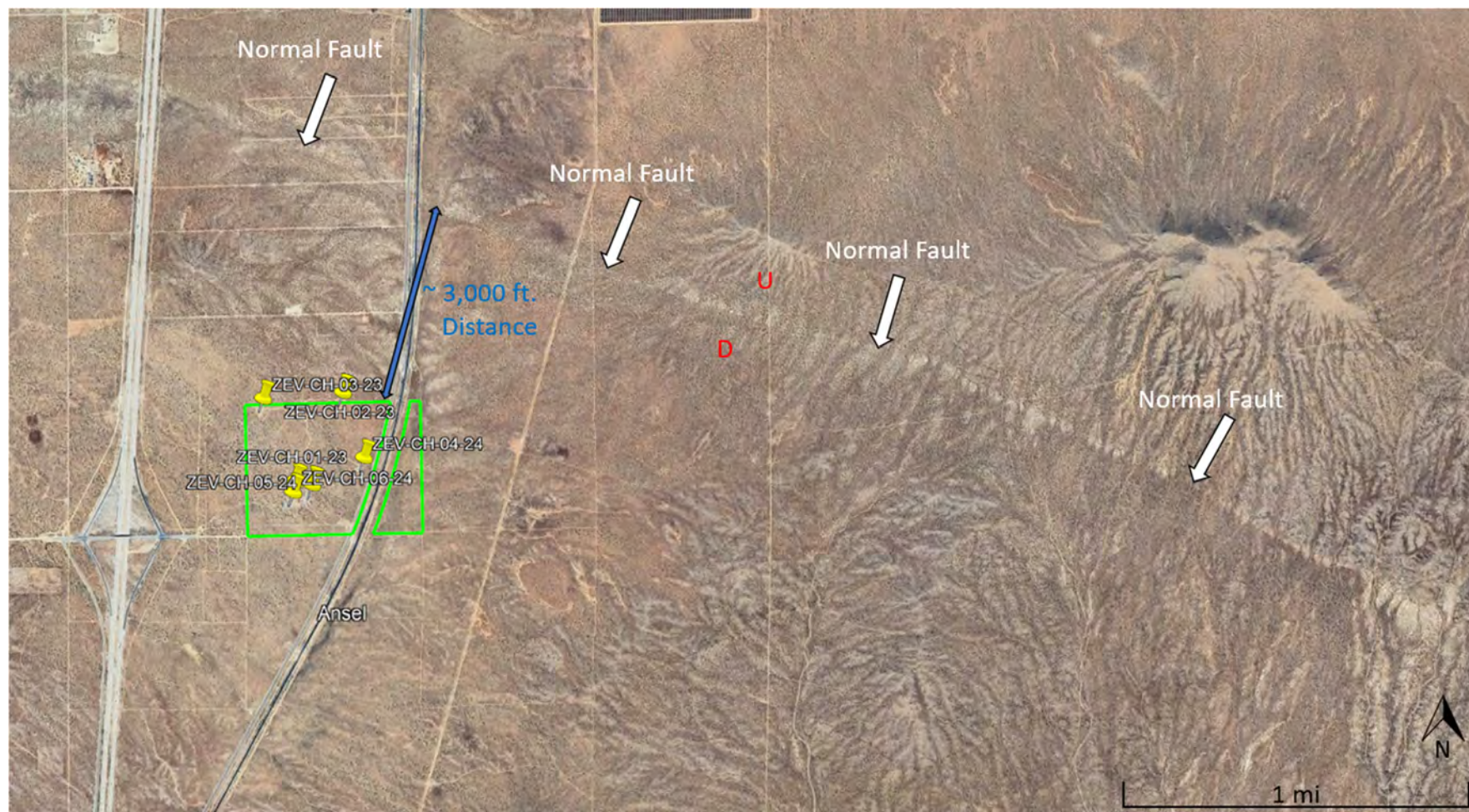
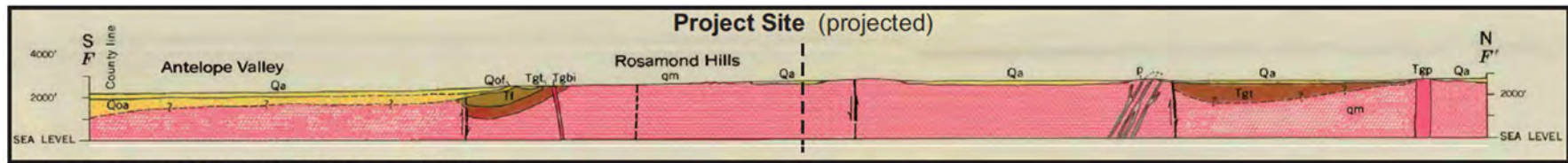


Figure 2-4. Satellite Image Showing the Project Site and the Surface Exposure of the Northwest-Southeast Trending Normal Fault



951-20 Lane [Lane Hydrostor Geol Map Project Site2\_Profile3.cdr].rjl (2-16-2024)

**Figure 2-5. Cross-Section Showing the Bedrock Geology around the Project Site (Dibblee 1963)**



### 3 SITE SPECIFIC GEOTECHNICAL CONDITIONS

The geotechnical conditions at the Project site have been determined from separate surface and subsurface geotechnical investigation programs. The surface geotechnical investigation collected geotechnical information from the soil and weathered bedrock underlying the site. The subsurface investigation involved core drilling to approximate depths of 2,200 to 3,100 ft below the surface. The results of the geotechnical investigations are summarized in the succeeding sections.

#### 3.1 Surficial Geotechnical Investigation

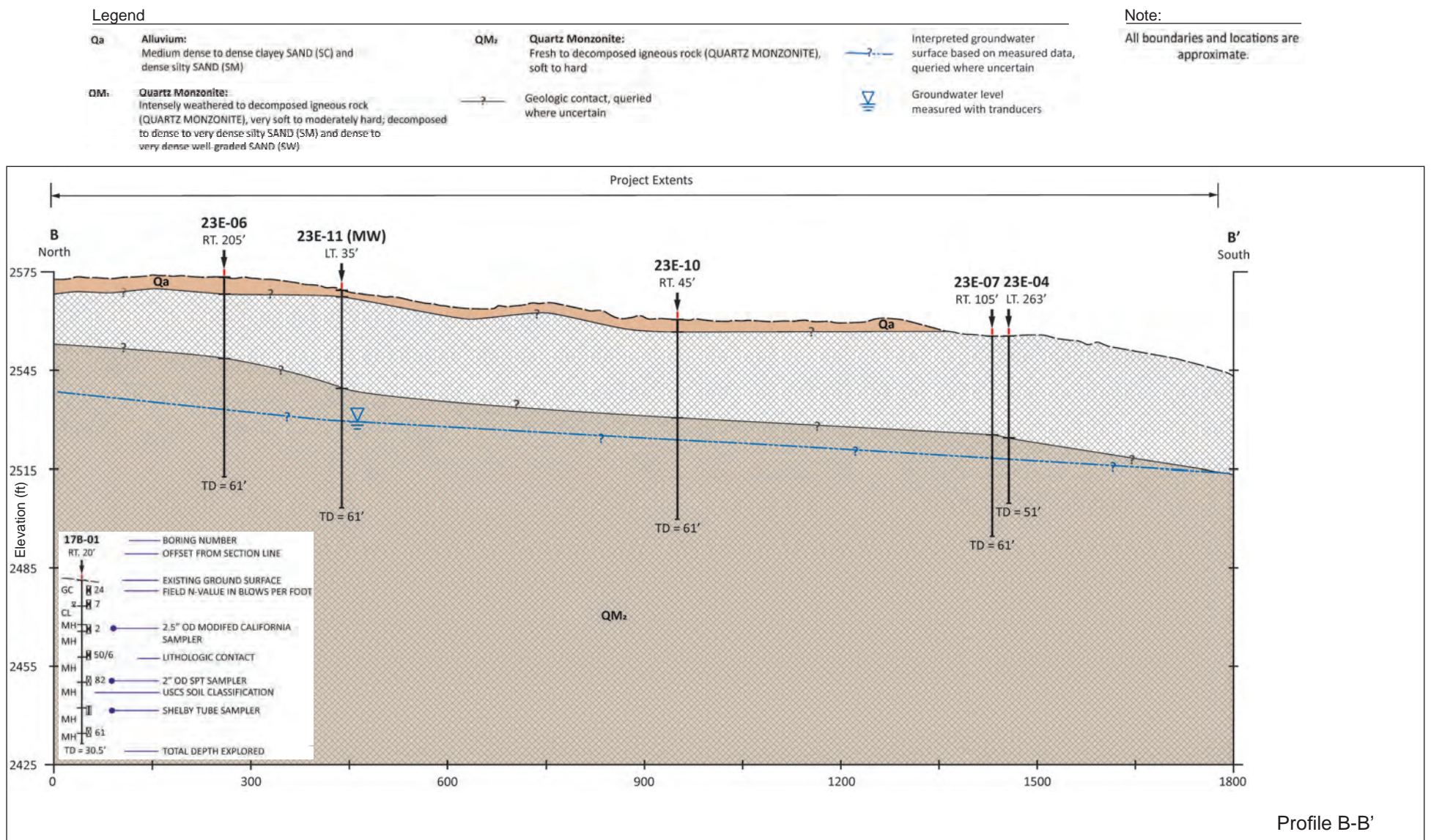
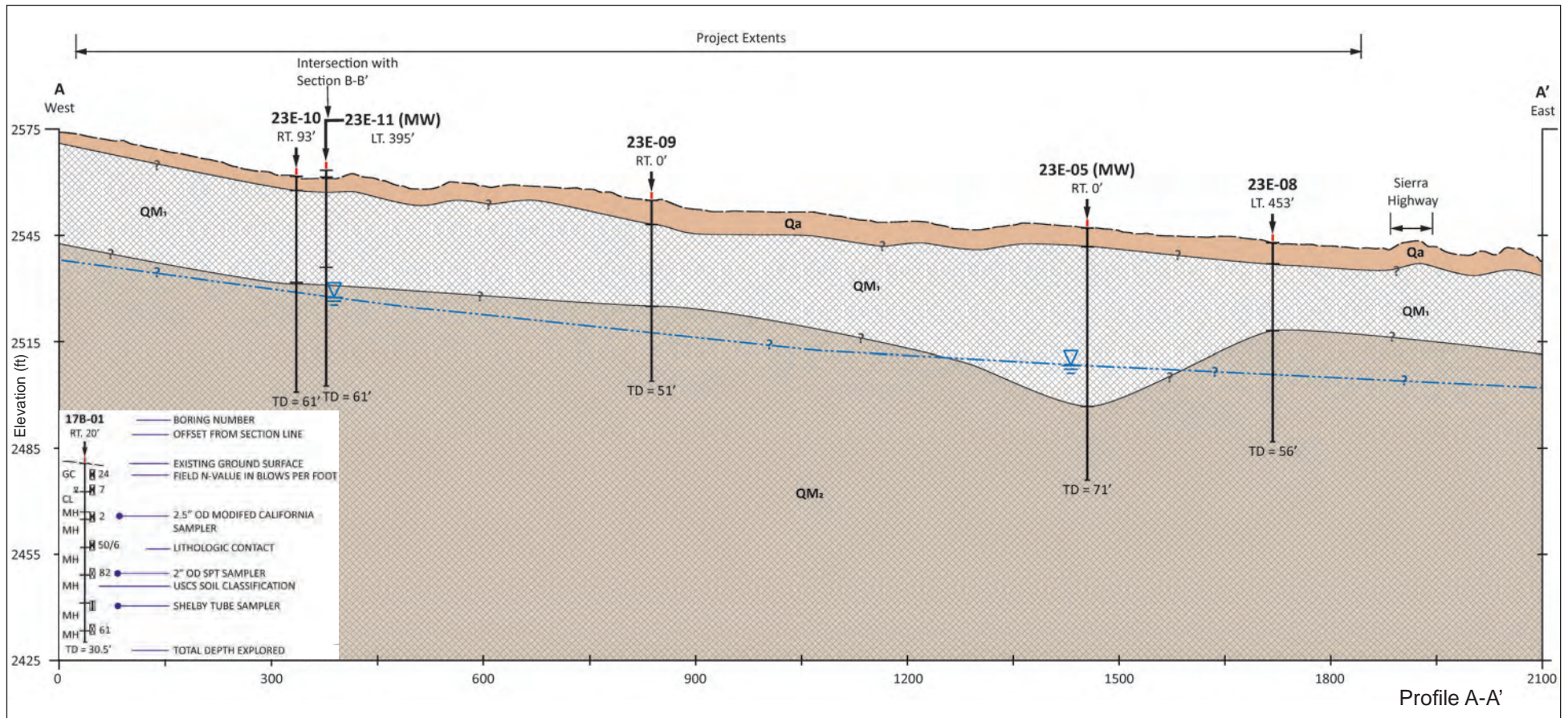
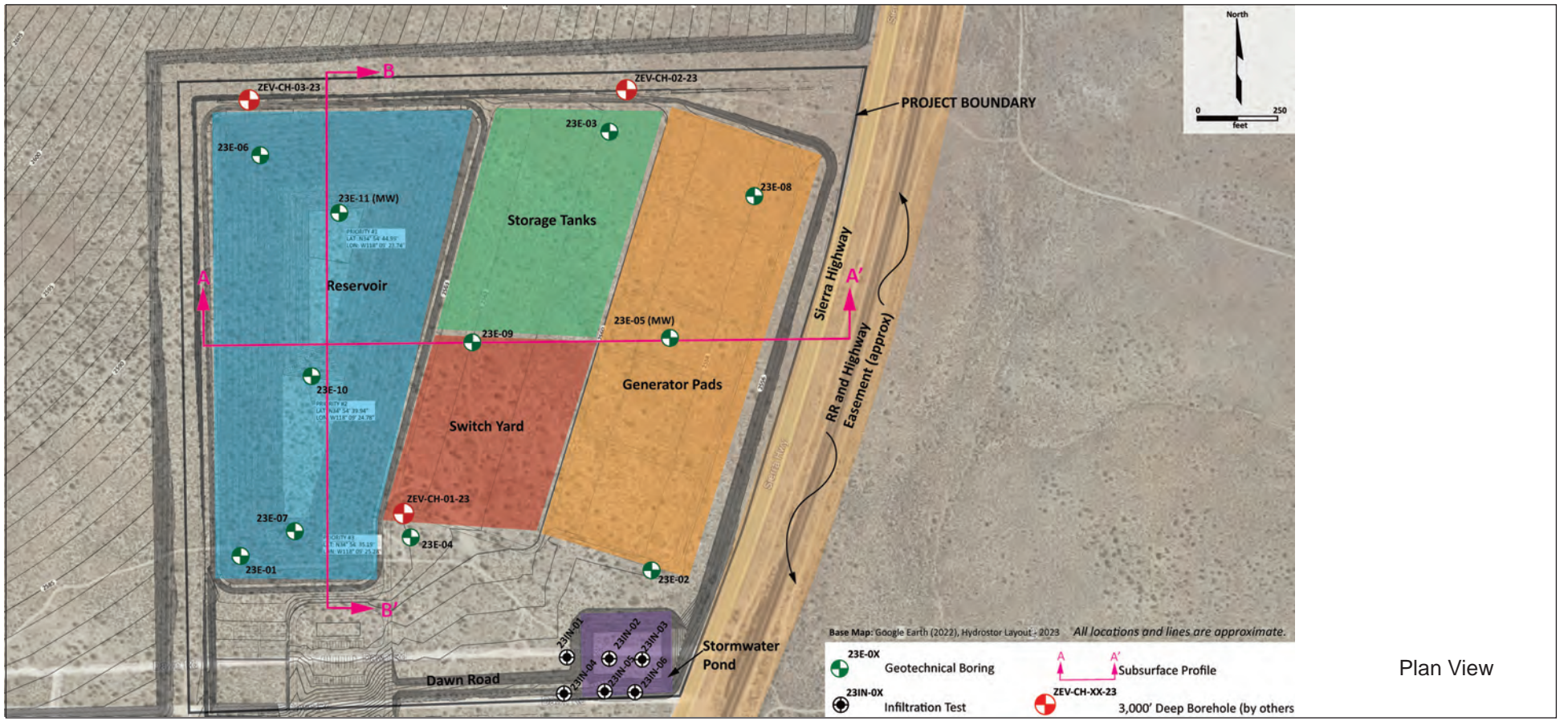
The characterization of the surficial deposits at the Project site is based on a geotechnical investigation carried out by Yeh and Associates, Inc. (2023). The logged and inferred geology of the surficial deposits determined from the investigation are shown in Figure 3-1. Most of the site is overlain by 3 to 7.5 ft of residual soils, which are comprised of loose to very dense, well-graded sand with varying amounts of silt and clay (SW, SM, SC). Underlying the soils is 20 to 45 ft of decomposed to intensely weathered quartz monzonite. The unit was described as very soft to moderately hard and very slightly fractured to moderately fractured. The decomposed zones were logged as silty to clayey sand (SM, SC). The borings continued to a depth of between 51 and 71 ft, where most of the quartz monzonite was logged as slightly to moderately weathered, very soft to hard, and intensely to slightly fractured. Isolated zones of intensely weathered to decomposed quartz monzonite were logged in this interval. The depth of the borings did not penetrate any significant amount of fresh rock at any of the sample locations.

Uniaxial compressive strength (UCS) tests carried out on rock core indicated intact strengths of between 70 and 5,770 pounds-per-square inch (psi), which is indicative of extremely weak to weak rock (ISRM 2007). The laboratory test results are provided in Table 3-1.

Monitoring wells indicate the groundwater depth at the site was around 40 ft below the surface (Figure 3-1). Yeh and Associates, Inc. suggests that groundwater conditions at the site will vary seasonally due to variations in storm runoff, irrigation, and groundwater pumping in the site vicinity.

**Table 3-1. Laboratory UCS Test Results from the Surface Geotechnical Investigation Program (Yeh and Associates, Inc 2023)**

Borehole	Material	Depth (ft)		Unit Weight (pcf)	Unconfined Compressive Strength (psi)
		From	To		
23E-02	Quartz monzonite, moderately weathered	67.5	68.0	153.4	77
23E-03	Quartz monzonite, moderately weathered	52.8	53.3	154.3	147
23E-04	Quartz monzonite, moderately weathered	39.0	39.5	155.3	647
23E-05	Quartz monzonite, moderately weathered	55.5	56.0	160.9	1,940
23E-05	Quartz monzonite, intensely weathered	57.2	57.7	155.2	97
23E-05	Quartz monzonite, fresh	65.0	65.5	162.9	5,770
23E-06	Quartz monzonite, slightly weathered	55.1	56.1	158.7	866
23E-06	Quartz monzonite, slightly weathered	59.1	59.6	158.4	218
23E-06	Quartz monzonite, moderately weathered	60.6	61.1	147.7	209



## 3.2 Subsurface Geotechnical Investigation

CRUX Subsurface Drilling advanced six core holes (ZEV-CH-01-23, ZEV-CH-02-23, ZEV-CH-03-23, ZEV-CH-04-24, ZEV-CH-05-24, and ZEV-CH-06-24) between March 17, 2023, and October 13, 2024, at the locations shown in Figure 3-2. The core holes were started with rotary drilling and setting HW casing to depths of between 20 and 171 ft. The borings were drilled using HQ-3-sized diamond bits and 10-ft-long wireline core barrels. This resulted in 2.41-inch-diameter cores, which were stored in 5-ft-long wooden core boxes. The end depth of core drilling ranged between 2,280 and 3,167 ft for the core holes, which equates to elevations between 268 ft above MSL and 618 ft below MSL.

Core logging was performed by Lane and Carboniferous, LLC geologist Chris Messinger. Core logging consisted of identifying the mineralogy and rock type for each run of core, the alteration of discontinuities for each run, noting the percentage core recovery for each 10-ft run, and noting the Rock Quality Designation (RQD) for each run based on the percentage of the run comprised of pieces longer than 4 inches.

### 3.2.1 Core Hole Lithology

The detailed lithology logged in each of the core holes is provided in the geotechnical logs in Appendix A. A brief summary of the lithology logged in each of the core holes is provided in Table 3-2. All six core holes indicate that the lithology is comprised of quartz monzonite. The only exception to this is frequent near vertical pegmatite dikes.

In all six core holes, the quartz monzonite has undergone various degrees of hydrothermal alteration. Hydrothermal alteration occurs when hot, mineral-rich fluids interact with rocks and minerals, causing them to change in terms of their mineral composition, texture, and structure. Dibble (1963) suggested that much of the alteration in the area occurs along fault or fracture zones. Table 3-3 outlines the various degrees of alteration used to classify the rock (ISRM 2007).

In ZEV-CH-01-23, between the elevations of 800 and 50 ft above MSL, the quartz monzonite is almost entirely fresh to slightly altered (Figure 3-3). In ZEV-CH-02-23, between the elevations of 700 and 355 ft above MSL, most of the quartz monzonite has been logged as fresh (Figure 3-4). The only exception to this is a zone of slightly to moderately altered quartz monzonite between the elevations of 650 and 620 ft above MSL and a moderately to highly altered zone between 470 to 430 ft above MSL. Elsewhere in the core hole, particularly below 355 ft above MSL, the quartz monzonite is slightly to highly altered. In ZEV-CH-03-23, most of the quartz monzonite between the elevations of 700 and 50 ft above MSL was logged as fresh to slightly altered (Figure 3-5). There are, however, isolated zones of moderately to highly altered quartz monzonite between the elevations of 620 to 345 ft above MSL. In ZEV-CH-04-24, most of the quartz monzonite between the elevations of 620 ft above MSL and 340 ft above MSL was logged as fresh to slightly altered (Figure 3-6). Both above and below these elevations, most of the quartz monzonite is slightly to moderately altered with isolated zones of moderately to highly altered rock. In core hole ZEV-CH-05-24, most of the quartz monzonite between the elevations of 750 to 260 ft above MSL was logged as fresh to slightly altered (Figure 3-7). There is, however, an isolated zone of highly altered quartz monzonite between the elevations of 790 to 750 ft above MSL. In ZEV-CH-06-24, most of the quartz monzonite between the elevations of 680 to 270 ft above MSL was logged as fresh to slightly altered (Figure 3-8). There are, however, two isolated

zones (approximately 10 ft) of slightly to moderately altered quartz monzonite around the elevations of 550 ft and 380 ft above MSL. Between the elevations of 800 and 680 ft above MSL, the quartz monzonite is, for the most part, slightly to highly altered.

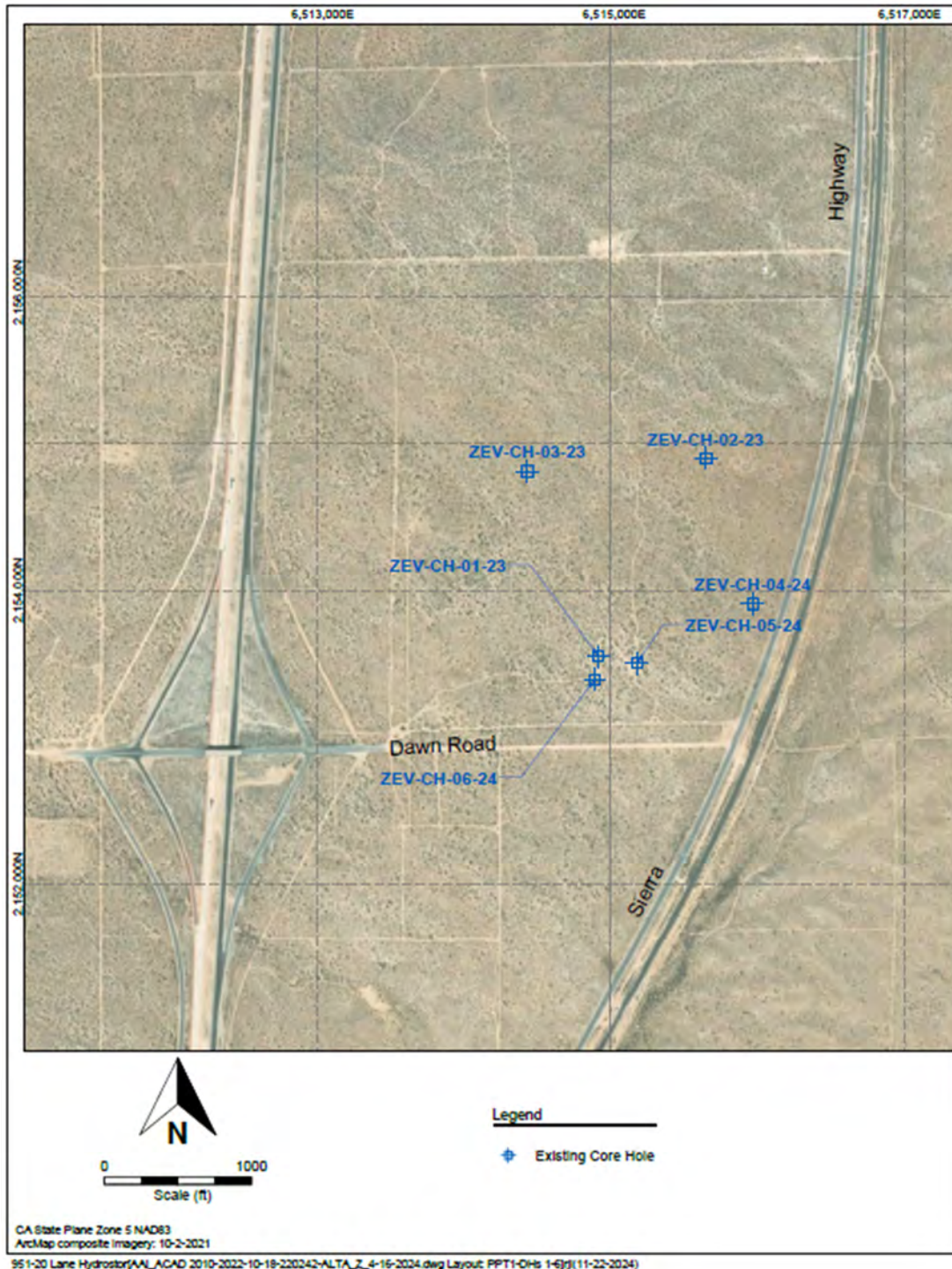


Figure 3-2. Location of Deep Subsurface Investigation Core Holes at the Project Site

**Table 3-2. Summary of Lithology in the Subsurface Core Holes**

Depth (ft)		Elevation (ft MSL)		Lithology
From:	To:	From:	To:	
<b>Core Hole: ZEV-CH-01-23</b>				
0	71	2,550	2,479	HW casing
71	133	2,479	2,417	Quartz monzonite, most of the core is moderately to highly altered
133	140	2,417	2,410	Pegmatite dike, slightly to moderately altered
140	295	2,410	2,255	Quartz monzonite, most of the core is slightly to moderately altered
295	401	2,255	2,149	Quartz monzonite, most of the core is fresh to slightly altered
401	620	2,149	1,930	Quartz monzonite, most of the core is moderately to completely altered
620	791	1,930	1,759	Quartz monzonite, most of the core is slightly to moderately altered
791	835	1,759	1,715	Quartz monzonite, most of the core is highly to completely altered
835	1,109	1,715	1,441	Quartz monzonite, most of the core is fresh to slightly altered
1,109	1,120	1,441	1,430	Pegmatite dike, fresh
1,120	1,166	1,430	1,384	Quartz monzonite, most of the core is fresh to slightly altered
1,166	1,312	1,384	1,238	Quartz monzonite, most of the core is slightly to highly altered
1,312	1,317	1,238	1,233	Pegmatite dike, moderately to highly altered
1,317	1,437	1,233	1,113	Quartz monzonite, most of the core is slightly to highly altered
1,437	1,442	1,113	1,108	Pegmatite dike, fresh
1,442	1,520	1,108	1,030	Quartz monzonite, most of the core is moderately to highly altered
1,520	1,524	1,030	1,026	Pegmatite dike, fresh
1,524	1,613	1,026	937	Quartz monzonite, most of the core is fresh to slightly altered
1,613	1,616	937	934	Pegmatite dike, fresh
1,616	1,829	934	721	Quartz monzonite, most of the core is fresh to slightly altered
1,829	1,847	721	703	Quartz monzonite, fresh
1,847	2,109	703	441	Quartz monzonite, most of the core is fresh to slightly altered
2,109	2,118	441	432	Pegmatite dike, fresh
2,118	2,318	432	232	Quartz monzonite, most of the core is fresh to slightly altered
2,318	2,326	232	224	Zone of thin pegmatite dikes, fresh
2,326	2,375	224	175	Quartz monzonite, most of the core is fresh to slightly altered
2,375	2,380	175	170	Pegmatite dike, fresh
2,380	2,682	170	-132	Quartz monzonite, most of the core is fresh to moderately altered
2,682	2,707	-132	-157	Pegmatite dike, fresh
2,707	2,721	-157	-171	Quartz monzonite, most of the core is slightly to moderately altered
2,721	2,777	-171	-227	Quartz monzonite, slightly to moderately altered
2,777	3,167	-227	-617	Quartz monzonite, most of the core is fresh to slightly altered

**Table 3-2. Summary of Lithology in the Subsurface Core Holes (continued)**

Depth (ft)		Elevation (ft MSL)		Lithology
From:	To:	From:	To:	
<b>Core Hole: ZEV-CH-02-23</b>				
0	70	2,578	2,508	HW casing
70	160	2,508	2,418	Quartz monzonite, most of the core is moderately to highly altered
160	606	2,418	1,972	Quartz monzonite, most of the core is fresh to slightly altered
606	612	1,972	1,966	Pegmatite dike, fresh
612	658	1,966	1,920	Quartz monzonite, most of the core is slightly altered
658	727	1,920	1,851	Zone of numerous thin pegmatite dikes, fresh to slightly altered
727	895	1,851	1,683	Quartz monzonite, most of the core is fresh to slightly altered
895	966	1,683	1,612	Quartz monzonite, most of the core is moderately to highly altered
966	980	1,612	1,598	Pegmatite dike, fresh
980	1,186	1,598	1,392	Quartz monzonite, most of the core is fresh to slightly altered
1,186	1,202	1,392	1,376	Quartz monzonite, fresh to slightly altered
1,202	1,206	1,376	1,372	Pegmatite dike, fresh
1,206	1,225	1,372	1,353	Quartz monzonite, fresh to slightly altered
1,225	1,270	1,353	1,308	Quartz monzonite, most of the core is moderately to highly altered
1,270	1,791	1,308	787	Quartz monzonite, most of the core is fresh to slightly altered
1,791	1,795	787	783	Quartz monzonite, fresh
1,795	2,114	783	464	Quartz monzonite, most of the core is fresh to slightly altered, numerous thin pegmatite dykes throughout
2,114	2,169	464	409	Quartz monzonite, most of the core is moderately to highly altered
2,169	2,245	409	333	Quartz monzonite, most of the core is fresh to slightly altered
2,245	2,320	333	258	Quartz monzonite, most of the core is moderately to highly altered
2,320	2,330	258	248	Quartz monzonite, fresh
2,330	2,351	248	227	Quartz monzonite, most of the core is fresh to moderately altered
2,351	2,358	227	220	Quartz monzonite, fresh
2,358	2,400	220	178	Quartz monzonite, most of the core is fresh to slightly altered
2,400	2,405	178	173	Pegmatite dike, moderately altered
2,405	2,427	173	151	Quartz monzonite, most of the core is moderately to highly altered
2,427	2,431	151	147	Pegmatite dike, fresh
2,431	2,504	147	74	Quartz monzonite, most of the core is fresh to slightly altered
2,504	2,508	74	70	Pegmatite dike, fresh
2,508	2,794	70	-216	Quartz monzonite, most of the core is fresh to moderately altered
2,794	2,800	-216	-222	Pegmatite dike, fresh
2,800	2,921	-222	-343	Quartz monzonite, most of the core is fresh to slightly altered
2,921	2,930	-343	-352	Diabase dike, fresh
2,930	3,045	-352	-467	Quartz monzonite, most of the core is fresh to slightly altered

**Table 3-2. Summary of Lithology in the Subsurface Core Holes (continued)**

Depth (ft)		Elevation (ft MSL)		Lithology
From:	To:	From:	To:	
<b>Core Hole: ZEV-CH-03-23</b>				
0	171	2,557	2,386	HW casing
171	264	2,386	2,293	Quartz monzonite, most of the core is fresh to slightly altered
264	306	2,293	2,251	Quartz monzonite, most of the core is moderately to highly altered
306	590	2,251	1,967	Quartz monzonite, most of the core is fresh to slightly altered
590	621	1,967	1,936	Quartz monzonite, most of the core is moderately to highly altered
621	1,083	1,936	1,474	Quartz monzonite, most of the core is fresh to slightly altered
1,083	1,086	1,474	1,471	Pegmatite dike, fresh
1,086	1,192	1,471	1,365	Quartz monzonite, most of the core is fresh to slightly altered
1,192	1,195	1,365	1,362	Pegmatite dike, fresh
1,195	1,197	1,362	1,360	Quartz monzonite, fresh
1,197	1,216	1,360	1,341	Quartz monzonite, most of the core is fresh to slightly altered
1,216	1,229	1,341	1,328	Quartz monzonite, fresh
1,229	1,246	1,328	1,311	Quartz monzonite, most of the core is fresh to slightly altered
1,246	1,251	1,311	1,306	Quartz monzonite, fresh
1,251	1,321	1,306	1,236	Quartz monzonite, most of the core is fresh to moderately altered
1,321	1,328	1,236	1,229	Quartz monzonite, fresh
1,328	1,338	1,229	1,219	Quartz monzonite, most of the core is slightly to moderately altered
1,338	1,343	1,219	1,214	Pegmatite dike, fresh
1,343	1,461	1,214	1,096	Quartz monzonite, most of the core is slightly to highly altered
1,461	1,793	1,096	764	Quartz monzonite, most of the core is fresh to slightly altered
1,793	1,799	764	758	Core loss
1,799	1,814	758	743	Quartz monzonite, most of the core is fresh to slightly altered
1,814	1,886	743	671	Quartz monzonite, most of the core is slightly to moderately altered
1,886	1,895	671	662	Quartz monzonite, fresh
1,895	2,000	662	557	Quartz monzonite, most of the core is fresh to slightly altered
2,000	2,151	557	406	Quartz monzonite, most of the core is moderately to highly altered
2,151	2,299	406	258	Quartz monzonite, most of the core is fresh to slightly altered
2,299	2,307	258	250	Core loss
2,307	2,496	250	61	Quartz monzonite, most of the core is fresh to slightly altered
2,496	2,525	61	32	Quartz monzonite, fresh to slightly altered
2,525	2,707	32	-150	Quartz monzonite, most of the core is fresh to slightly altered
2,707	2,716	-150	-159	Quartz monzonite, fresh
2,716	2,766	-159	-209	Quartz monzonite, most of the core is fresh to slightly altered
2,766	2,841	-209	-284	Quartz monzonite, most of the core is moderately to completely altered
2,841	2,906	-284	-349	Quartz monzonite, most of the core is fresh to slightly altered
2,906	3,015	-349	-458	Quartz monzonite, most of the core is slightly to moderately altered

**Table 3-2. Summary of Lithology in the Subsurface Core Holes (continued)**

Depth (ft)		Elevation (ft MSL)		Lithology
From:	To:	From:	To:	
<b>Core Hole: ZEV-CH-04-24</b>				
0	76	2,543	2,467	HW casing
76	115	2,467	2,428	Significant core loss
115	140	2,428	2,403	Quartz monzonite, most of the core is slightly to highly altered
140	154	2,403	2,389	Quartz monzonite, most of the core is fresh to slightly altered
154	157	2,389	2,386	Pegmatite dike, slightly altered
157	339	2,386	2,204	Quartz monzonite, most of the core is fresh to moderately altered
339	376	2,204	2,167	Quartz monzonite, most of the core is highly to completely altered
376	691	2,167	1,852	Quartz monzonite, most of the core is fresh to slightly altered
691	691	1,852	1,852	Quartz monzonite, most of the core is slightly to moderately altered
691	820	1,852	1,723	Quartz monzonite, most of the core is fresh to slightly altered
820	823	1,723	1,720	Pegmatite dike, fresh to slightly altered
823	1,078	1,720	1,465	Quartz monzonite, most of the core is fresh to slightly altered
1,078	1,306	1,465	1,237	Quartz monzonite, most of the core is highly to completely altered
1,306	1,776	1,237	767	Quartz monzonite, most of the core is moderately to completely altered
1,776	1,799	767	744	Quartz monzonite, most of the core is slightly to moderately altered
1,799	1,801	744	742	Pegmatite dike, fresh
1,801	1,806	742	737	Quartz monzonite, most of the core is slightly to moderately altered
1,806	1,808	737	735	Pegmatite dike, fresh
1,808	1,823	735	720	Quartz monzonite, most of the core is slightly to moderately altered
1,823	1,826	720	717	Pegmatite dike, fresh
1,826	1,936	717	607	Quartz monzonite, most of the core is slightly to highly altered
1,936	2,131	607	412	Quartz monzonite, most of the core is fresh to slightly altered
2,131	2,142	412	401	Pegmatite dike, fresh
2,142	2,211	401	332	Quartz monzonite, most of the core is fresh to slightly altered
2,211	2,246	332	297	Quartz monzonite, most of the core is moderately to completely altered
2,246	2,361	297	182	Quartz monzonite, most of the core is fresh to moderately altered
2,361	2,371	182	172	Quartz monzonite, fresh to slightly
2,371	2,511	172	32	Quartz monzonite, most of the core is fresh to moderately altered
2,511	2,518	32	25	Core loss
2,518	2,581	25	-38	Quartz monzonite, most of the core is fresh to slightly altered



**Table 3-2. Summary of Lithology in the Subsurface Core Holes (continued)**

Depth (ft)		Elevation (ft MSL)		Lithology
From:	To:	From:	To:	
<b>Core Hole: ZEV-CH-05-24</b>				
0	75	2,541	2,466	HW casing
75	80	2,466	2,461	Quartz monzonite, most of the core is slightly to moderately altered
80	82	2,461	2,460	Core loss
82	305	2,459	2,236	Quartz monzonite, most of the core is slightly to moderately altered
305	435	2,236	2,106	Quartz monzonite, most of the core is moderately to completely altered
435	469	2,106	2,072	Quartz monzonite, most of the core is slightly to moderately altered
469	479	2,072	2,062	Quartz monzonite, most of the core is moderately to completely altered
479	568	2,062	1,973	Quartz monzonite, most of the core is fresh to moderately altered
568	580	1,973	1,961	Quartz monzonite, most of the core is moderately to highly altered
580	673	1,961	1,868	Quartz monzonite, most of the core is fresh to moderately altered
673	690	1,868	1,851	Quartz monazite, most of the core is moderately to highly altered
690	716	1,851	1,825	Quartz monzonite, most of the core is fresh to slightly altered
716	730	1,825	1,811	Quartz monzonite, most of the core is highly to completely altered
730	767	1,811	1,774	Quartz monzonite, most of the core is slightly to moderately altered
767	1,135	1,774	1,406	Quartz monzonite, most of the core is fresh to slightly altered
1,135	1,140	1,406	1,401	Quartz monazite, most of the core is highly altered
1,140	1,200	1,401	1,341	Quartz monzonite, most of the core is fresh to slightly altered
1,200	1,275	1,341	1,266	Quartz monzonite, most of the core is slightly to moderately altered
1,275	1,298	1,266	1,243	Quartz monzonite, most of the core is fresh to slightly altered
1,298	1,800	1,243	741	Quartz monzonite, most of the core is moderately to completely altered, two thin pegmatite dikes throughout
1,800	2,033	741	508	Quartz monzonite, most of the core is fresh to slightly altered, numerous thin pegmatite dikes throughout
2,033	2,047	508	494	Quartz monzonite, most of the core is fresh to moderately altered
2,047	2,053	494	488	Quartz monzonite, fresh
2,053	2,102	488	439	Quartz monzonite, most of the core is fresh to slightly altered
2,102	2,104	439	437	Pegmatite dike, fresh
2,104	2,135	437	406	Quartz monzonite, most of the core is fresh to slightly altered
2,135	2,136	406	405	Quartz monzonite, fresh
2,136	2,162	405	379	Quartz monzonite, most of the core is slightly to moderately altered
2,162	2,224	379	317	Quartz monzonite, most of the core is fresh
2,224	2,228	317	313	Core loss
2,228	2,285	313	256	Quartz monzonite, most of the core is fresh to moderately altered

**Table 3-2. Summary of Lithology in the Subsurface Core Holes (continued)**

Depth (ft)		Elevation (ft MSL)		Lithology
From:	To:	From:	To:	
<b>Core Hole: ZEV-CH-06-24</b>				
0	20	2,549	2,529	HW Casing
20	100	2,529	2,449	Quartz monzonite, fresh
100	101	2,449	2,448	Core loss
101	153	2,448	2,396	Quartz monzonite, slightly to moderately altered
153	303	2,396	2,246	Quartz monzonite, fresh to slightly altered
303	304	2,246	2,245	Core loss
304	402	2,245	2,147	Quartz monzonite, most of the core is fresh
402	426	2,147	2,123	Quartz monzonite, slightly to moderately altered
426	516	2,123	2,033	Quartz monzonite, most of the core is fresh
516	581	2,033	1,968	Quartz monzonite, moderately altered
581	606	1,968	1,943	Quartz monzonite, fresh
606	621	1,943	1,928	Quartz monzonite, highly altered
621	719	1,928	1,830	Quartz monzonite, most of the core is fresh to slightly altered
719	746	1,830	1,803	Quartz monzonite, highly altered
746	846	1,803	1,703	Quartz monzonite, slightly altered
846	854	1,703	1,695	Quartz monzonite, completely altered
854	887	1,695	1,662	Quartz monzonite, slightly altered
887	912	1,662	1,637	Quartz monzonite, highly altered
912	920	1,637	1,629	Quartz monzonite, most of the core is slightly to moderately altered
920	966	1,629	1,583	Quartz monzonite, most of the core is fresh to slightly altered
966	976	1,583	1,573	Quartz monzonite, completely altered
976	1,028	1,573	1,521	Quartz monzonite, most of the core is slightly altered
1,028	1,156	1,521	1,393	Quartz monzonite, most of the core is fresh to slightly altered
1,156	1,236	1,393	1,313	Quartz monzonite, most of the core is fresh to moderately altered
1,236	1,276	1,313	1,273	Quartz monzonite, completely altered
1,276	1,311	1,273	1,238	Quartz monzonite, slightly to moderately altered
1,311	1,363	1,238	1,186	Quartz monzonite, fresh to slightly altered
1,363	1,364	1,186	1,185	Core loss
1,364	1,389	1,185	1,160	Quartz monzonite, fresh to slightly altered
1,389	1,394	1,160	1,155	Pegmatite dike, fresh to slightly altered
1,394	1,497	1,155	1,052	Quartz monzonite, fresh to slightly altered
1,497	1,746	1,052	803	Quartz monzonite, most of the core is moderately altered
1,746	1,844	803	705	Quartz monzonite, most of the core is fresh to moderately altered
1,844	1,866	705	683	Quartz monzonite, moderately to highly altered
1,866	2,064	683	485	Quartz monzonite, most of the core is fresh to slightly altered
2,064	2,065	485	484	Core loss
2,065	2,166	484	383	Quartz monzonite, most of the core is fresh to slightly altered
2,166	2,177	383	372	Quartz monzonite, most of the core is slightly to moderately altered
2,177	2,280	372	269	Quartz monzonite, most of the core is slightly altered

**Table 3-3. Effect of Alteration on Fresh Rock (ISRM 2007)**

Classification	Symbol	Description
Fresh	Fr	No visible signs of alteration; perhaps slight discoloration on defect surfaces.
Slightly Altered	SA	Alteration confined to veins and/or veinlets. Little or no penetration of alteration beyond vein/veinlet boundaries. No discernable effect on the strength properties of the parent rock type.
Moderately Altered	MA	Alteration is controlled by veins and may penetrate wall rock as narrow vein selvages or envelopes. Alteration may also be pervasive but weakly developed. Modifications to the rock are small.
Highly Altered	HA	Pervasive alteration of rock-forming minerals and intact rock to assemblages that significantly change the strength properties of the parent rock type.
Completely Altered	CA	Intensive, pervasive, complete alteration of rock-forming minerals. The rock mass may resemble soil. For hydrothermal alteration, any alteration assemblages that results in the nearly complete or complete change in rock strength relative to the parent rock type.



**Figure 3-3. Degree of Alteration Logged in Core Hole ZEV-CH-01-23**



Figure 3-4. Degree of Alteration Logged in Core Hole ZEV-CH-02-23

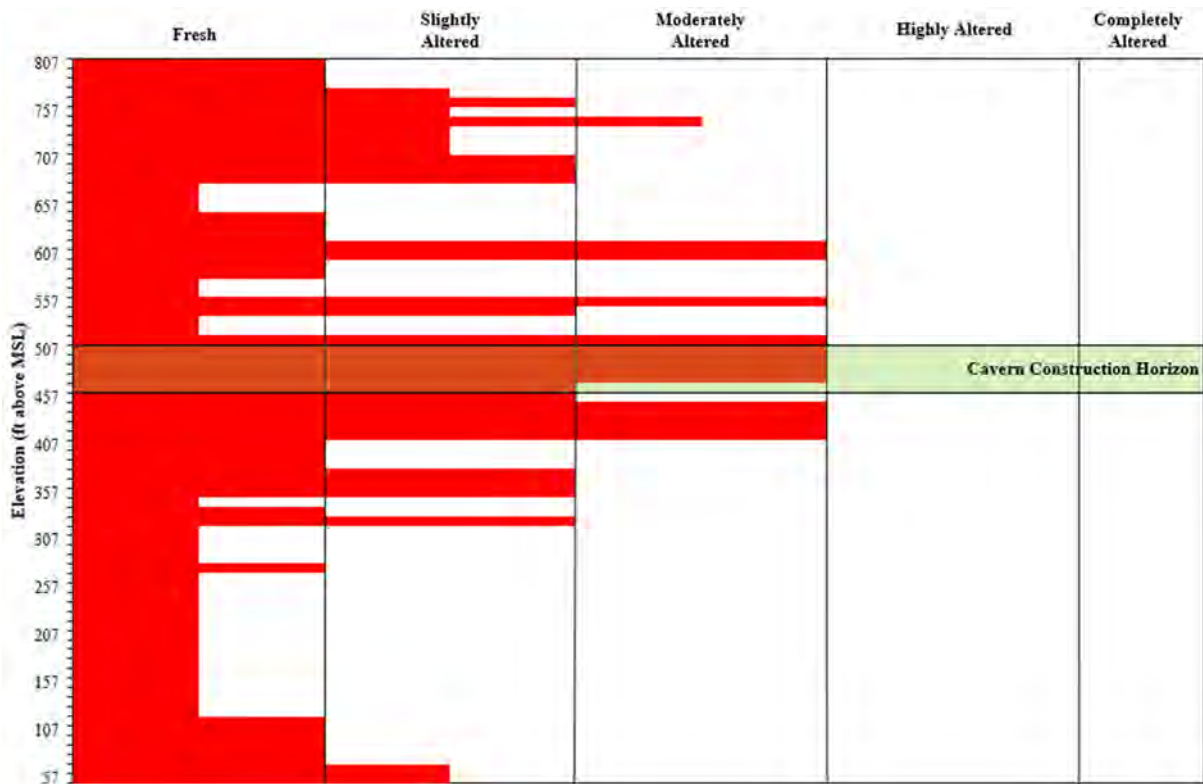


Figure 3-5. Degree of Alteration Logged in Core Hole ZEV-CH-03-23



Figure 3-6. Degree of Alteration Logged in Core Hole ZEV-CH-04-24



Figure 3-7. Degree of Alteration Logged in Core Hole ZEV-CH-05-24



**Figure 3-8. Degree of Alteration Logged in Core Hole ZEV-CH-06-24**

### 3.2.2 Rock Quality

The Rock Quality Designation (RQD) classification system has been used to classify the degree of jointing or block size of the recovered core (Deere 1963). The rock quality descriptors corresponding to the RQD values are given in Table 3-4. The core holes show a wide range in rock quality from “Very Poor” to “Excellent”. In core holes ZEV-CH-01-23 and ZEV-CH-02-23, the logging indicates that the highest rock quality is generally between the elevations of 600 and 300 ft above MSL, where most of the rock mass is classed as “Fair” to “Good” (Figures 3-9 and 3-10). Immediately above and below these elevations, the logging indicates decreasing rock quality, where most of the rock mass is classed as “Very Poor” to “Poor”. In core holes ZEV-CH-03-23 and ZEV-CH-04-24, the logging indicates a distinctly lower rock quality, with most of the rock mass classed as “Very Poor” to “Poor” (Figures 3-11 and 3-12). In core hole ZEV-CH-03-23, the highest rock quality is generally located between the elevations of 360 and 100 ft above MSL (Figure 3-11). In core hole ZEV-CH-04-24, the highest rock quality is located between the elevations of 510 and 315 ft above MSL (Figure 3-12). In core holes ZEV-CH-05-24 and ZEV-CH-06-24, the logging indicates a slightly higher rock quality than the previous two holes, with most of the rock mass classed as “Poor” to “Fair” (Figures 3-13 and 3-14). The highest rock quality logged in ZEV-CH-05-24 is located between the elevations of 800 and 675 ft above MSL (Figure 3-13). The highest rock quality logged in ZEV-CH-06-24 is located between the elevations of 800 and 730 ft above MSL (Figure 3-14).

**Table 3-4. RQD Classification System (Deere and Deere 1988)**

RQD	Description of Rock Quality
0 to <25	Very Poor
25 to <50	Poor
50 to <75	Fair
75 to <90	Good
90 to 100	Excellent

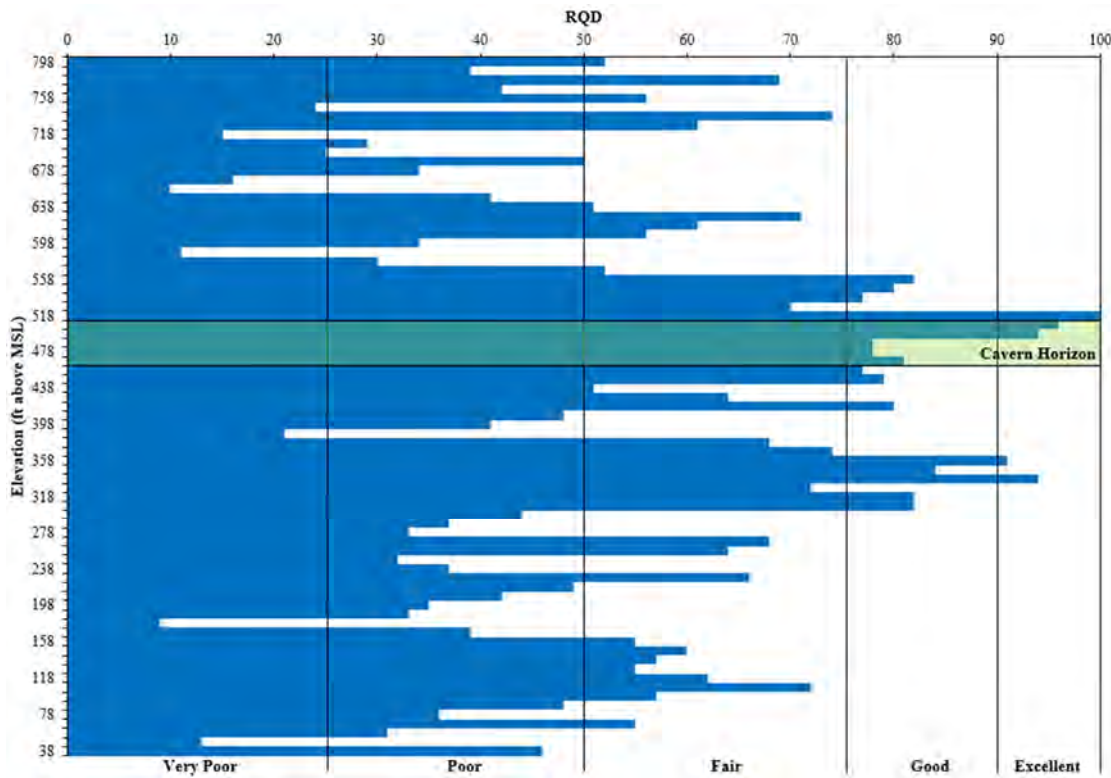


**Figure 3-9. Rock Quality Logged in Core Hole ZEV-CH-01-23**

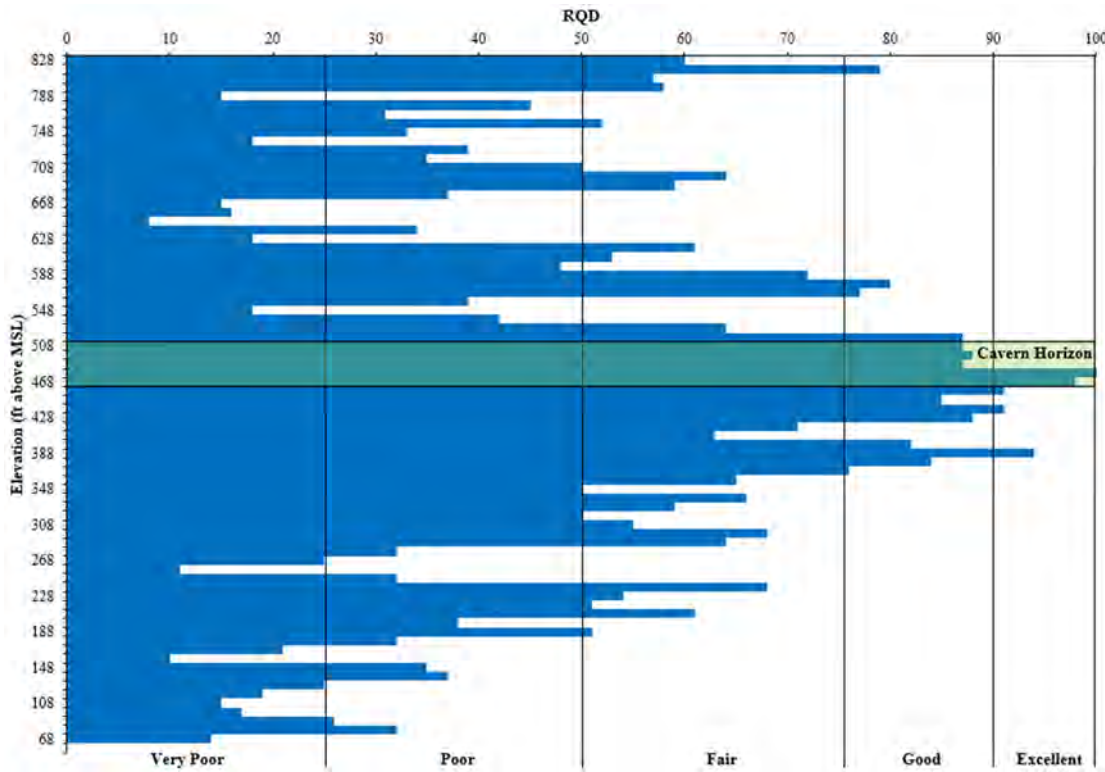


Figure 3-10. Rock Quality Logged in Core Hole ZEV-CH-02-23

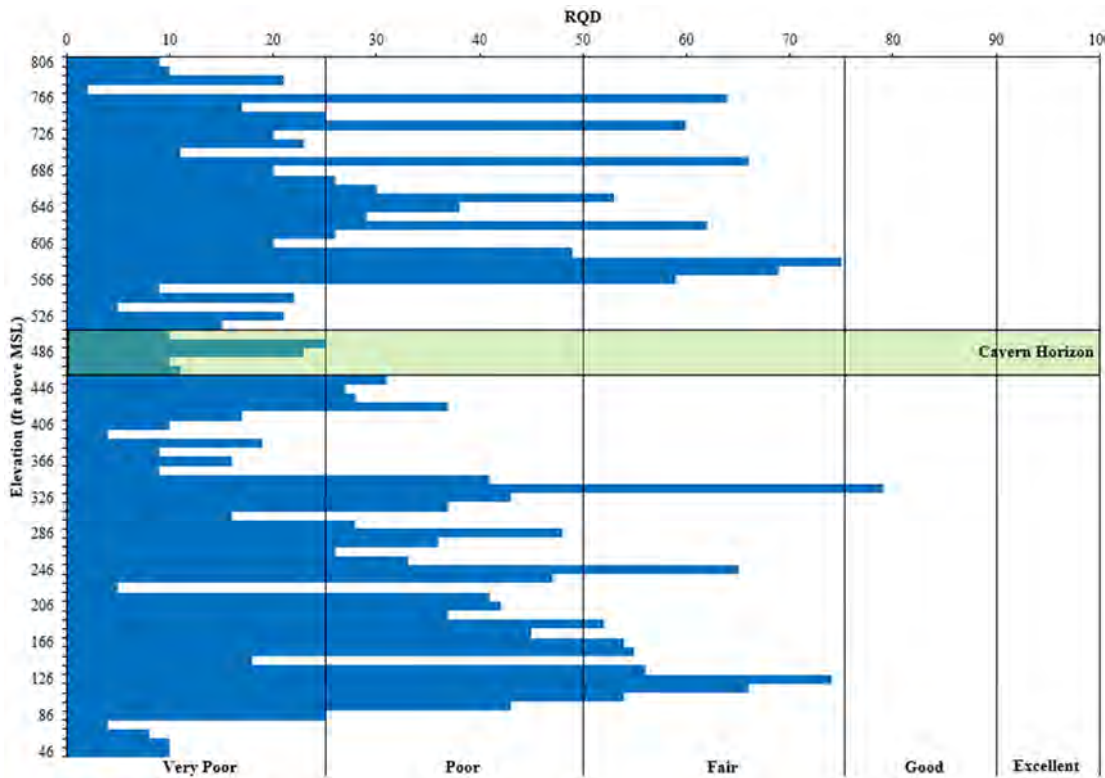


Figure 3-11. Rock Quality Logged in Core Hole ZEV-CH-03-23



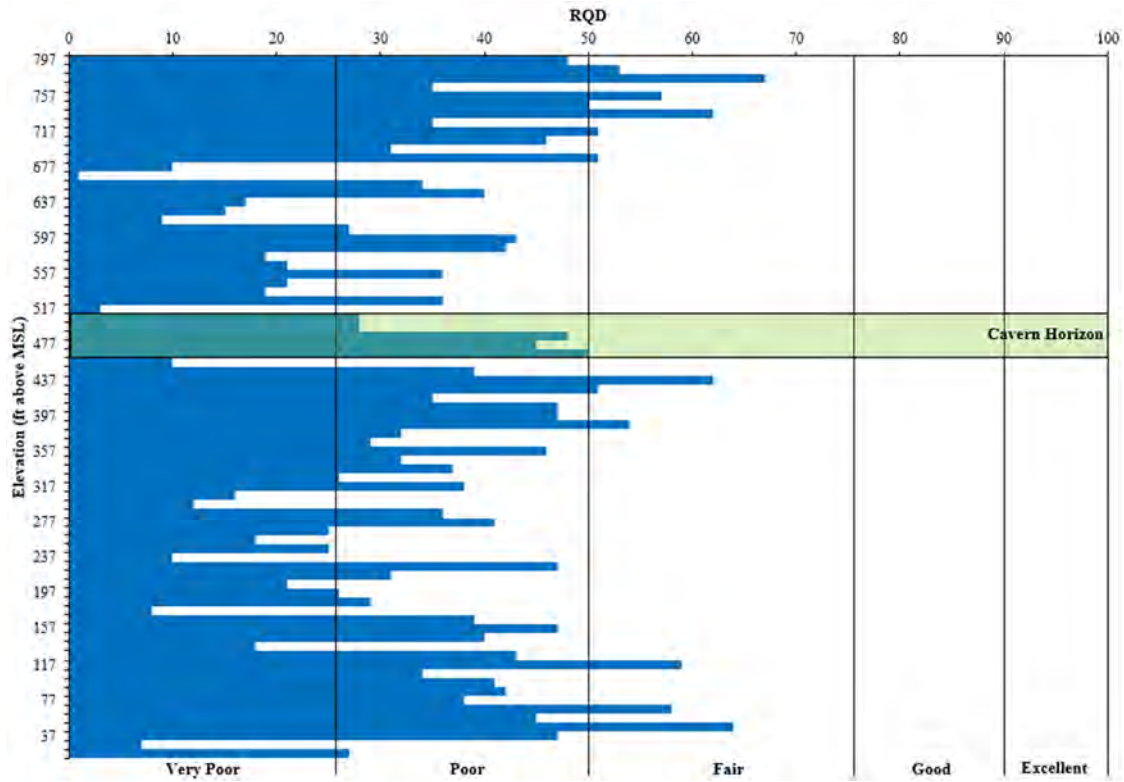


Figure 3-12. Rock Quality Logged in Core Hole ZEV-CH-04-24

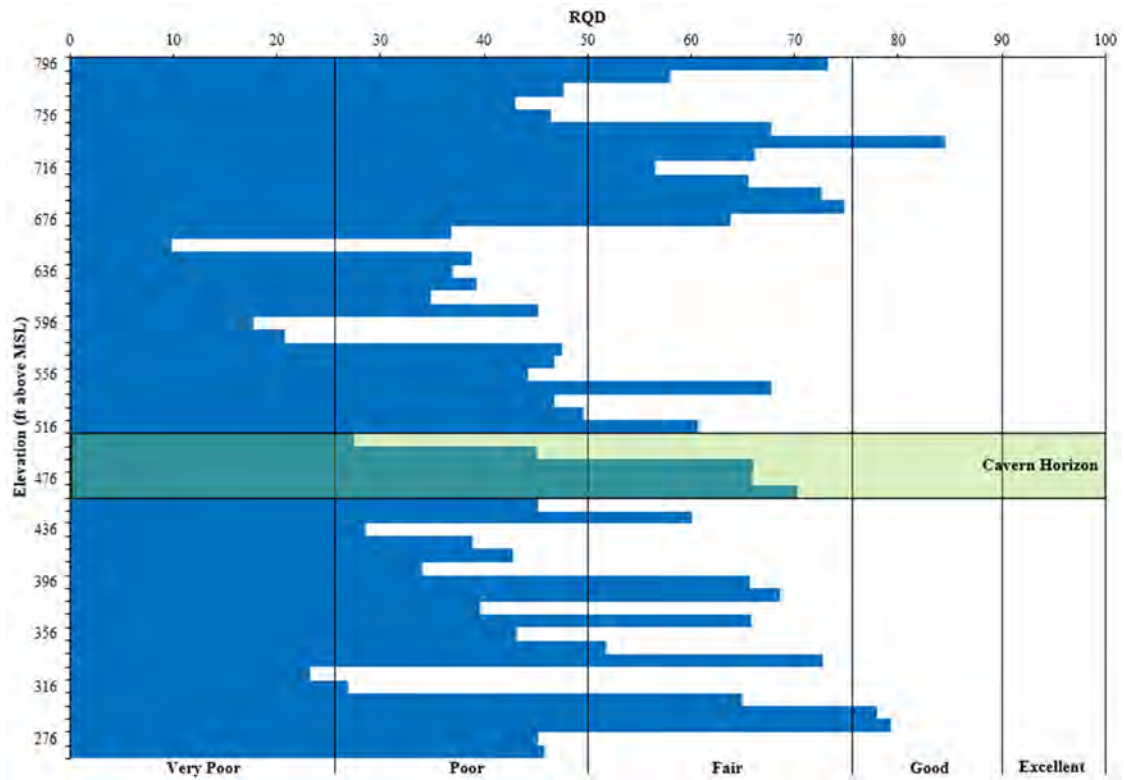
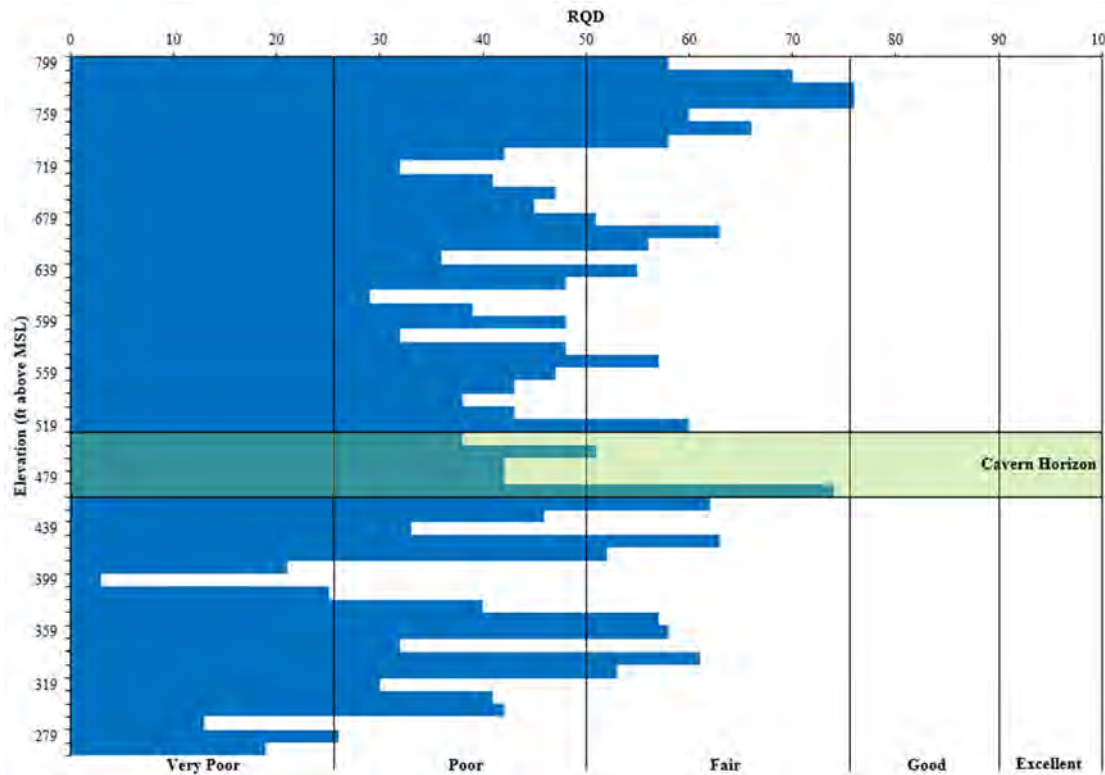


Figure 3-13. Rock Quality Logged in Core Hole ZEV-CH-05-24



**Figure 3-14. Rock Quality Logged in Core Hole ZEV-CH-06-24**

### 3.2.3 Packer Testing

Packer testing was performed by project geologist Chris Messinger to estimate the hydraulic conductivity of the rock mass at a depth suitable for A-CAES operation. Packers were set along the core hole length to isolate consecutive 21.8 ft intervals for testing. For each test, a small amount of water was added to the test interval after which the interval was pressurized to 80 psi above the hydrostatic pressure. Changes in the water level are then measured, first at 1-minute intervals for 5 minutes and 5-minute intervals thereafter, until the flow rate into the rock stabilized. Packer testing began at the bottom of the core holes and worked higher in elevation until a final depth of 1,800 and 1,900 ft below the ground surface for the first four holes. Core holes ZEV-CH-05-24 and ZEV-CH-06-24 were tested up to the bottom of the surface casing.

The recorded flow rates in core holes ZEV-CH-01-23, ZEV-CH-02-23, and ZEV-CH-03-23 are all less than 4.5 gallons-per-hour (gph), with most of the rates less than 2.0 gph (Figures 3- 15 to 3-17). The hydraulic conductivity of the rock mass, which was derived from an average of three different methodologies, ranges between  $1.90 \times 10^{-8}$  and  $8.55 \times 10^{-7}$  centimeters per second (cm/s) in these three core holes (Figures 3-15 to 3-17). In core holes ZEV-CH-04-24, ZEV-CH-05-24, and ZEV-CH-06-24 between the elevations of 350 and 200 ft above MSL, higher flow rates ranging from 5.5 to 12 gph were measured (Figures 3-18 to 3-20). Above these elevations, the flow rates are mostly less than 3.0 gph. The hydraulic conductivity in these core holes ranges between  $1.94 \times 10^{-8}$  to  $2.33 \times 10^{-6}$  cm/s (Figures 3-18 to 3-20).

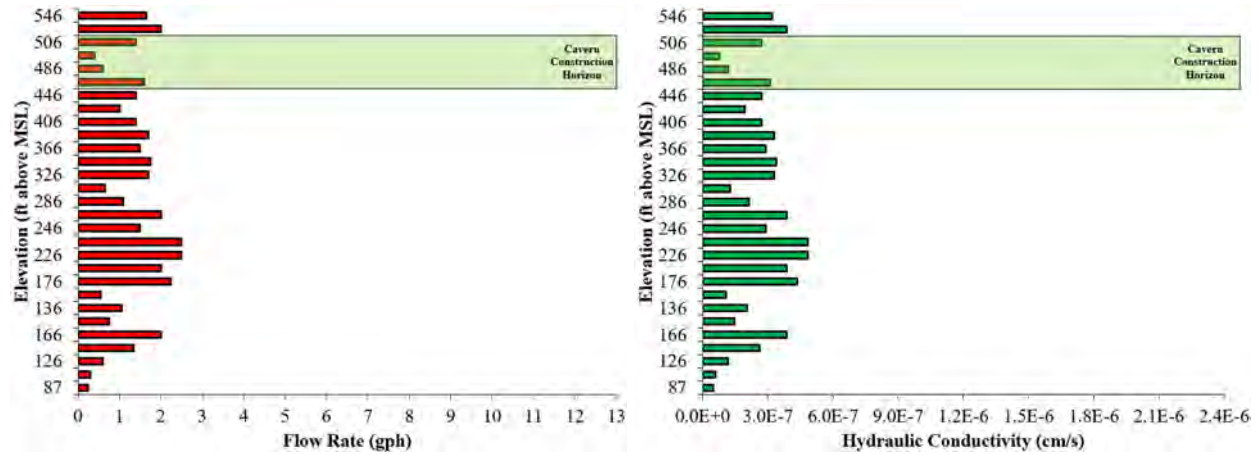


**Figure 3-15. Flow Rate and Permeability Recorded in Core Hole ZEV-CH-01-23**

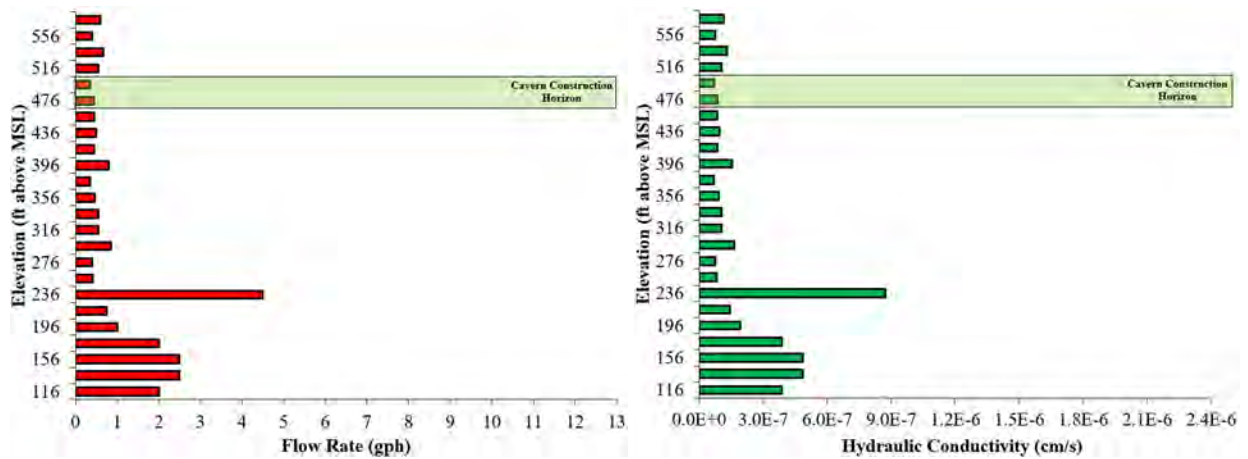


**Figure 3-16. Flow Rate and Permeability Recorded in Core Hole ZEV-CH-02-23**

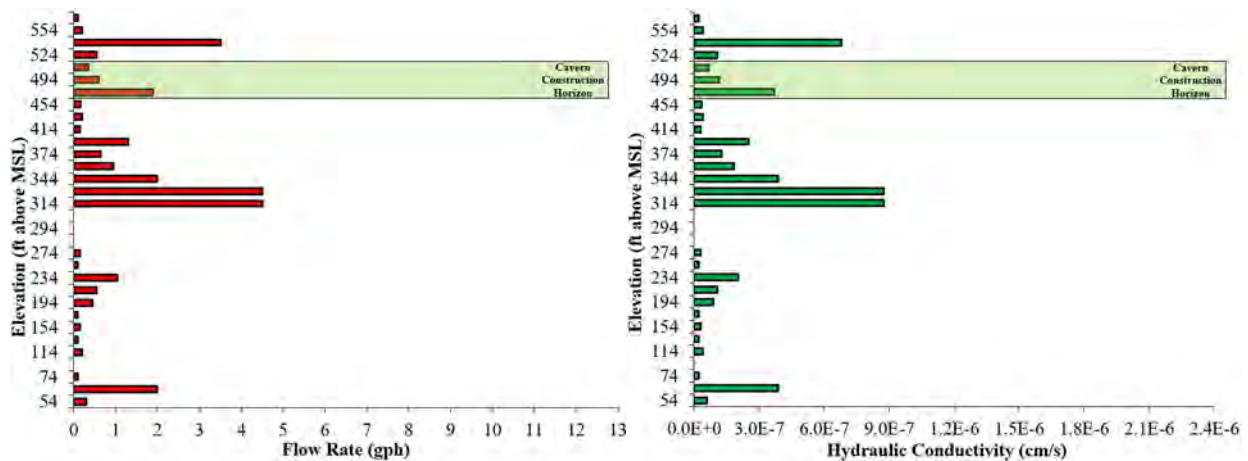


**Figure 3-17. Flow Rate and Permeability Recorded in Core Hole ZEV-CH-03-23**

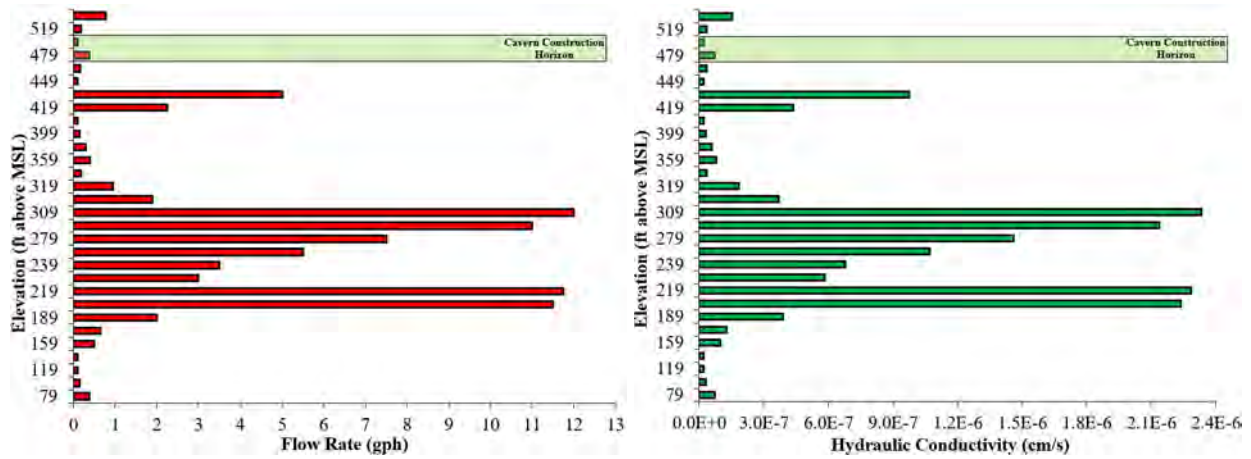


Figure 3-18. Flow Rate and Permeability Recorded in Core Hole ZEV-CH-04-24

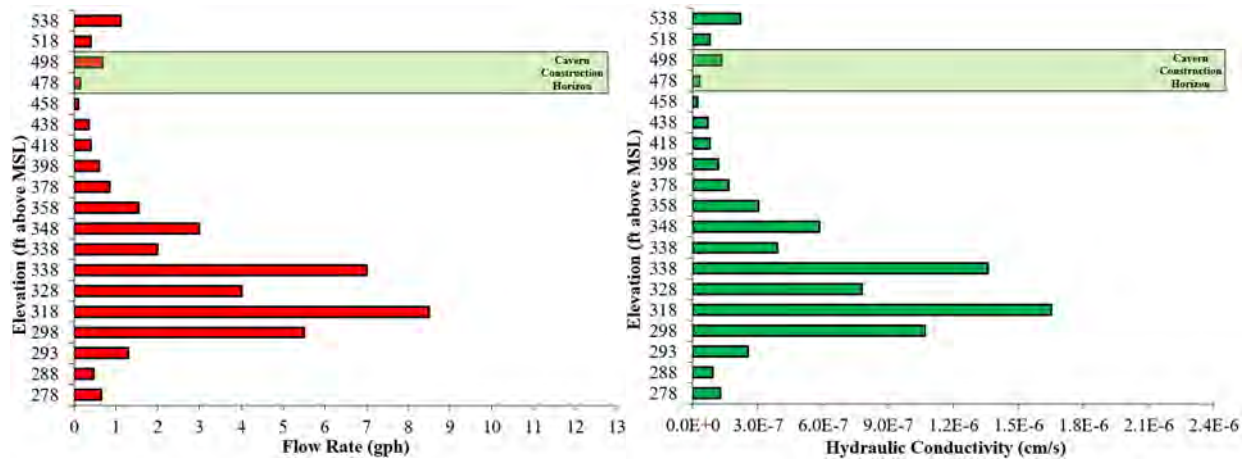


Figure 3-19. Flow Rate and Permeability Recorded in Core Hole ZEV-CH-05-24

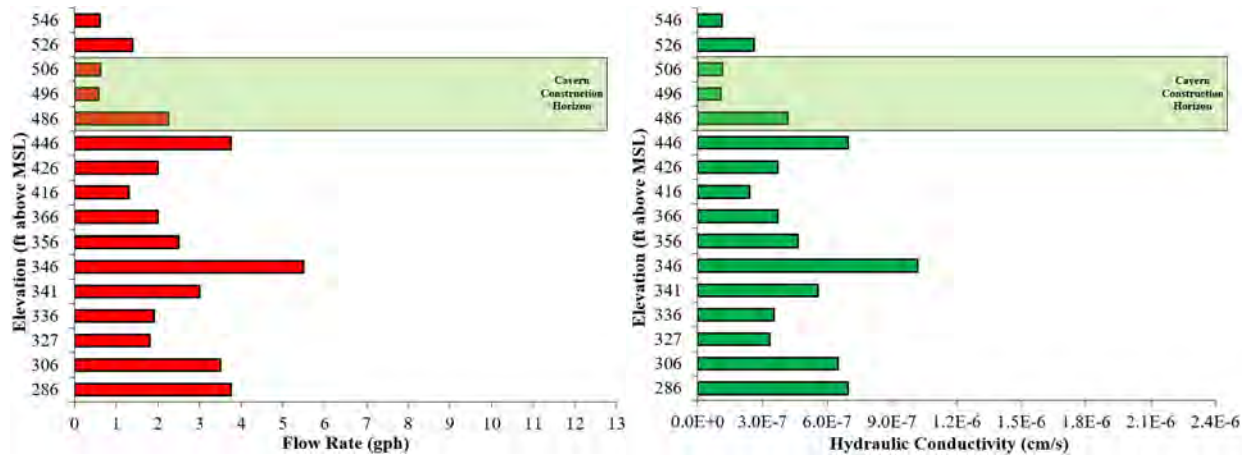


Figure 3-20. Flow Rate and Permeability Recorded in Core Hole ZEV-CH-06-24

The derived hydraulic conductivity values can be used to infer the condition of the rock mass discontinuities according to Table 3-5 (Quinones-Rozo 2010). The condition of the rock mass discontinuities can therefore be classed as “Very Tight” throughout the tested horizon.

**Table 3-5. Condition of Rock Mass Discontinuities Associated with Different Hydraulic Conductivities (Quinones-Rozo 2010)**

Hydraulic Conductivity Range (cm/s)	Condition of Rock Mass Discontinuities
$<1 \times 10^{-5}$	Very Tight
$1 \times 10^{-5}$ to $6 \times 10^{-5}$	Tight
$6 \times 10^{-5}$ to $2 \times 10^{-4}$	Few Partly Open
$2 \times 10^{-4}$ to $6 \times 10^{-4}$	Some Open
$6 \times 10^{-4}$ to $1 \times 10^{-3}$	Many Open
$>1 \times 10^{-3}$	Open Closely Spaced or Voids

### 3.2.4 Falling Head Testing

Following core drilling in core hole ZEV-CH-05-24, a series of falling head tests were undertaken between the depths of 401 and 1,383 ft (2,140 ft and 1,158 ft above MSL) by adding water to a sealed off 21.8 ft test zone using downhole packers. The outflow from the bore was estimated using a dip meter and a pressure data logger. The testing intervals were selected based on the observation of water making zones from the recovered core and from interpretation of the geophysical log. Table 3-6 summarizes the dates and intervals when falling head tests were performed.

### 3.2.5 Rising Head Testing

In addition to the falling head tests, a series of rising head tests were undertaken between the depths of 1,101 and 2,242 ft (1,440 and 299 ft above MSL) in core hole ZEV-CH-05-24 by sealing off test zones with packers and removing water to allow the inflow from the bore to be estimated using a dip meter and pressure data logger. Table 3-7 summarizes the dates and location when rising head tests were performed.

**Table 3-6. Falling Head Test Summary for Core Hole ZEV-CH-05-24**

Test No.	Date	Depth of Testing Interval (ft)	Length of Testing Interval (ft)	Water Level Drop in Testing Interval (ft)	Elapsed Time (min)	Hydraulic Conductivity (ft/min)	Initial Outflow (ft <sup>3</sup> /min)	Initial Outflow (gal/min)
ZEVCH05 RH 423-401	7/17/2024	401 - 423	21.8	3.55	304	$6.6 \times 10^{-8}$	$5.2 \times 10^{-4}$	$3.9 \times 10^{-3}$
ZEVCH05 FH 543-521	7/16/2024	521 - 543	21.8	1.05	92	$5.1 \times 10^{-8}$	$5.1 \times 10^{-4}$	$3.9 \times 10^{-3}$
ZEVCH05 FH 553-531	7/16/2024	531 - 553	21.8	Invalid Test				
ZEVCH05 FH 963-941	7/15/2024	941 - 963	21.8	19.12	49	$1.0 \times 10^{-6}$	$1.9 \times 10^{-2}$	$1.4 \times 10^{-1}$
ZEVCH05 FH 1143-1121	7/15/2024	1,121 - 1,143	21.8	9.44	44	$4.8 \times 10^{-7}$	$1.1 \times 10^{-2}$	$7.9 \times 10^{-2}$
ZEVCH05 FH 1383-1361	7/14/2024	1,361 - 1,383	21.8	19.72	187	$2.0 \times 10^{-7}$	$5.2 \times 10^{-3}$	$3.9 \times 10^{-2}$

**Table 3-6. Rising Head Test Summary for Core Hole ZEV-CH-05-24**

Test No.	Date	Depth of Testing Interval (ft)	Length of Testing Interval (ft)	Water Level Increase in Testing Interval (ft)	Elapsed Time (min)	Hydraulic Conductivity (ft/min)	Initial Inflow (ft <sup>3</sup> /min)	Initial Inflow (gal/min)
ZEVCH05 FH 1123-1101	7/15/2024	1,101 - 1,123	21.8	9.02	26	$8.0 \times 10^{-7}$	$1.7 \times 10^{-2}$	$1.3 \times 10^{-1}$
ZEVCH05 FH 2221-2200	7/11/2024	2,200 - 2,221	21.8	14.38	8	$2.2 \times 10^{-6}$	$9.1 \times 10^{-2}$	$6.7 \times 10^{-1}$
ZEVCH05 FH 2242-2221	7/10/2024	2,221 - 2,242	21.8	17.34	13	$1.6 \times 10^{-6}$	$6.7 \times 10^{-2}$	$5.0 \times 10^{-1}$

**3.2.6 Geophysical Logging**

Geophysical logging was performed by GEOVision, Inc. (GEOVision). The core hole geophysical logging program consisted of running a sonde containing temperature and conductivity sensors, optical (OTV) and acoustic (ATV) televiwers, an acoustic caliper, and a borehole deviation sensor. The interpretation of the directions and inclinations of discontinuities in the rock was plotted as tadpoles (filled circles with tails indicating dip direction) on plots of dip versus depth. The OTV and ATV logs for the six core holes are included in Appendix B.

**3.2.7 Structural Defects**

Utilizing the ATV and OTV logs for the six core holes, discontinuities in the borehole wall and their inclination were identified by GEOVision. The summary data for the discontinuities are presented in the geophysical reports included in Appendix B. Agapito grouped the discontinuities together for each core hole and plotted the joints on stereonet and rosette diagrams to confirm dip and dip azimuth of the structure, and to identify joint sets within the fracture data. Representative stereonet and rosette diagrams are provided in Figures 3-21 to 3-26. A summary of the joint set trends identified is given in Table 3-7.

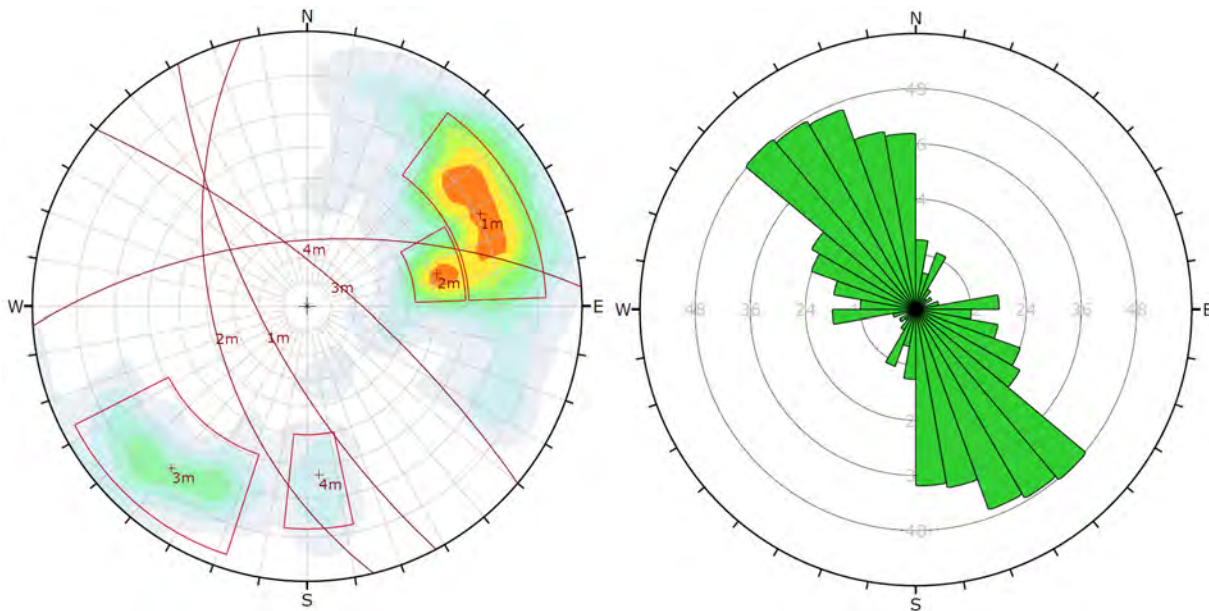


**Figure 3-21. Stereonet (left) and Rosette Diagram (right) of the Joints between the Elevations of 560 and 60 ft above MSL for ZEV-CH-01-23**

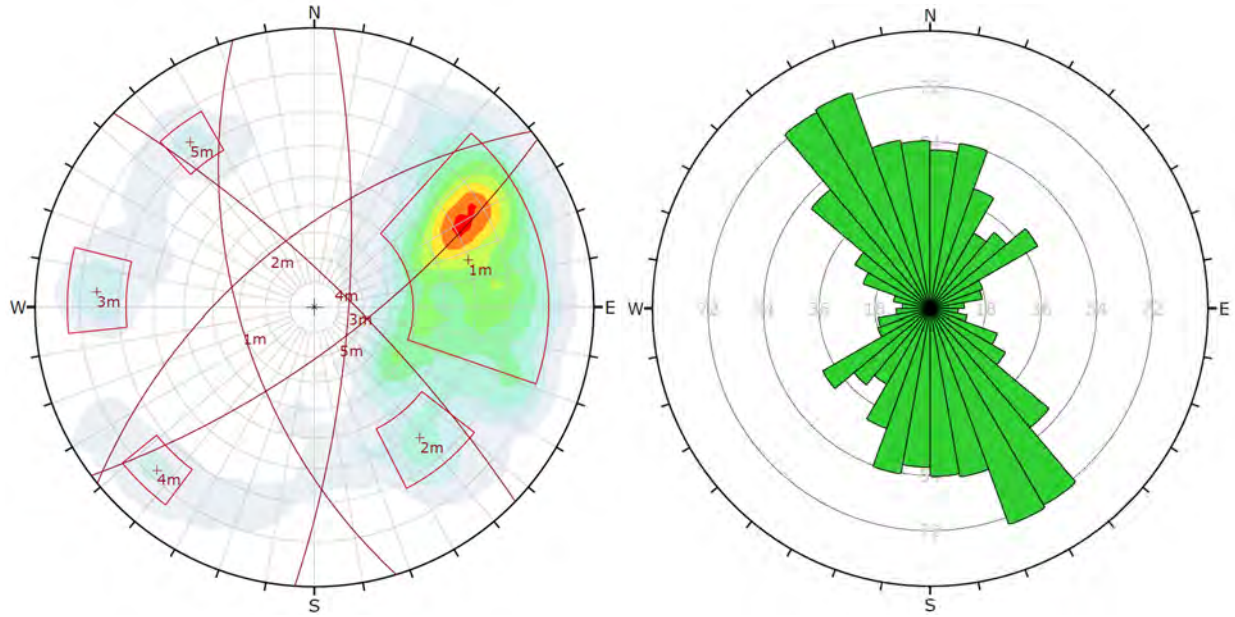


**Figure 3-22. Stereonet (left) and Rosette Diagram (right) of the Joints between the Elevations of 560 and 60 ft above MSL for ZEV-CH-02-23**

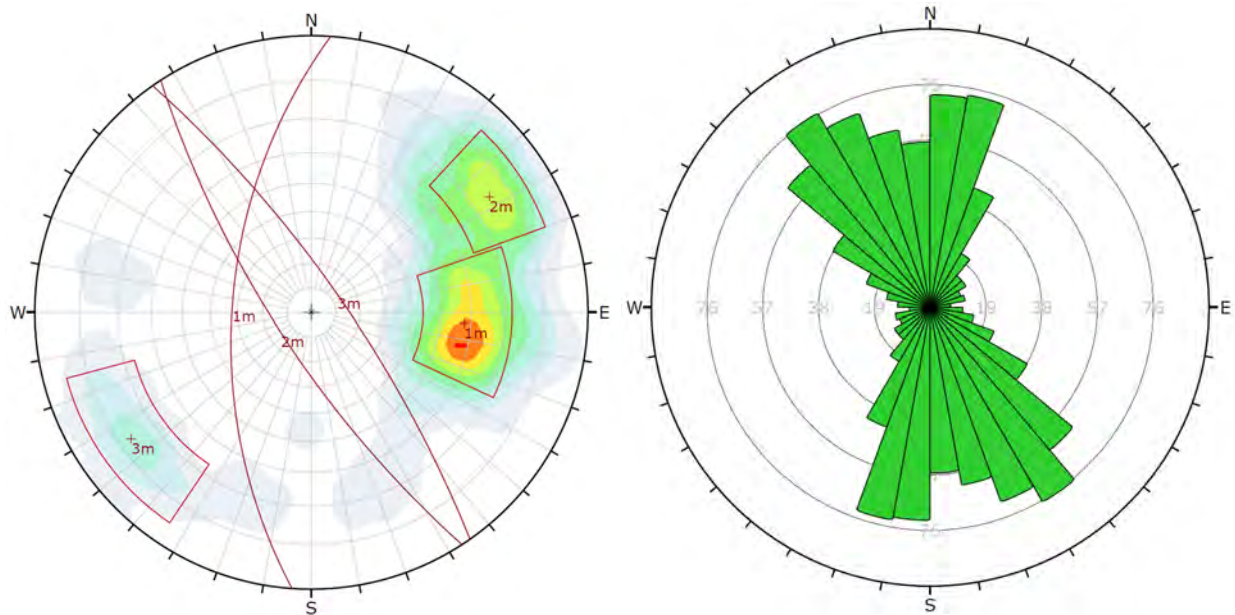


**Figure 3-23. Stereonet (left) and Rosette Diagram (right) of the Joints between the Elevations of 560 and 60 ft above MSL for ZEV-CH-03-23**

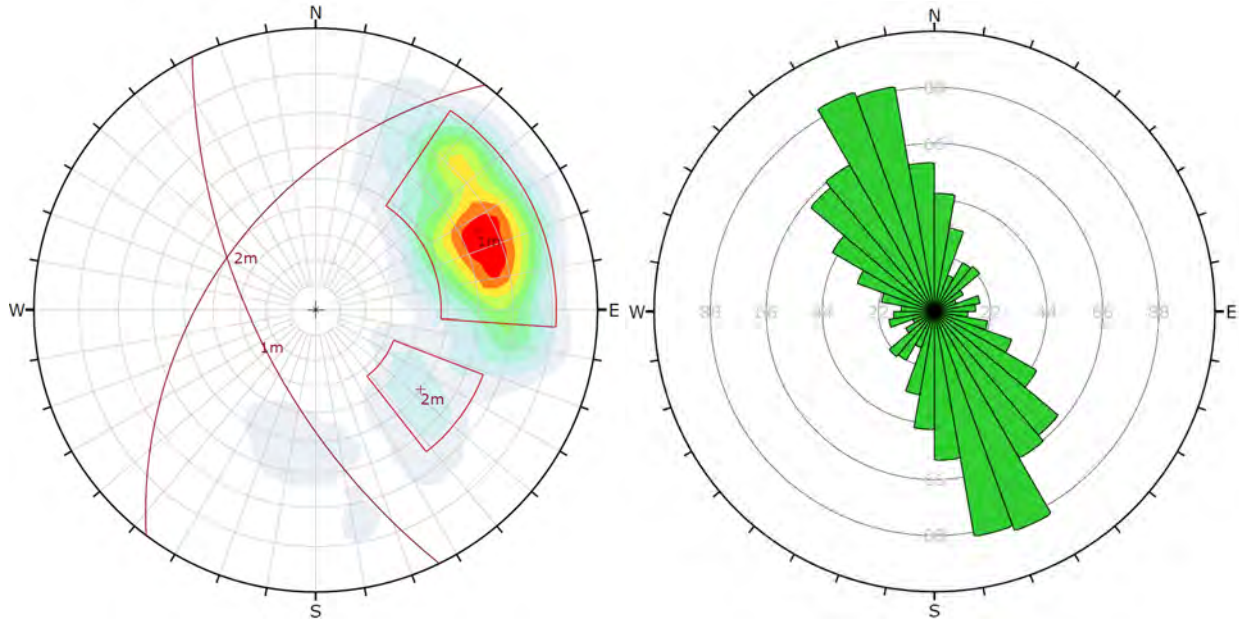


**Figure 3-24. Stereonet (left) and Rosette Diagram (right) of the Joints between the Elevations of 560 and 60 ft above MSL for ZEV-CH-04-24**

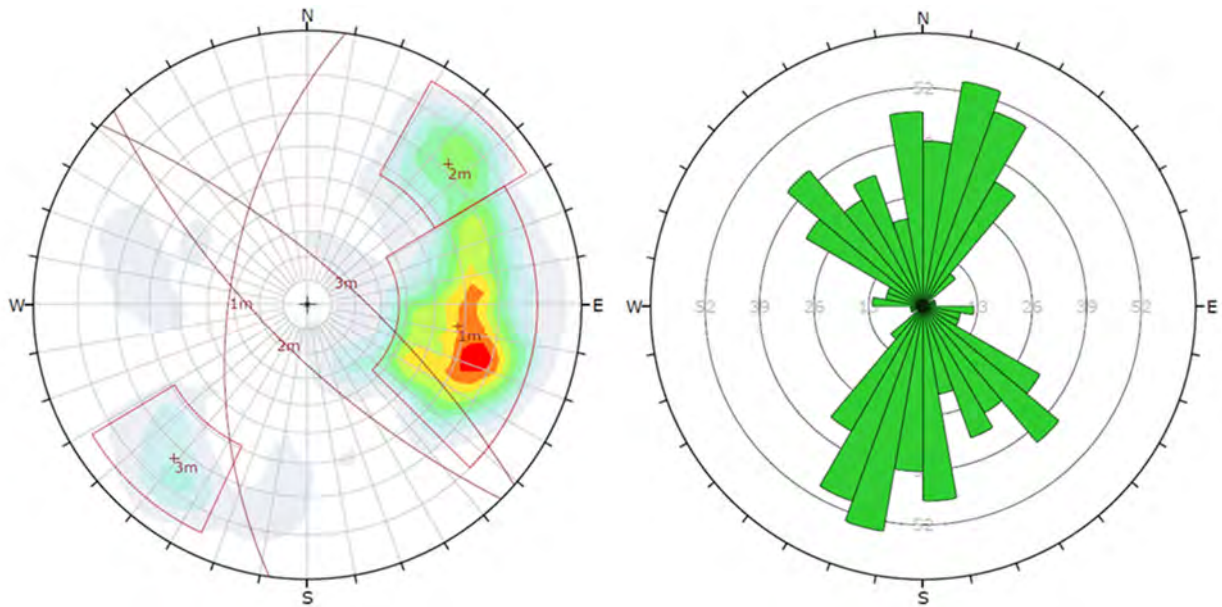


**Figure 3-25. Stereonet (left) and Rosette Diagram (right) of the Joints between the Elevations of 560 and 60 ft above MSL ZEV-CH-05-24**



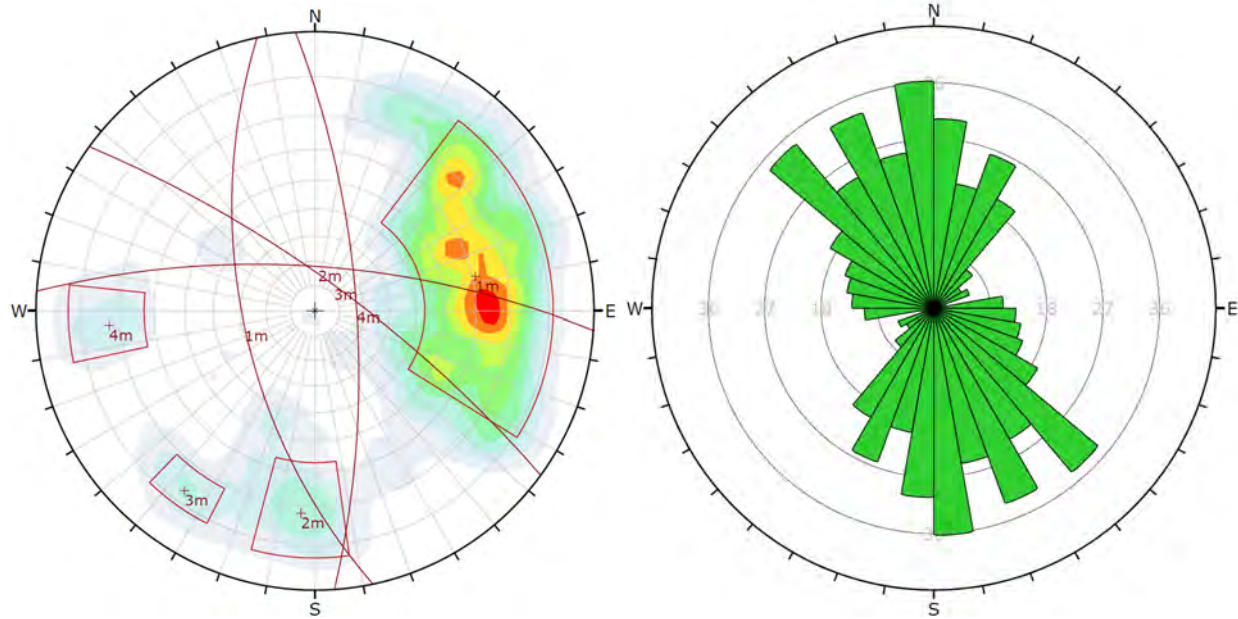


**Figure 3-26. Stereonet (left) and Rosette Diagram (right) of the Joints between the Elevations of 560 and 60 ft above MSL ZEV-CH-06-24**

**Table 3-7. Summary of Structure Orientation and Dip in the Investigation Horizon**

Borehole	Joints			
	Joint Set	Dip Direction	Strike	Dip (°)
ZEV-CH-01-23	JS1	242	N28°W	71
		256	N14°W	52
		040	S50°E	75
	JS2	356	N86°E	63
ZEV-CH-02-23	JS1	253	N28°W	60
		044	S46°E	78
		094	S04°W	76
	JS2	321	N51°E	62
		143	N53°E	72
ZEV-CH-03-23	JS1	274	N04°E	58
		237	N33°W	75
	JS2	055	S35°E	77
ZEV-CH-04-24	JS1	244	N26°W	65
	JS2	307	N37°E	50
ZEV-CH-05-24	JS1	278	N08°E	58
		225	N45°W	72
	JS2	041	S49°E	73
ZEV-CH-06-24	JS1	258	N12°W	61
		086	S04°E	73
	JS2	004	S86°E	72
		036	S54°E	77

From Table 3-7, it appears that the primary joint set has two subsets that mainly strike in a northwest-southeast direction. The most common subset is moderately to steeply dipping (40 to 70°) to the southwest. A secondary subset is steeply dipping (70 to 85°) to the northeast. This subset is more prevalent in core hole ZEV-CH-01-24 and is not observed in core hole ZEV-CH-04-24. In core holes ZEV-CH-03-23, ZEV-CH-05-24, and ZEV-CH-06-24 the main cluster of the primary jointing rotates to a more north-south strike direction.

A secondary joint set that strikes in a northeast-southwest direction is observed in all core holes. Similar to the primary joint set, two subsets are observed in the core holes. The first subset is moderately dipping (30 to 60°) to the northwest, while the second subset, mainly visible in ZEV-CH-02-23, is steeply dipping (70 to 80°) to the southeast. Other random steeply dipping joints were measured in all six core holes.

The discontinuity spacing can be classified using the descriptions provided in Table 3-8. The spacing of most of the combined joints in the potential cavern horizon can, therefore, be classed as close to moderate with the majority of the discontinuities spaced between 80 and 400 mm (0.25 and 1.30 ft). A histogram showing the distribution of all joints is provided in Figure 3-27. A similar spacing distribution is evident for primary and secondary joint sets within the potential cavern horizon (Figures 3-28 and 3-29).

The persistence, or length, of the joints cannot be determined from the core drilling. This could be estimated from nearby extensive surface exposures of the quartz monzonite, but Agapito is not aware of any such studies.

**Table 3-8. Discontinuity Spacing Classification (ISRM 2007)**

Description of Discontinuity Spacing	Spacing (mm)
Extremely Close	< 20
Very Close	20 to < 60
Close	60 to < 200
Moderate	200 to < 600
Wide	600 to < 2000
Very Wide	2000 to < 6000
Extremely Wide	> 6000

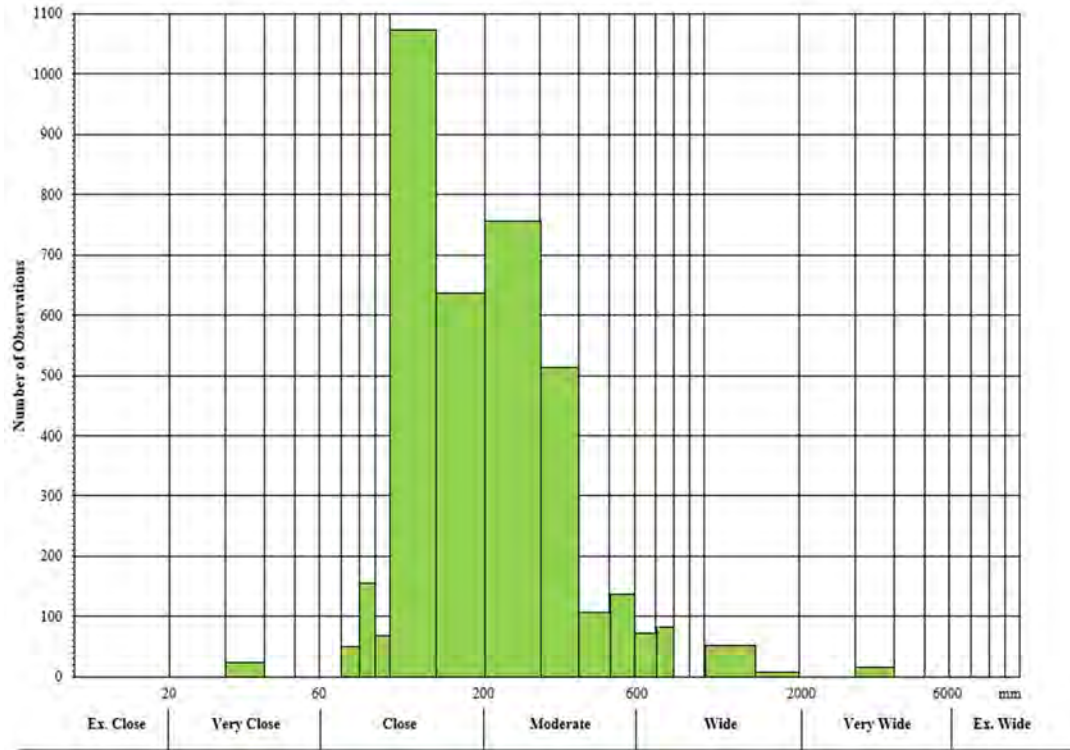


**Figure 3-27. Histogram Showing the Distribution of Discontinuity Spacing for All Joints in the Investigation Horizon**

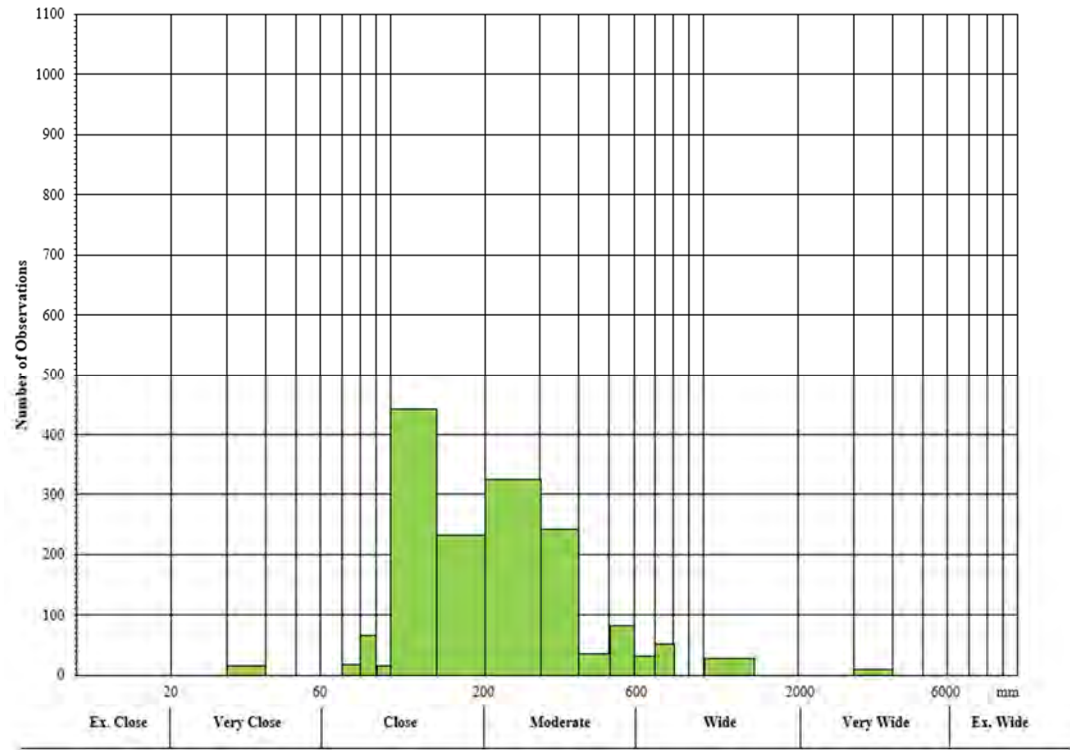


**Figure 3-28. Histogram Showing the Distribution of Discontinuity Spacing for the Primary Joint Set in the Investigation Horizon**

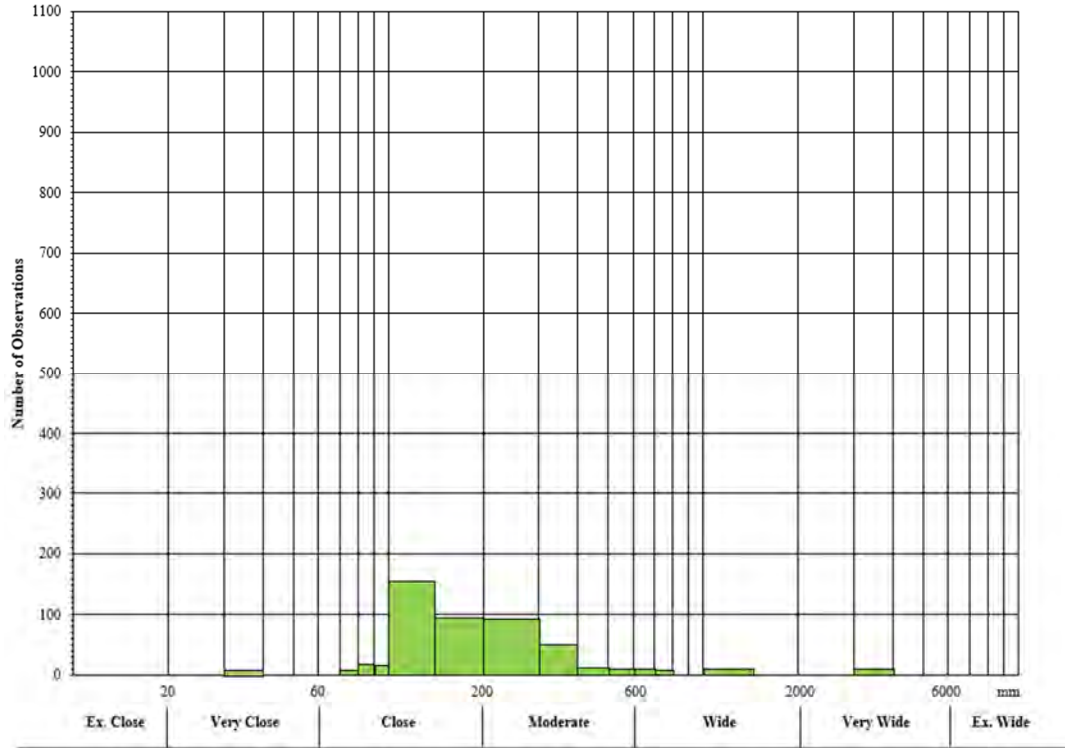


**Figure 3-29. Histogram Showing the Distribution of Discontinuity Spacing for the Secondary Set in the Investigation Horizon**

## 4 GEOTECHNICAL CHARACTERIZATION

### 4.1 Geomechanical Properties of the Intact Rock

Agapito conducted laboratory testing on a large number of core samples collected from the six core holes. The core samples were analysed from each hole beginning at depths of around 1,500 ft. The sampling frequency was increased between the depths of 2,000 and 3,000 ft to account for the investigation of potential cavern horizons. The samples were packaged and shipped to Agapito's laboratory in Grand Junction, Colorado, for testing according to Agapito's recommended testing program. The samples were tested for UCS, splitting tensile strength (Brazilian), triaxial compression strength, slake durability index, axial point load strength index (PLT-A and PLT-D), density, moisture content, Young's modulus (E), and Poisson's ratio ( $\nu$ ). Table 4-1 summarizes all data from the testing program for the various rock types.

**Table 4-1. Summary of Laboratory Rock Mechanics Testing Results from the Exploration Core Holes**

Rock Type	Density (pcf)	UCS (psi)	E ( $\times 10^6$ psi)	$\nu$	Tensile Strength (psi)	Point Load Index		Moisture (%)	Slake Durability Index (%)	Durability
						Axial $I_s$ (50)	Diametral $I_s$ (50)			
Quartz Monzonite (all)	164.5	15,163	7.94	0.28	912	550	372	0.52%	93.0	Medium High
Quartz Monzonite (Fr to Fr-SA)	166.0	16,956	8.94	0.26	983	685	609	0.38%	96.8	High
Quartz Monzonite (SA to SA-MA)	164.0	11,848	6.39	0.30	974	517	471	0.58%	93.9	Medium High
Quartz Monzonite (MA to MA-HA)	159.0	9,603	3.95	0.35	650	315	122	0.96%	80.6	Medium
Quartz Monzonite (HA to HA-CA)	154.0	3,561	1.09	0.28	193	57	117	1.29%	41.7	Low
Pegmatite	155.0	12,953	7.08	0.24	121	173	385	0.41%	94.8	Medium High

#### 4.1.1 Unit Weight

The density of the quartz monzonite was determined from laboratory testing on a total of 413 samples. The density ranged from 138.0 pounds per cubic foot (pcf) to 174.6 pcf with a mean of 164.5 pcf. The degree of alteration does not affect the density unless the samples are moderately to highly altered, where the average density is 159.0 pcf or unless the samples are highly to completely altered, where the average density is 154.0 pcf.

#### 4.1.2 Uniaxial Compressive Strength

UCS tests were performed on rock core samples and the individual test results are summarized in Appendix C. Samples were prepared from as-shipped core. Failures were denoted as being "structural" where failure occurred along obvious pre-existing planes of weakness (i.e., joints). These results, where the structure failure was obvious in the testing photos, were omitted from the analysis.

A correlation factor can be used to convert the axial point load strength to UCS for rock. A graphical comparison of the UCS and corrected axial point load strength for each core hole indicates a correlation factor of 26 is appropriate (Figures 4-1 to 4-6). As shown in the figures, most of the intact rock located below the elevation of 550 ft above MSL can be classed as medium to high strength (ISRM 2007). A noted reduction in strength is recorded in the slightly to moderately altered rock, where intact strength is typically classed as moderate to medium. The low to moderate intact rock strength recorded in the core is indicative of areas that have undergone high to complete alteration.

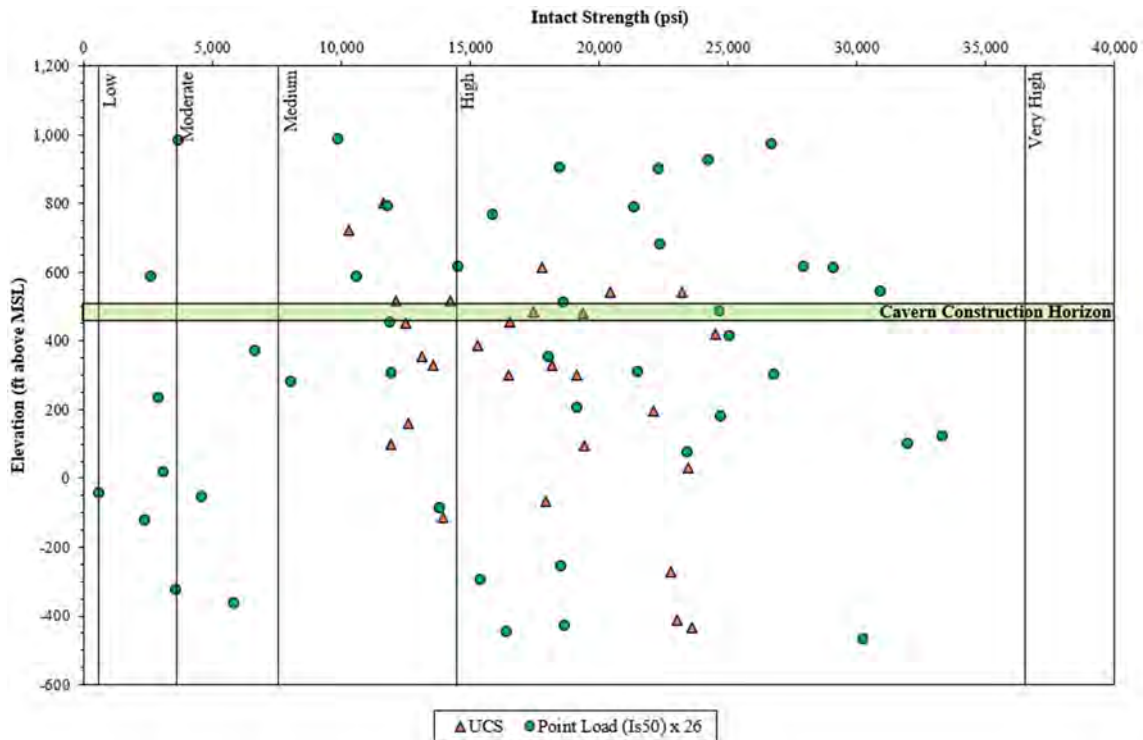


Figure 4-1. Intact Rock Strength Recorded in Core Hole ZEV-CH-01-23

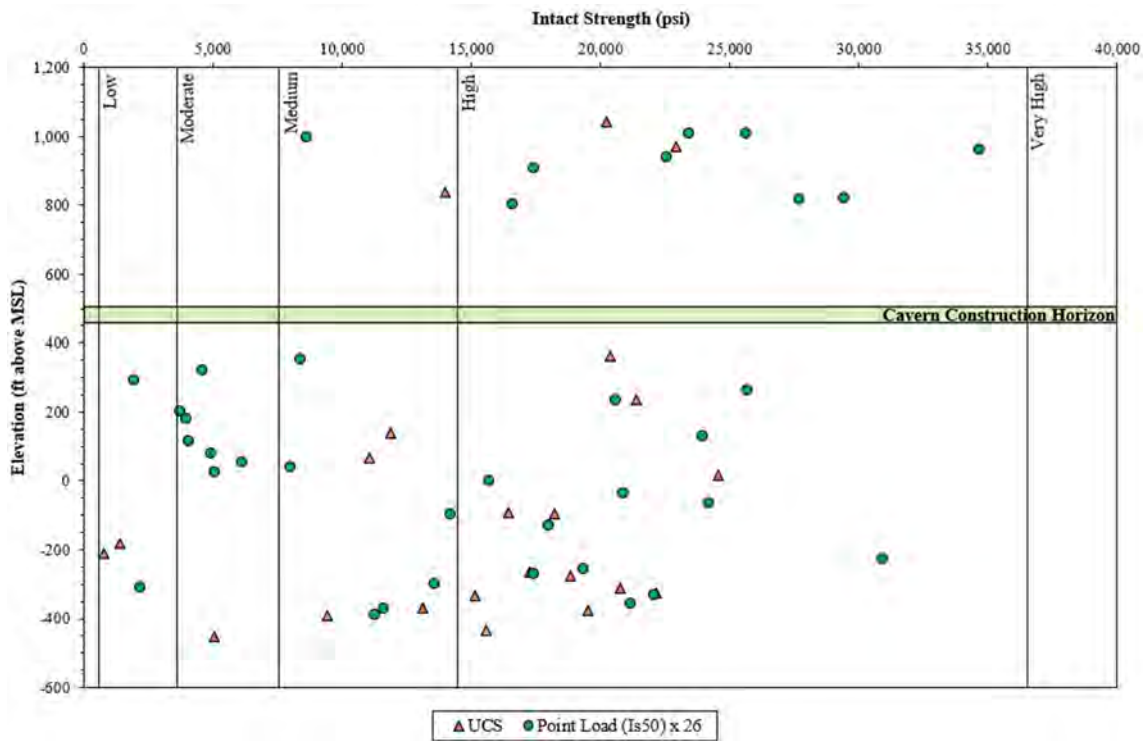


Figure 4-2. Intact Rock Strength Recorded in Core Hole ZEV-CH-02-23

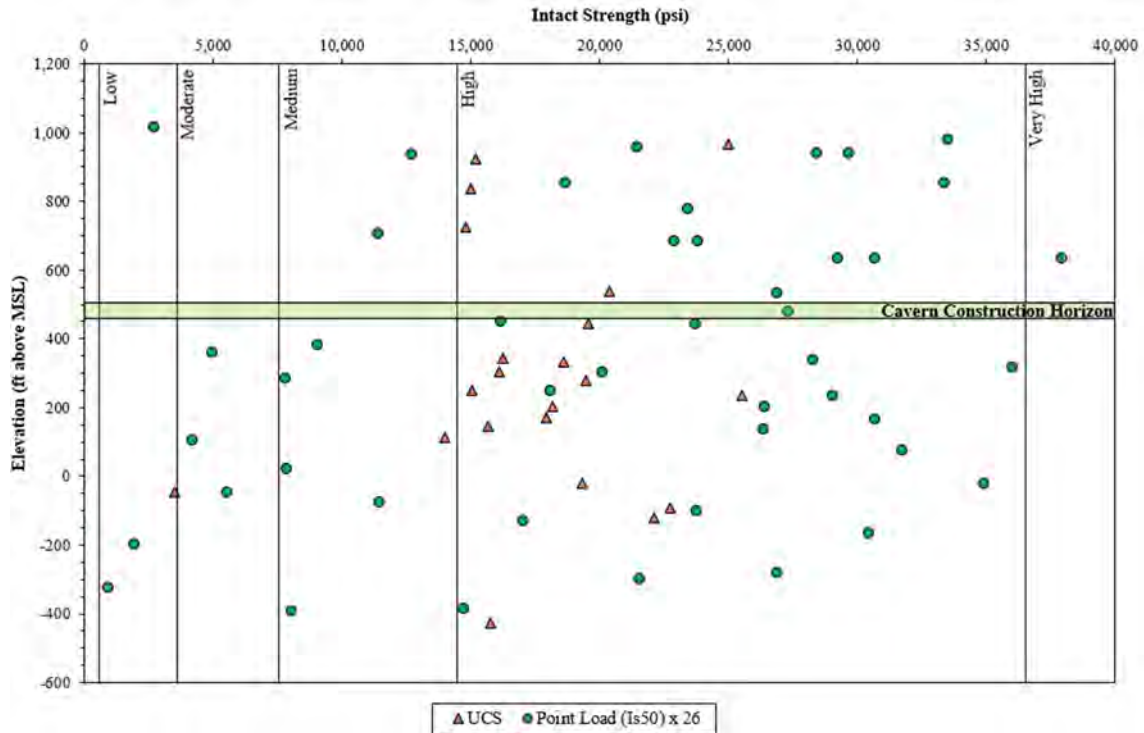


Figure 4-3. Intact Rock Strength Recorded in Core Hole ZEV-CH-03-23

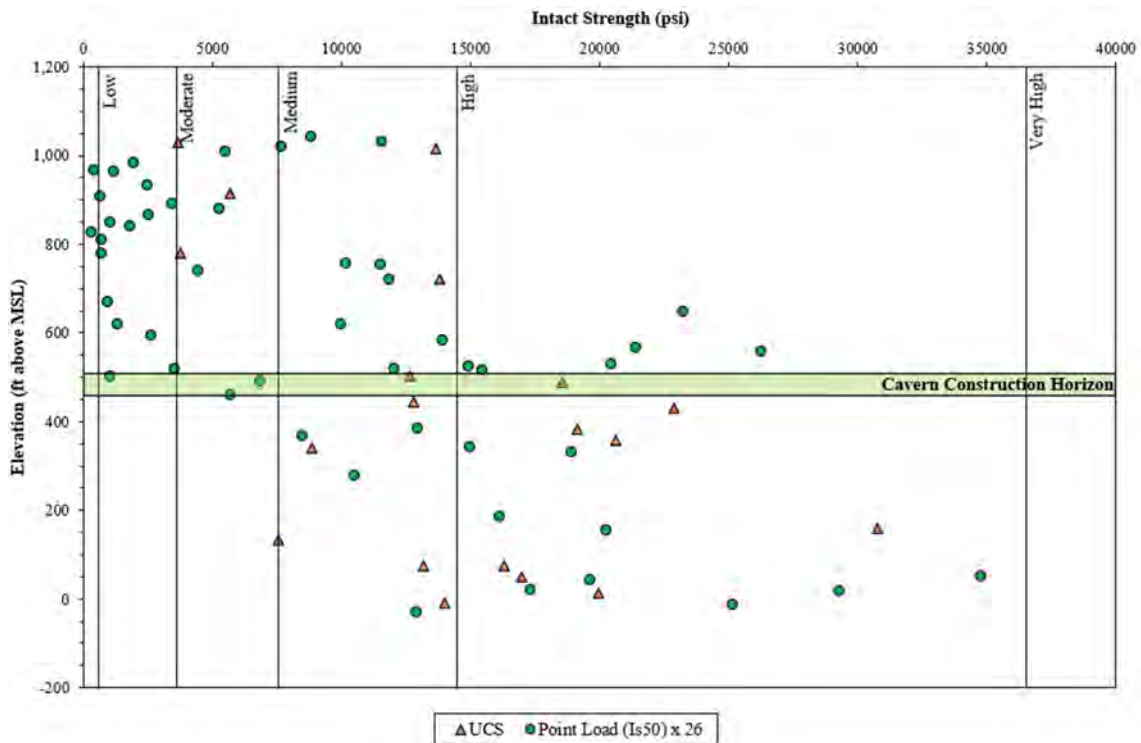


Figure 4-4. Intact Rock Strength Recorded in Core Hole ZEV-CH-04-24

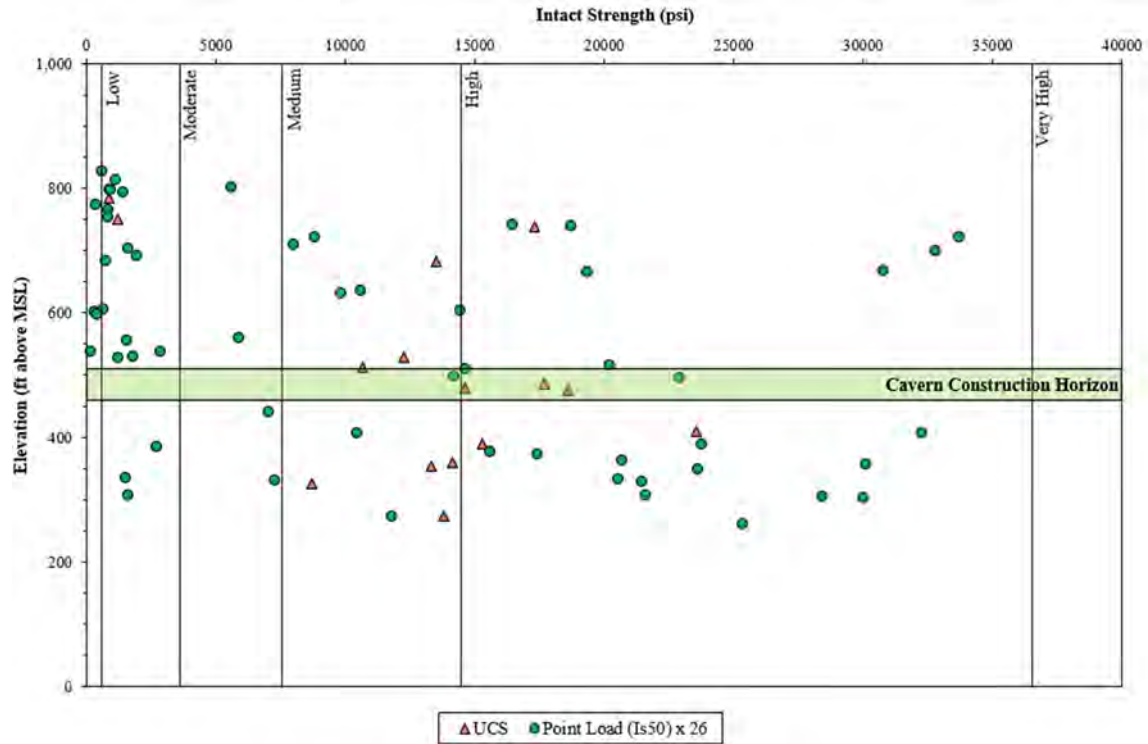


Figure 4-5. Intact Rock Strength Recorded in Core Hole ZEV-CH-05-24

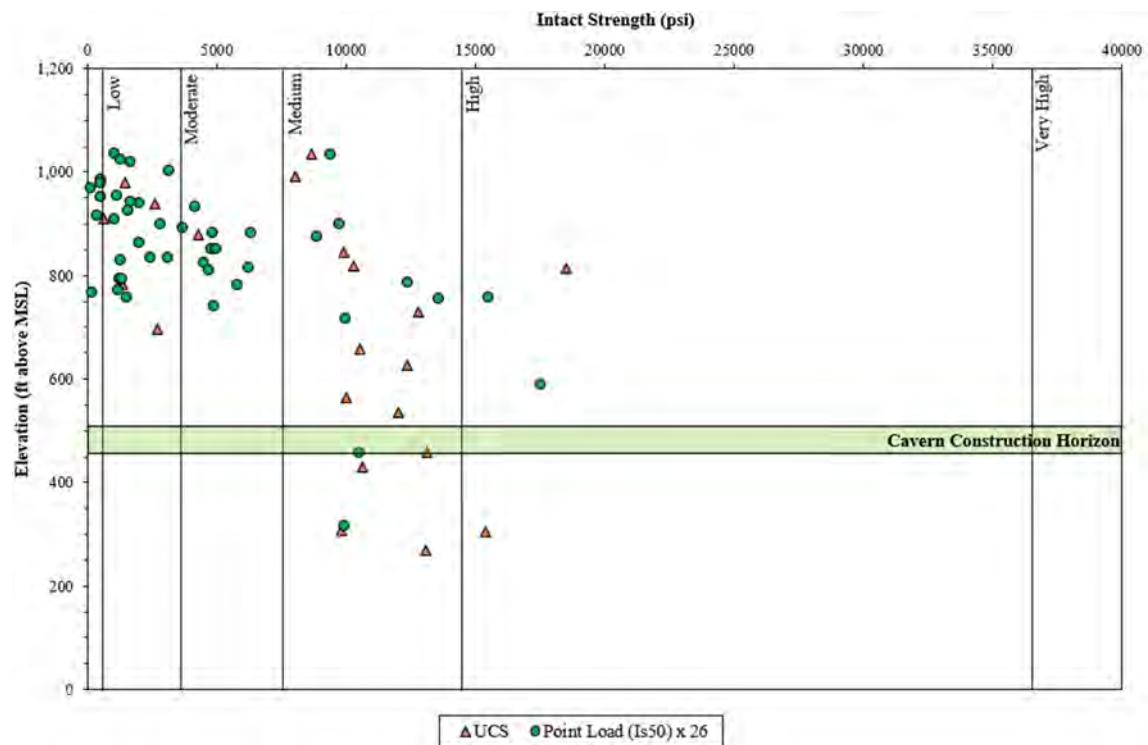


Figure 4-6. Intact Rock Strength Recorded in Core Hole ZEV-CH-06-24



### 4.1.3 Triaxial Compressive Strength

A summary of the Mohr-Coulomb failure criteria derived from the triaxial data from the successful tests performed, with confining pressures ranging from 1,500 to 2,500 psi, is shown in Table 4-2.

**Table 4-2. Summary of Triaxial Test Results from the Exploration Core Holes**

Rock Type	$\phi$ (degrees)	$c$ (psi)
Quartz Monzonite (all)	36.0	7,065
Quartz Monzonite (Fr-SA)	36.0	7,066
Quartz Monzonite (MA-HA)	36.3	4,638

### 4.1.4 Elastic Properties

Laboratory testing for uniaxial compressive strength rock samples produced plots of stress versus strain up to a peak strength level in the unconfined state. The average slope of these lines at 50% strength level was used to derive the intact Young's modulus. The individual test results for both Young's modulus and Poisson's ratio are summarized in Appendix C. As shown in Table 4-1, stiffness generally decreases with the degree of alteration in the quartz monzonite.

### 4.1.5 Slake Durability

The slake durability test is used to estimate qualitatively the durability of weak rocks through weakening and disintegration resulting from cycles of wetting and drying. This is an important test to help understand the rock behavior in the A-CAES cavern when subjected to repeated cycles of water infiltration and hot compressed air. Both two- and four-cycle tests were performed on the samples. Most of the rock anticipated in the cavern horizon can be classed as medium high to very high durability (Figures 4-7 to 4-12). The quartz monzonite that has been logged as moderately to highly altered typically exhibits medium durability. Low and Medium durability is indicative of specimens that contain exclusively small, and large and small fragments respectively after two cycles of wetting and drying (ASTM D4644-08). This means that some of the retained specimen has broken down into smaller fragments.

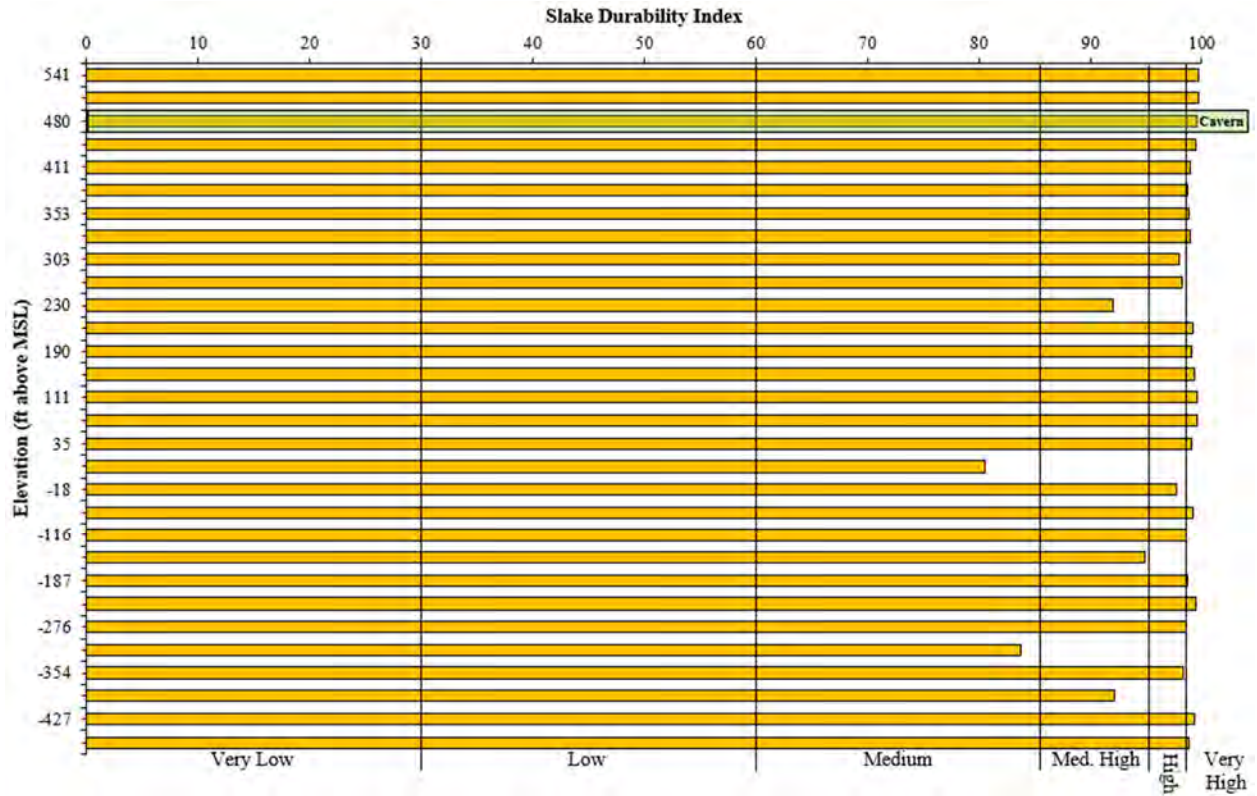


**Figure 4-7. Slake Durability Index Recorded in Core Hole ZEV-CH-01-23**

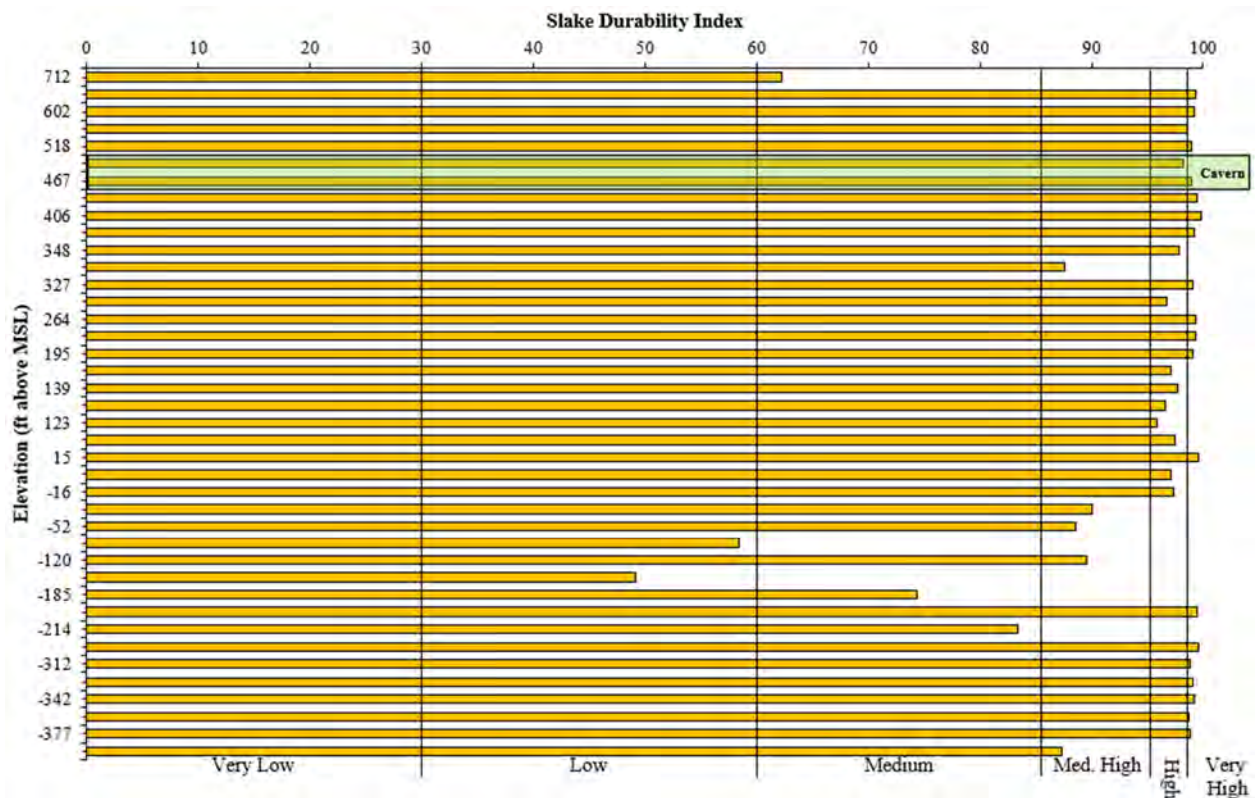


**Figure 4-8. Slake Durability Index Recorded in Core Hole ZEV-CH-02-23**

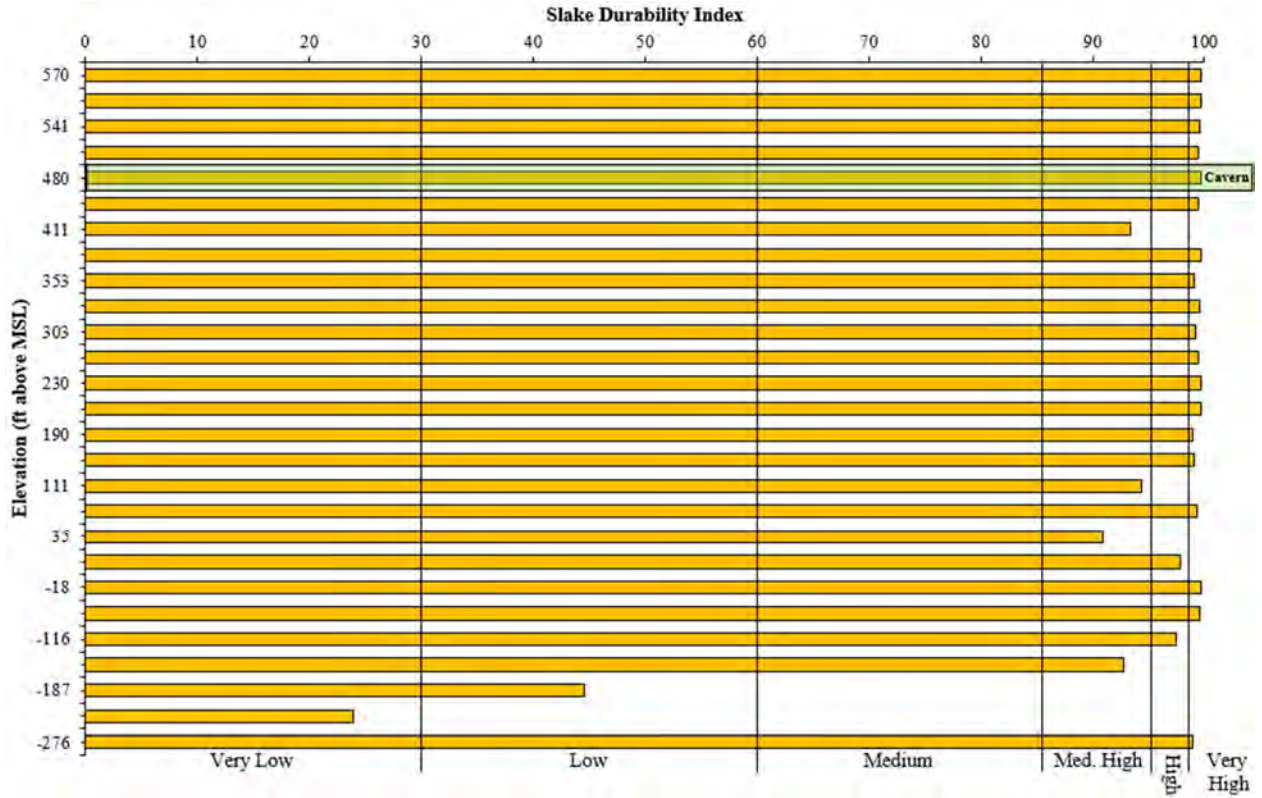


**Figure 4-9. Slake Durability Index Recorded in Core Hole ZEV-CH-03-23**

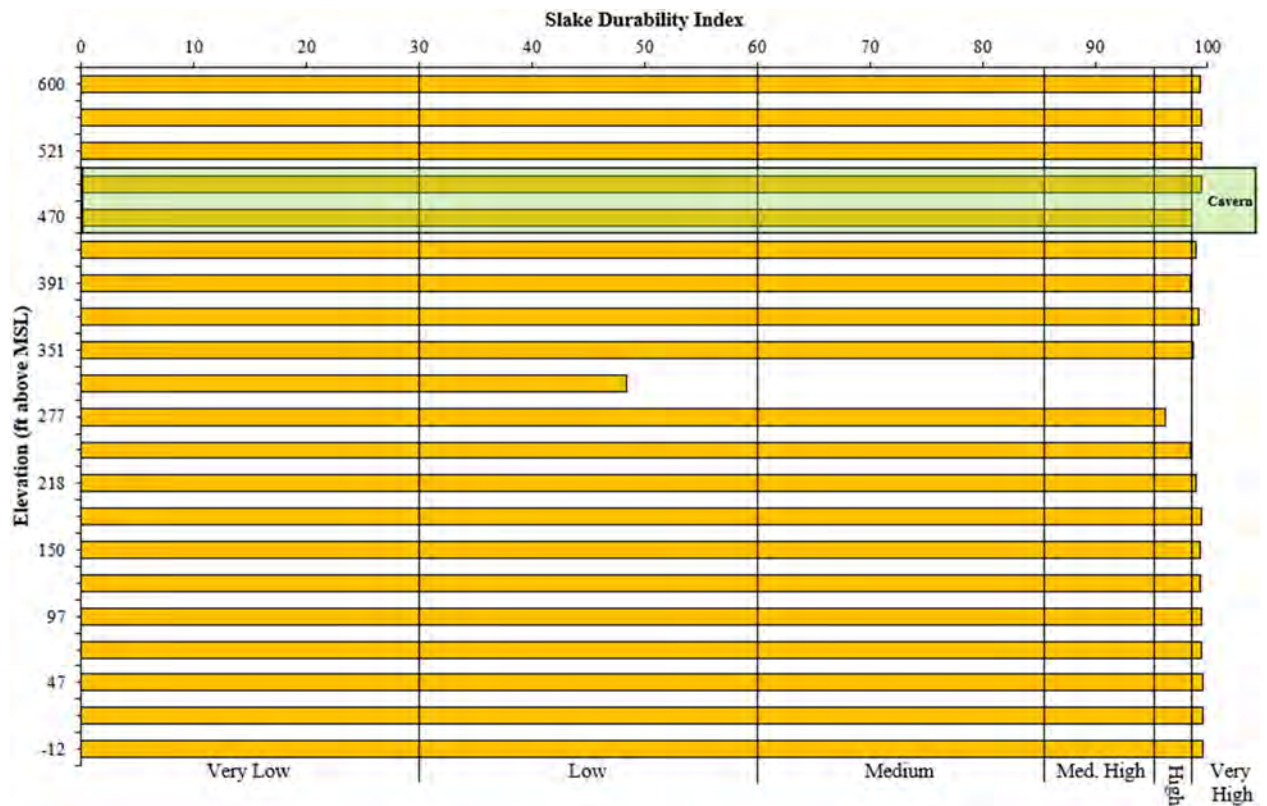


**Figure 4-10. Slake Durability Index Recorded in Core Hole ZEV-CH-04-24**

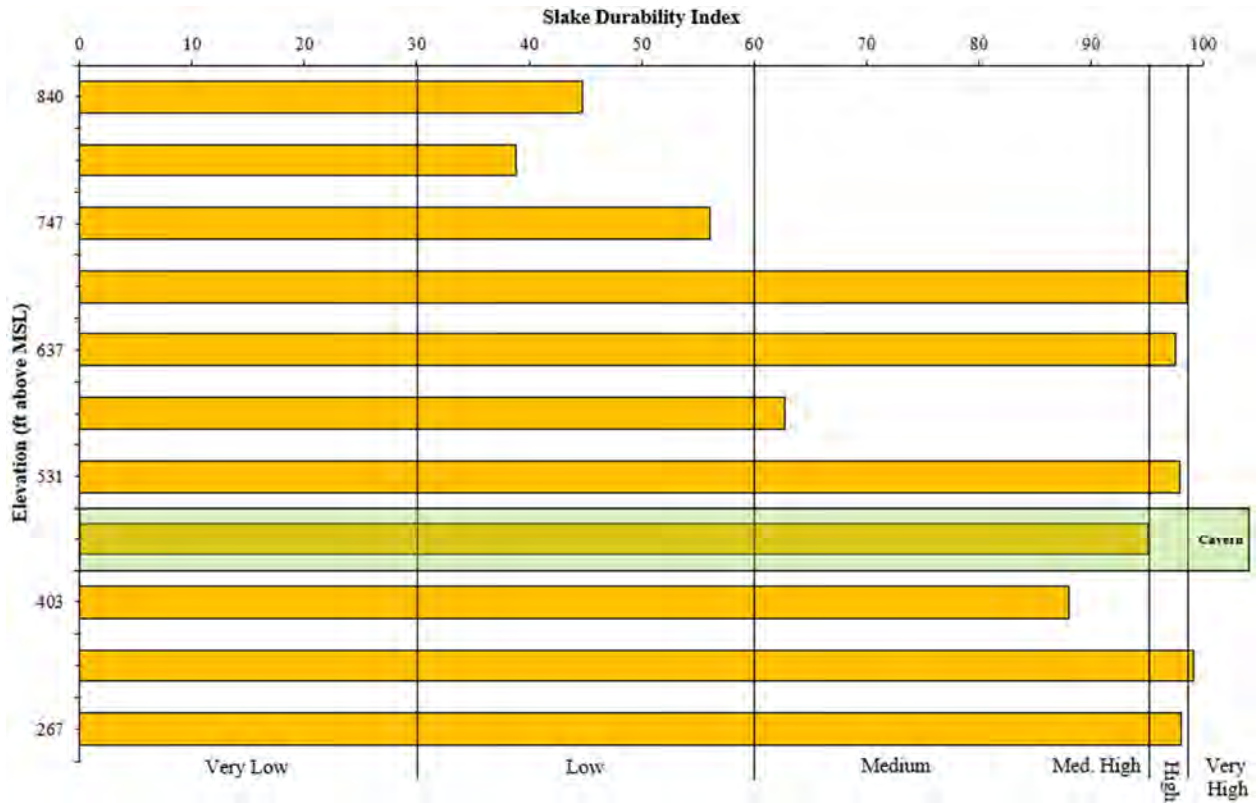


**Figure 4-11. Slake Durability Index Recorded in Core Hole ZEV-CH-05-24**



**Figure 4-12. Slake Durability Index Recorded in Core Hole ZEV-CH-06-24**

#### *4.1.6 Petrographic Analysis*

Petrographic analysis was conducted on the rock collected from core holes ZEV-CH-05-24 and ZEV-CH-06-24 at the intervals shown in Table 4-3. The analysis consisted of reflected polarized light microscopy and transmitted polarized light microscopy. The results indicate that most of the samples are a coarse-grained quartz monzonite. Two samples near the top of the potential cavern horizon in core hole ZEV-CH-05-24 were identified as coarse-grained granite, which has a higher quartz content than the quartz monzonite rock. Four samples near the top and within the potential cavern horizon in core hole ZEV-CH-06-24 were identified as fine to medium grained monzogranite, which also has a higher quartz content than the quartz monzonite rock. Alteration and microfractures were observed in a number of the samples. These rock type definitions correlate well with the rock types identified by Carboniferous Energy Consultants' logging. The samples are high in plagioclase, potassium feldspar, and quartz. Lesser amounts of biotite, zeolite, clay, chlorite, calcite, magnetite, sphene, hornblende, and amphibole are also observed in some samples. The zeolite, clay and chlorite mineral assemblages correlate with altered rock samples.

#### *4.1.7 CERCHAR Abrasivity*

Abrasivity tests were conducted by Advanced Terra Testing. Fourteen samples were tested in core hole ZEV-CH-05-24, and sixteen samples were tested in core hole ZEV-CH-06-24. Sample details and results are presented in Table 4-4. The test results indicate a CERCHAR Abrasivity Index (CAI) of between 2.64 and 5.10, which, depending on the classification system, suggests very abrasive to extremely abrasive rock.

**Table 4-3. Summary of Petrographic Analysis from Core Holes ZEV-CH-05-24 and ZEV-CH-06-24**

Depth From (ft)	Depth To (ft)	Elevation From (ft)	Elevation To (ft)	Rock Type	Plagioclase	K-Feldspar	Quartz	Biotite	Zeolite	Clay	Chlorite	Calcite	Magnetite	Sphene	Hornblende
					Percent (%)	Percent (%)	Percent (%)	Percent (%)	Percent (%)	Percent (%)	Percent (%)	Percent (%)	Percent (%)	Percent (%)	Percent (%)
<b>Core Hole: ZEV-CH-05-24</b>															
166.10	166.60	2,375.00	2,374.50	Quartz Monzonite	46%	31%	17%	4%	0%	0%	0%	2%	0%	0%	0%
236.00	237.00	2,305.10	2,304.10	Quartz Monzonite	37%	29%	20%	2%	0%	8%	2%	2%	0%	0%	0%
351.30	352.30	2,189.80	2,188.80	Quartz Monzonite	40%	35%	17%	3%	0%	0%	0%	5%	0%	0%	0%
458.80	459.60	2,082.30	2,081.50	Quartz Monzonite	41%	39%	17%	3%	0%	0%	0%	0%	0%	0%	0%
585.00	586.00	1,956.10	1,955.10	Quartz Monzonite	39%	33%	20%	6%	0%	0%	0%	0%	1%	1%	0%
679.10	680.00	1,862.00	1,861.10	Quartz Monzonite	45%	35%	15%	5%	0%	0%	0%	0%	0%	0%	0%
713.10	714.00	1,828.00	1,827.10	Quartz Monzonite	46%	30%	20%	4%	0%	0%	0%	0%	0%	0%	0%
856.20	857.00	1,684.90	1,684.10	Quartz Monzonite	48%	40%	10%	2%	0%	0%	0%	0%	0%	0%	0%
961.30	962.40	1,579.80	1,578.70	Quartz Monzonite	45%	30%	20%	5%	0%	0%	0%	0%	0%	0%	0%
1,088.60	1,089.60	1,452.50	1,451.50	Quartz Monzonite	44%	35%	15%	5%	0%	0%	0%	0%	1%	0%	0%
1,126.80	1,127.60	1,414.30	1,413.50	Quartz Monzonite	43%	35%	18%	4%	0%	0%	0%	0%	0%	0%	0%
1,242.20	1,244.00	1,298.90	1,297.10	Quartz Monzonite	48%	31%	15%	5%	0%	0%	0%	0%	1%	0%	0%
1,396.50	1,397.40	1,144.60	1,143.70	Quartz Monzonite	40%	30%	15%	5%	2%	8%	0%	0%	0%	0%	0%
1,450.20	1,451.50	1,090.90	1,089.60	Quartz Monzonite	34%	20%	15%	0%	15%	10%	3%	3%	0%	0%	0%
1,517.70	1,518.70	1,023.40	1,022.40	Quartz Monzonite	30%	25%	18%	0%	15%	6%	6%	0%	0%	0%	0%
1,671.10	1,672.20	870.00	868.90	Quartz Monzonite	32%	22%	10%	0%	15%	15%	6%	0%	0%	0%	0%
1,763.00	1,764.00	778.10	777.10	Quartz Monzonite	44%	34%	10%	2%	0%	8%	2%	0%	0%	0%	0%
1,791.50	1,792.40	749.60	748.70	Quartz Monzonite	35%	25%	12%	0%	15%	8%	5%	0%	0%	0%	0%
1,802.00	1,804.00	739.10	737.10	Quartz Monzonite	35%	25%	25%	0%	12%	2%	1%	0%	0%	0%	0%
1,846.50	1,847.70	694.60	693.40	Quartz Monzonite	45%	35%	13%	4%	2%	0%	0%	0%	1%	0%	0%
1,917.50	1,918.00	623.60	623.10	Granite	37%	33%	29%	1%	0%	0%	0%	0%	0%	0%	0%
1,980.50	1,981.80	560.60	559.30	Quartz Monzonite	48%	35%	11%	5%	0%	0%	0%	0%	1%	0%	0%
2,050.00	2,050.80	491.10	490.30	Granite	37%	35%	27%	1%	0%	0%	0%	0%	0%	0%	0%
2,104.00	2,105.00	437.10	436.10	Quartz Monzonite	49%	37%	8%	5%	0%	0%	0%	0%	1%	0%	0%
2,211.40	2,212.90	329.70	328.20	Quartz Monzonite	44%	37%	13%	4%	0%	0%	1%	0%	0%	0%	1%

**Table 4-3. Summary of Petrographic Analysis from Core Holes ZEV-CH-05-24 and ZEV-CH-06-24 (continued)**

Depth From (ft)	Depth To (ft)	Elevation From (ft)	Elevation To (ft)	Rock Type	Plagioclase	K-Feldspar	Quartz	Biotite	Zeolite	Clay	Chlorite	Calcite	Magnetite	Amphibole	
					Percent (%)	Percent (%)	Percent (%)	Percent (%)	Percent (%)	Percent (%)	Percent (%)	Percent (%)	Percent (%)	Percent (%)	
<b>Core Hole: ZEV-CH-06-24</b>															
58.90	59.70	2,489.90	2,489.10	Quartz Monzonite	43%	36%	15%	4%	0%	1%	0%	1%	0%	0%	
124.70	125.50	2,424.10	2,423.30	Quartz Monzonite	47%	36%	12%	4%	0%	1%	0%	0%	0%	0%	
258.00	258.90	2,290.80	2,289.90	Quartz Monzonite	46%	32%	15%	4%	0%	3%	0%	0%	0%	0%	
336.45	337.25	2,212.35	2,211.55	Quartz Monzonite	46%	35%	14%	2%	2%	1%	0%	0%	0%	0%	
472.75	473.45	2,076.05	2,075.35	Quartz Monzonite	44%	30%	17%	4%	2%	5%	0%	0%	0%	0%	
559.30	560.15	1,989.50	1,988.65	Quartz Monzonite	38%	29%	14%	2%	5%	0%	0%	12%	0%	0%	
654.90	655.10	1,893.90	1,893.70	Quartz Monzonite	38%	31%	17%	4%	10%	0%	0%	0%	0%	0%	
746.35	746.75	1,802.45	1,802.05	Quartz Monzonite	46%	35%	14%	4%	1%	0%	0%	0%	0%	0%	
854.85	855.85	1,693.95	1,692.95	Quartz Monzonite	43%	35%	15%	3%	2%	1%	0%	1%	0%	0%	
952.20	952.60	1,596.60	1,596.20	Quartz Monzonite	42%	30%	20%	4%	4%	0%	0%	0%	0%	0%	
1,079.30	1,080.40	1,469.50	1,468.40	Quartz Monzonite	45%	30%	20%	4%	0%	0%	0%	0%	1%	0%	
1,123.10	1,124.25	1,425.70	1,424.55	Quartz Monzonite	46%	30%	20%	3%	0%	0%	0%	0%	1%	0%	
1,262.10	1,262.70	1,286.70	1,286.10	Quartz Monzonite	40%	30%	13%	2%	15%	0%	0%	0%	0%	0%	
1,356.60	1,357.15	1,192.20	1,191.65	Quartz Monzonite	46%	37%	15%	2%	0%	0%	0%	0%	0%	0%	
1,441.80	1,442.75	1,107.00	1,106.05	Quartz Monzonite	47%	37%	14%	2%	0%	0%	0%	0%	0%	0%	
1,553.40	1,553.90	995.40	994.90	Quartz Monzonite	39%	30%	13%	3%	12%	3%	0%	0%	0%	0%	
1,642.90	1,643.40	905.90	905.40	Quartz Monzonite	40%	30%	12%	3%	14%	1%	0%	0%	0%	0%	
1,754.25	1,755.05	794.55	793.75	Quartz Monzonite	36%	27%	12%	0%	20%	1%	4%	0%	0%	0%	
1,878.10	1,878.55	670.70	670.25	Quartz Monzonite	35%	27%	12%	2%	20%	1%	2%	0%	0%	0%	
1,946.00	1,946.50	602.80	602.30	Quartz Monzonite	47%	33%	15%	3%	0%	0%	0%	0%	1%	1%	
1,978.10	1,979.07	570.70	569.73	Monzogranite	38%	33%	28%	1%	0%	0%	0%	0%	0%	0%	
2,022.91	2,024.38	525.89	524.42	Monzogranite	34%	30%	25%	1%	10%	0%	0%	0%	0%	0%	
2,046.60	2,047.75	502.20	501.05	Quartz Monzonite	46%	36%	15%	3%	0%	0%	0%	0%	0%	0%	
2,068.38	2,068.78	480.42	480.02	Monzogranite	35%	31%	30%	2%	2%	0%	0%	0%	0%	0%	
2,078.80	2,079.18	470.00	469.62	Monzogranite	35%	32%	30%	1%	2%	0%	0%	0%	0%	0%	

**Table 4-4. Summary of CERCHAR Abrasivity Test Results from Core Holes ZEV-CH-05-24 and ZEV-CH-06-24**

Depth From (ft)	Depth To (ft)	Elevation From (ft)	Elevation To (ft)	Lithology	CERCHAR Abrasivity Index (CAI)	Sandvik Mining Test Classification of CAI (2007)	ASTMD7625-22 Classification of CAI (2022)	Moh's Hardness
<b>Core Hole: ZEV-CH-05-24</b>								
232.50	234.20	2,308.60	2,306.90	Quartz Monzonite	2.64	Very Abrasive	High Abrasiveness	3.8
436.50	438.00	2,104.60	2,103.10	Quartz Monzonite	4.26	Highly Abrasive	Extreme Abrasiveness	5.0
623.50	624.50	1,917.60	1,916.60	Quartz Monzonite	3.76	Highly Abrasive	High Abrasiveness	5.2
859.00	859.70	1,682.10	1,681.40	Quartz Monzonite	4.92	Extremely Abrasive	Extreme Abrasiveness	6.1
1,000.20	1,001.10	1,540.90	1,540.00	Quartz Monzonite	3.11	Highly Abrasive	High Abrasiveness	4.1
1,399.00	1,400.00	1,142.10	1,141.10	Quartz Monzonite	3.89	Highly Abrasive	High Abrasiveness	4.9
1,502.40	1,503.30	1,038.70	1,037.80	Quartz Monzonite	3.01	Highly Abrasive	High Abrasiveness	4.8
1,655.20	1,656.40	885.90	884.70	Quartz Monzonite	4.49	Highly Abrasive	Extreme Abrasiveness	6.5
1,802.00	1,804.00	739.10	737.10	Quartz Monzonite	4.64	Extremely Abrasive	Extreme Abrasiveness	5.9
1,997.50	1,998.70	543.60	542.40	Quartz Monzonite	4.63	Extremely Abrasive	Extreme Abrasiveness	6.6
2,031.40	2,033.17	509.70	507.93	Quartz Monzonite	5.04	Extremely Abrasive	Extreme Abrasiveness	7.2
2,050.00	2,050.80	491.10	490.30	Quartz Monzonite	4.75	Extremely Abrasive	Extreme Abrasiveness	6.8
2,100.00	2,101.00	441.10	440.10	Quartz Monzonite	4.35	Highly Abrasive	Extreme Abrasiveness	6.5
2,235.35	2,236.45	305.75	304.65	Quartz Monzonite	4.73	Extremely Abrasive	Extreme Abrasiveness	6.8



**Table 4-4. Summary of CERCHAR Abrasivity Test Results from Core Holes ZEV-CH-05-24 and ZEV-CH-06-24 (continued)**

Depth From (ft)	Depth To (ft)	Elevation From (ft)	Elevation To (ft)	Lithology	CERCHAR Abrasivity Index (CAI)	Sandvik Mining Test Classification of CAI (2007)	ASTMD7625-22 Classification of CAI (2022)	Moh's Hardness
<b>Core Hole: ZEV-CH-06-24</b>								
119.10	119.90	2,429.70	2,428.90	Quartz Monzonite	2.86	Very Abrasive	High Abrasiveness	4.4
367.15	368.75	2,181.65	2,180.05	Quartz Monzonite	4.53	Extremely Abrasive	Extreme Abrasiveness	4.8
499.35	500.65	2,049.45	2,048.15	Quartz Monzonite	4.35	Highly Abrasive	Extreme Abrasiveness	5.9
698.65	699.50	1,850.15	1,849.30	Quartz Monzonite	3.91	Highly Abrasive	High Abrasiveness	4.9
796.15	796.70	1,752.65	1,752.10	Quartz Monzonite	2.88	Very Abrasive	High Abrasiveness	4.4
1,001.50	1,002.15	1,547.30	1,546.65	Quartz Monzonite	4.72	Extremely Abrasive	Extreme Abrasiveness	5.7
1,208.95	1,209.15	1,339.85	1,339.65	Quartz Monzonite	4.17	Highly Abrasive	Extreme Abrasiveness	6.1
1,409.50	1,410.35	1,139.30	1,138.45	Quartz Monzonite	4.73	Extremely Abrasive	Extreme Abrasiveness	6.8
1,555.15	1,555.90	993.65	992.90	Quartz Monzonite	5.10	Extremely Abrasive	Extreme Abrasiveness	3.2
1,622.20	1,622.75	926.60	926.05	Quartz Monzonite	4.70	Extremely Abrasive	Extreme Abrasiveness	5.4
1,805.00	1,805.70	743.80	743.10	Quartz Monzonite	2.96	Very Abrasive	High Abrasiveness	4.2
1,978.10	1,978.71	570.70	570.09	Quartz Monzonite	4.47	Highly Abrasive	Extreme Abrasiveness	5.4
2,007.15	2,007.50	541.65	541.30	Quartz Monzonite	3.54	Highly Abrasive	High Abrasiveness	3.8
2,022.91	2,024.38	525.89	524.42	Quartz Monzonite	4.33	Highly Abrasive	Extreme Abrasiveness	5.8
2,068.38	2,068.78	480.42	480.02	Quartz Monzonite	4.18	Highly Abrasive	Extreme Abrasiveness	4.0
2,076.40	2,076.78	472.40	472.02	Quartz Monzonite	4.37	Highly Abrasive	Extreme Abrasiveness	4.0

## 4.2 Rock Mass Classification

Two rock mass classification systems have been used to evaluate the competency of the rock mass anticipated in the potential cavern horizons. These systems will be used to characterize the condition of the rock mass to assess ground behavior and establish rock mass geomechanical properties for empirical and numerical modeling. These systems include the Rock Mass Rating (RMR), and the Tunneling Quality Index (Q). A summary of the rock mass classification results is presented in the following sections, and the details of the analysis are included in Appendix D.

### 4.2.1 Rock Mass Rating (RMR)

The Rock Mass Rating (RMR) is a geomechanical classification system for rocks (Bieniawski 1976, 1989). The system uses the following six parameters to classify rock mass quality: UCS, the RQD, spacing of discontinuities, condition of discontinuities, groundwater condition, and orientation of discontinuities. The reported RMR values in this assessment do not consider the orientation of discontinuities.

The results of the analysis indicate that the rock mass in the core holes can be classified as “Fair” to “Good” within the potential cavern horizons (Figures 4-13 and 4-18). As a general trend within the cavern horizons, the rock mass quality is higher between the elevations of 580 and 320 ft above MSL. The exception to this trend is in core hole ZEV-CH-03-23, where most of the best quality rock mass is located between the elevations of 360 and 100 ft above MSL (Figure 4-15). The lower RMRs in core holes ZEV-CH-03-23 and ZEV-CH-04-24 can be attributed to increased fracturing of the rock.

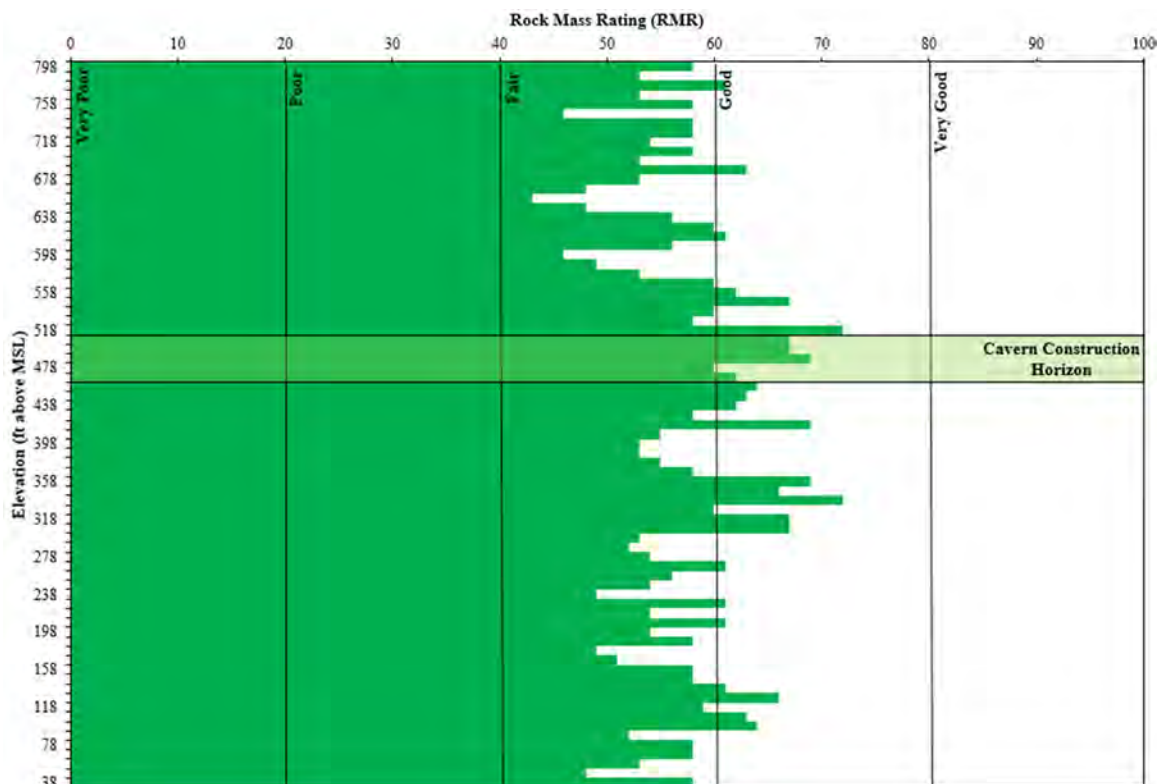


Figure 4-13. Rock Mass Rating for Core Hole ZEV-CH-01-23

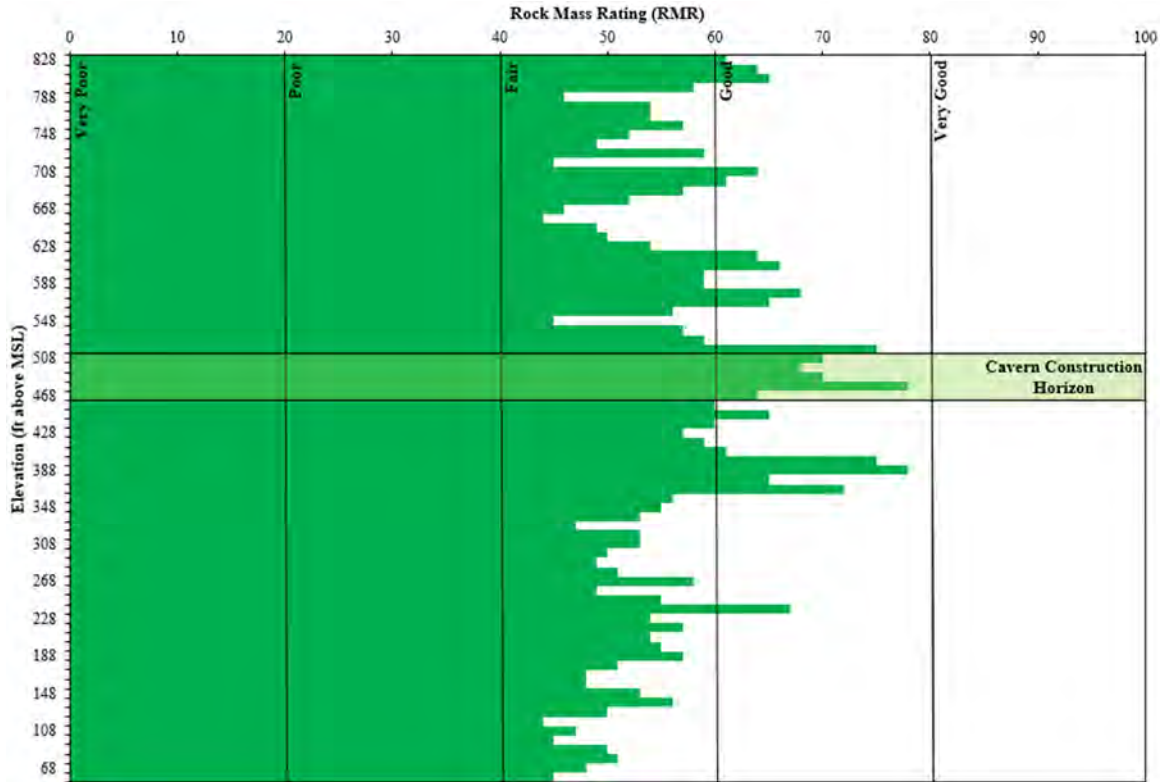


Figure 4-14. Rock Mass Rating for Core Hole ZEV-CH-02-23

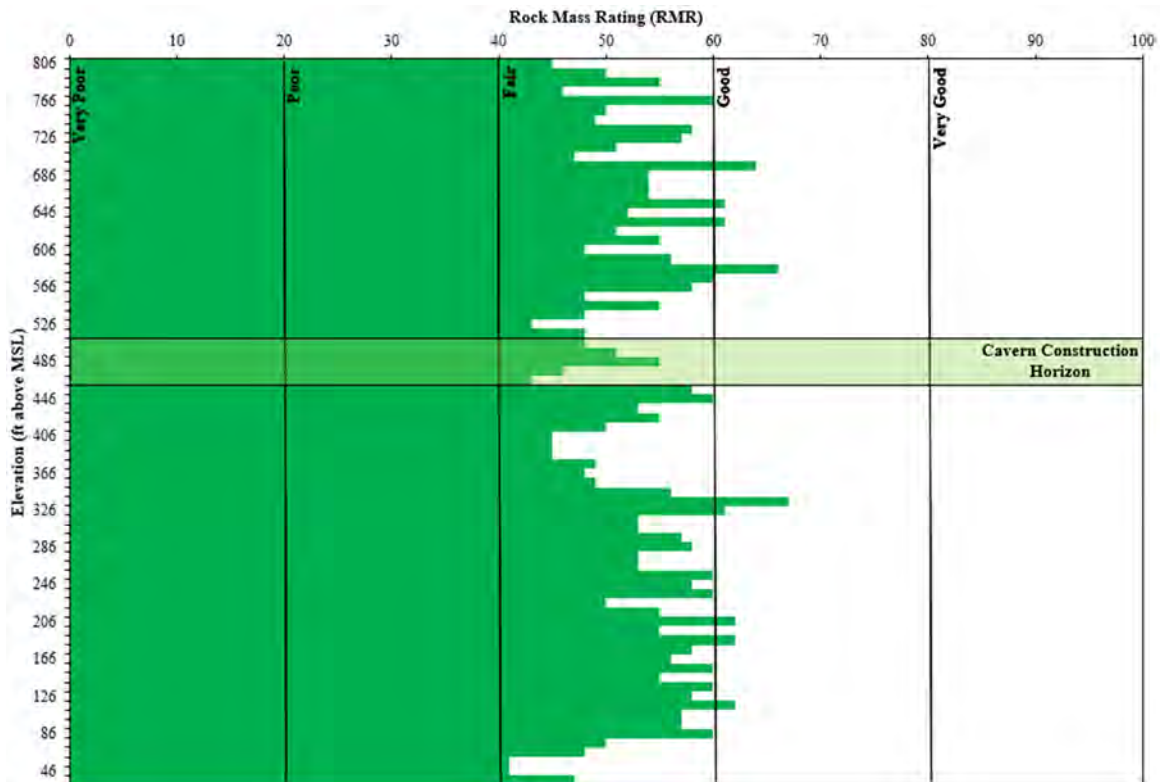


Figure 4-15. Rock Mass Rating for Core Hole ZEV-CH-03-23

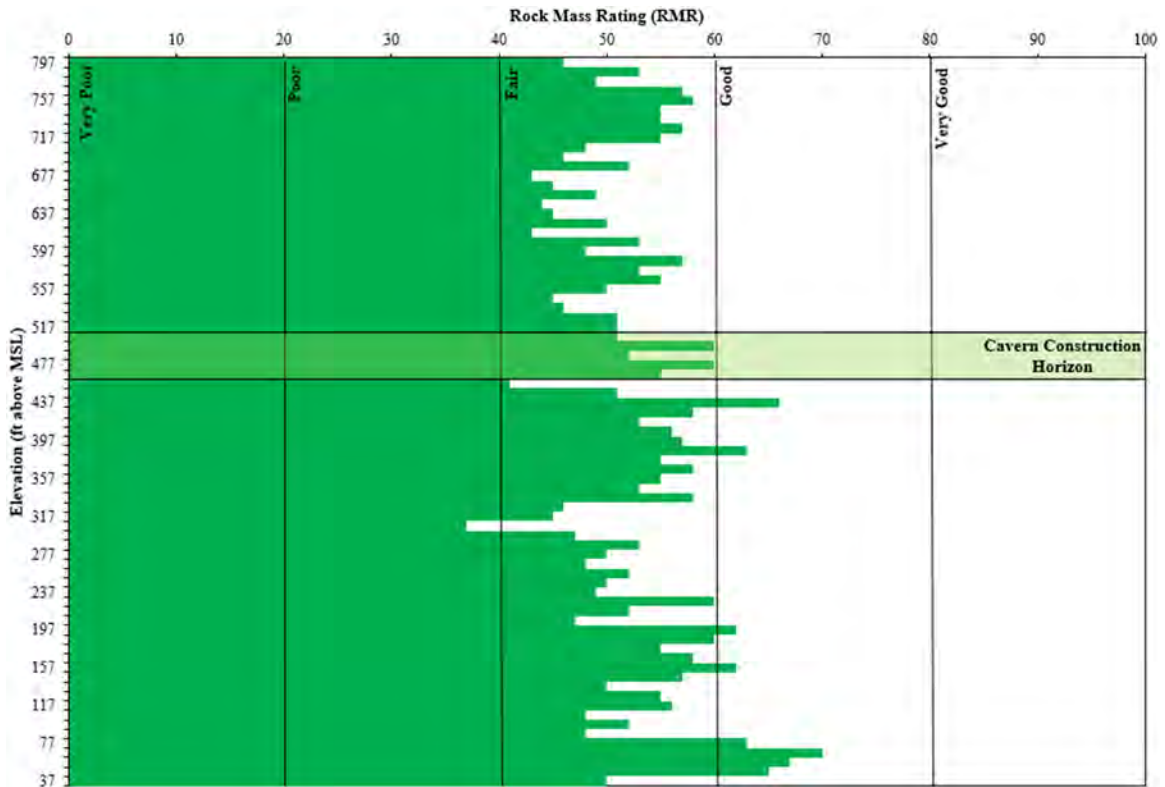


Figure 4-16. Rock Mass Rating for Core Hole ZEV-CH-04-24

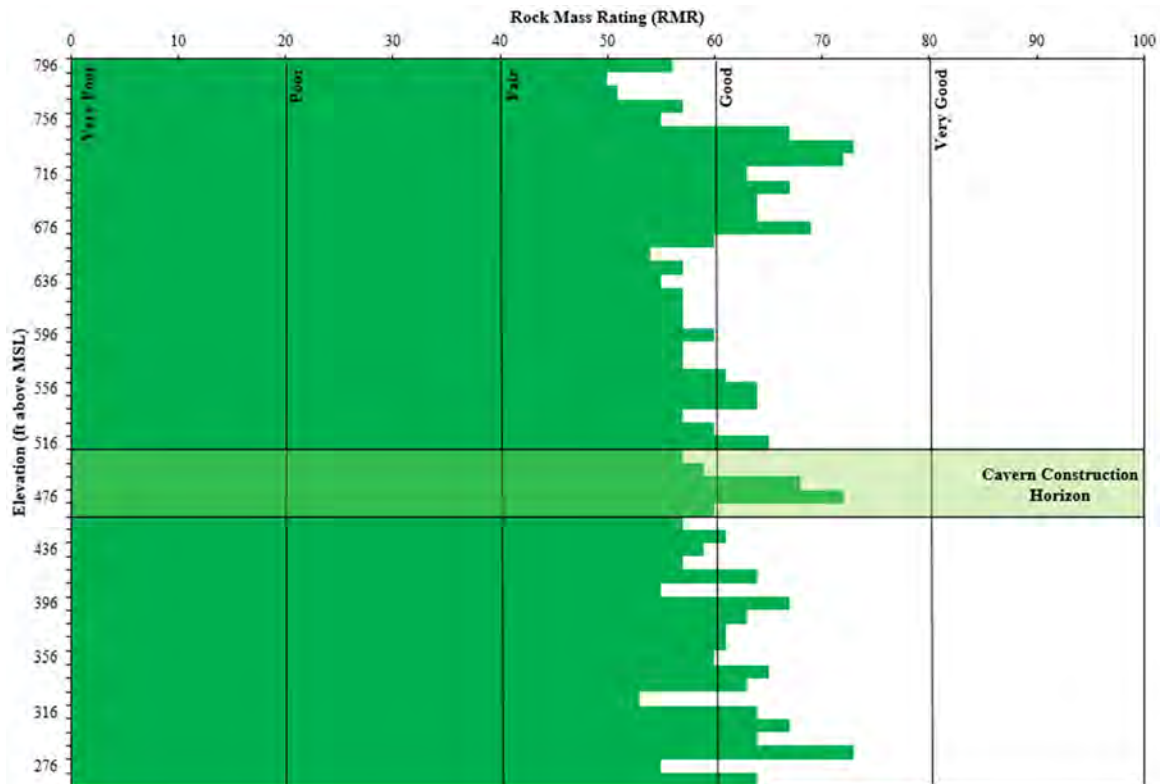
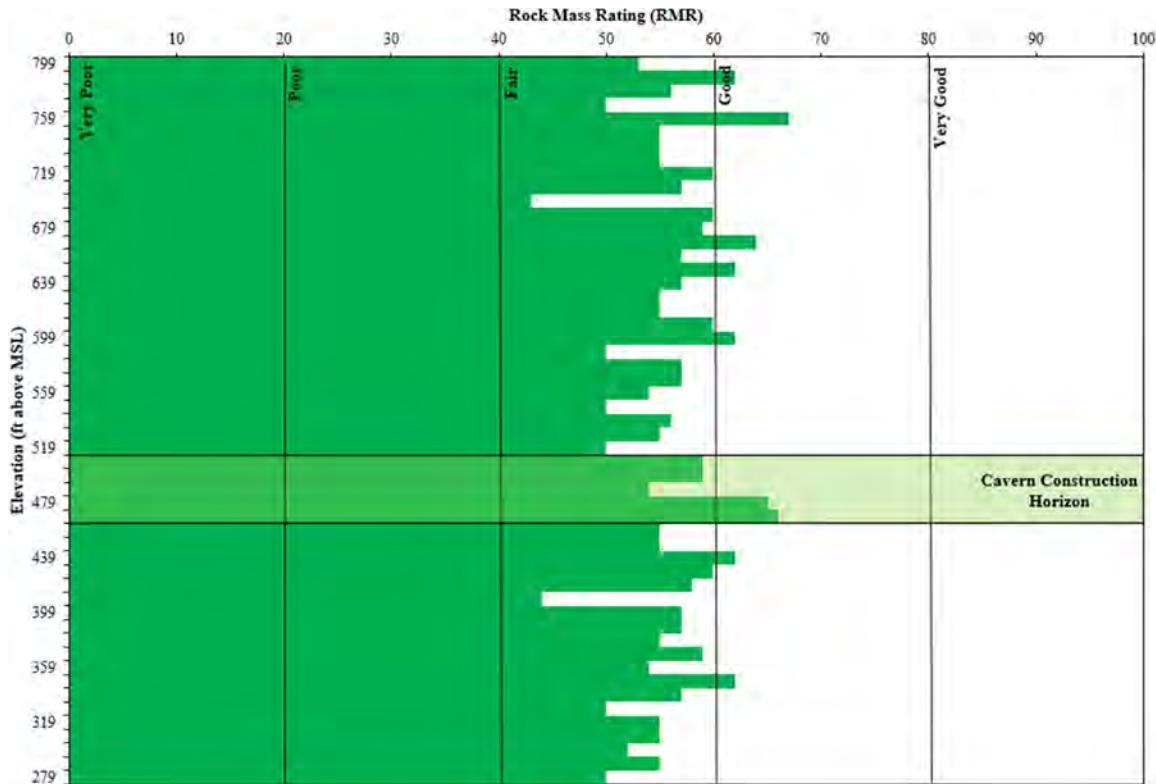


Figure 4-17. Rock Mass Rating for Core Hole ZEV-CH-05-24



**Figure 4-18. Rock Mass Rating for Core Hole ZEV-CH-06-24**

4.2.2 *NGI Q-system*

The Norwegian Geotechnical Institute’s Q-system is an empirical rock mass classification system developed by Barton et al. (1974), which is used to facilitate the selection of ground support. The Q-system is based on a numerical evaluation of rock mass properties similar to RMR, except the system does not account directly for the strength of the intact rock. The system assigns a degree of rock quality based on six key parameters, specifically: the RQD, the number of joint sets, the roughness of the most unfavorable joint or discontinuity, the degree of joint alteration or infilling, water inflow, and the in situ stress environment.

The parameters are grouped into three quotients to give the rock mass quality using the following equation:

$$Q = \frac{RQD}{J_n} \times \frac{J_r}{J_a} \times \frac{J_w}{SRF} \tag{Eqn. 4-1}$$

In the core holes, most of the rock mass within the potential cavern horizons is classed as “Very Poor” to “Fair” with isolated zones of “Good” rock mass (Figures 4-19 and 4-24). In core holes ZEV-CH-01-23, ZEV-CH-02-23, ZEV-CH-05-24, and ZEV-CH-06-24 the highest quality rock mass is generally located between the elevations of 650 and 320 ft above MSL, where the Q values range between 0.3 and 33 (Figures 4-19, 4-20, 4-23, and 4-24). Similar to the RMR rating system, the lower zones of rock mass quality in the core holes are related to the increased fracturing of the rock.

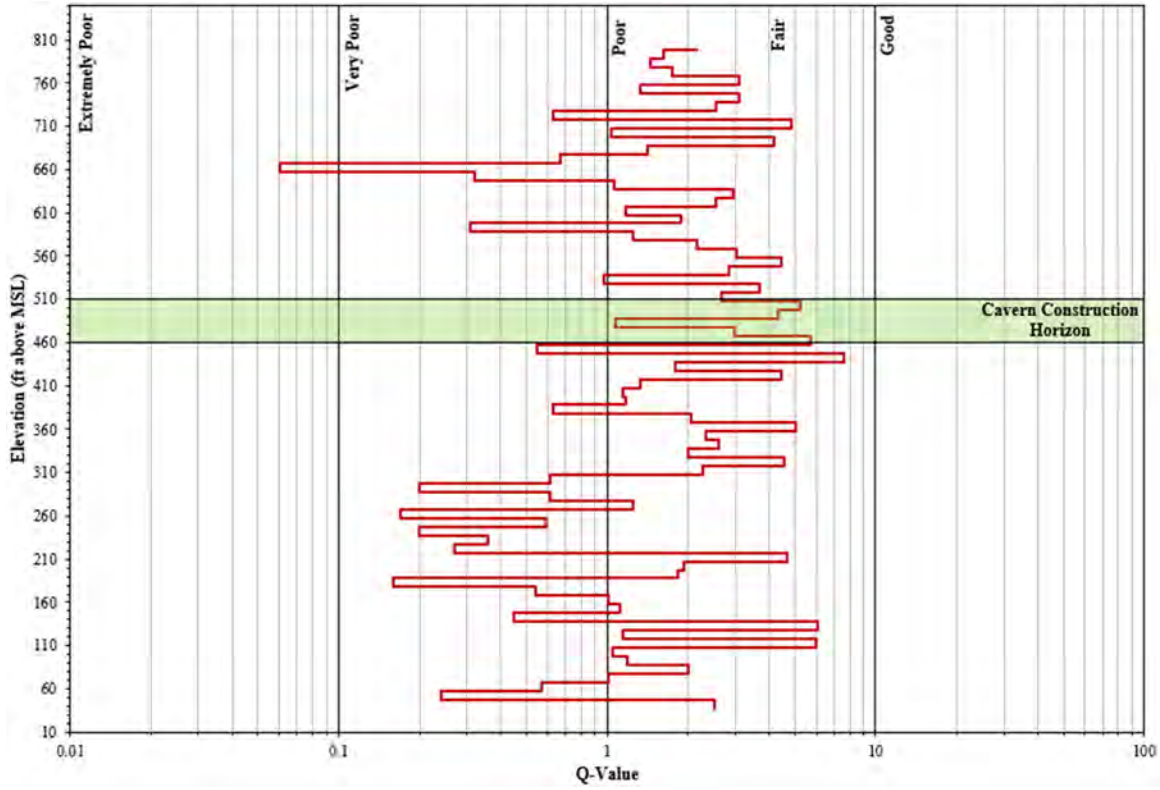


Figure 4-19. Q Ratings for Core Hole ZEV-CH-01-23

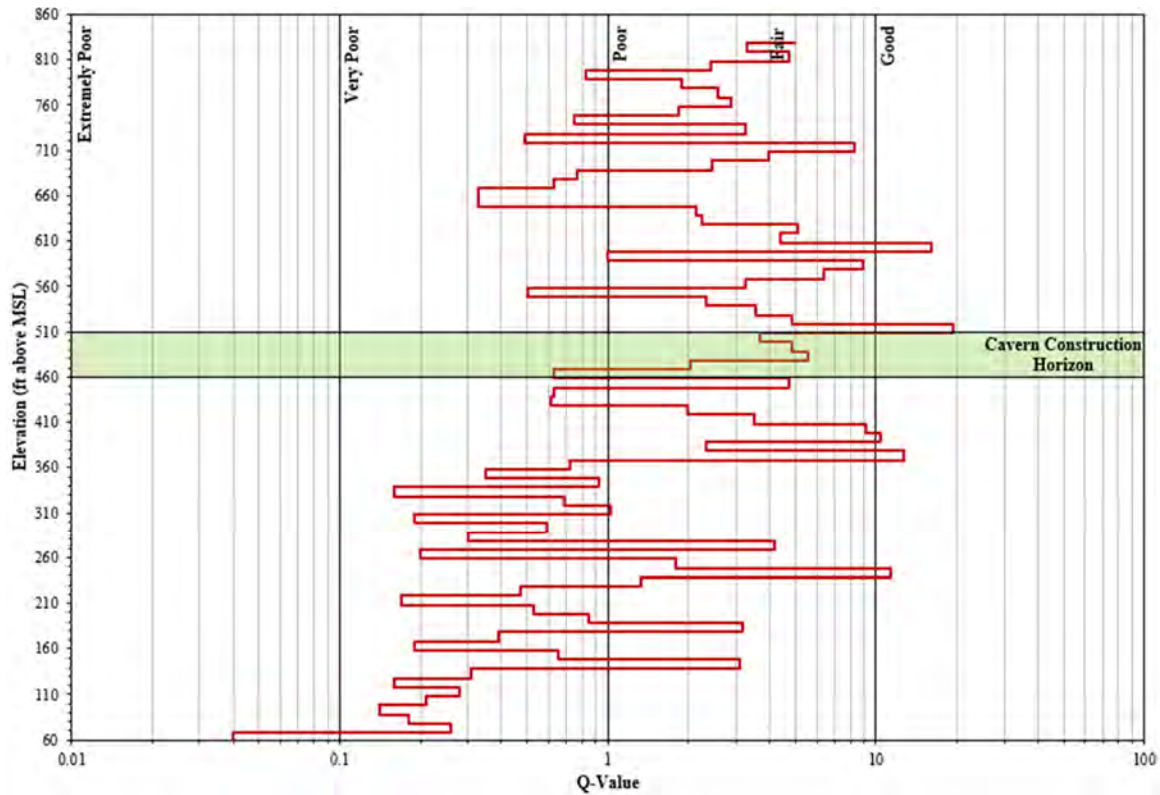


Figure 4-20. Q Ratings for Core Hole ZEV-CH-02-23

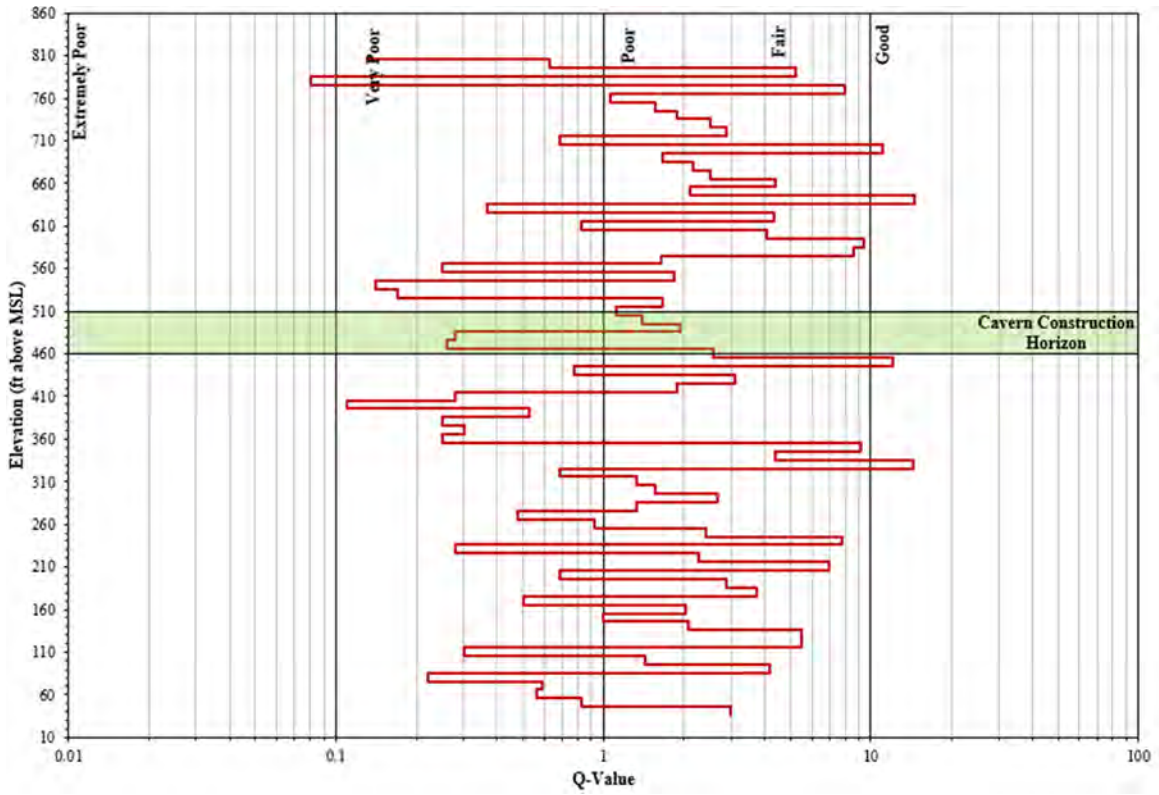


Figure 4-21. Q Ratings for Core Hole ZEV-CH-03-23

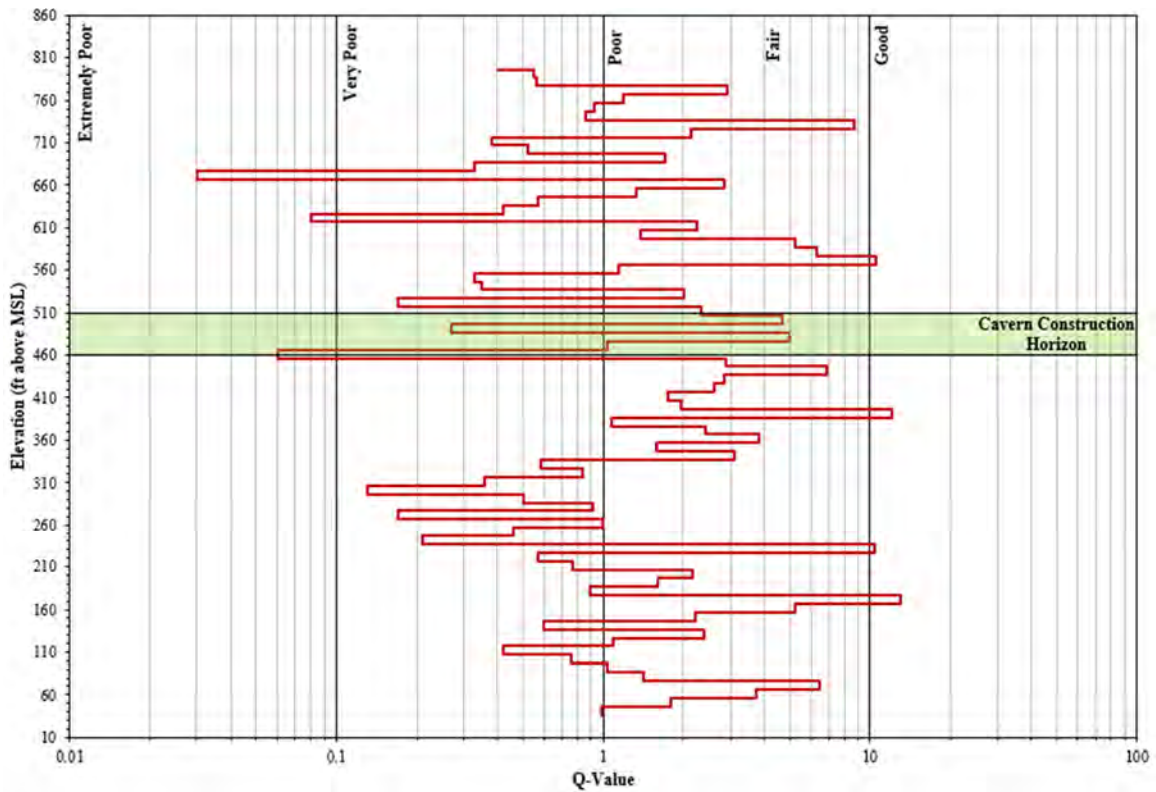


Figure 4-22. Q Ratings for Core Hole ZEV-CH-04-24

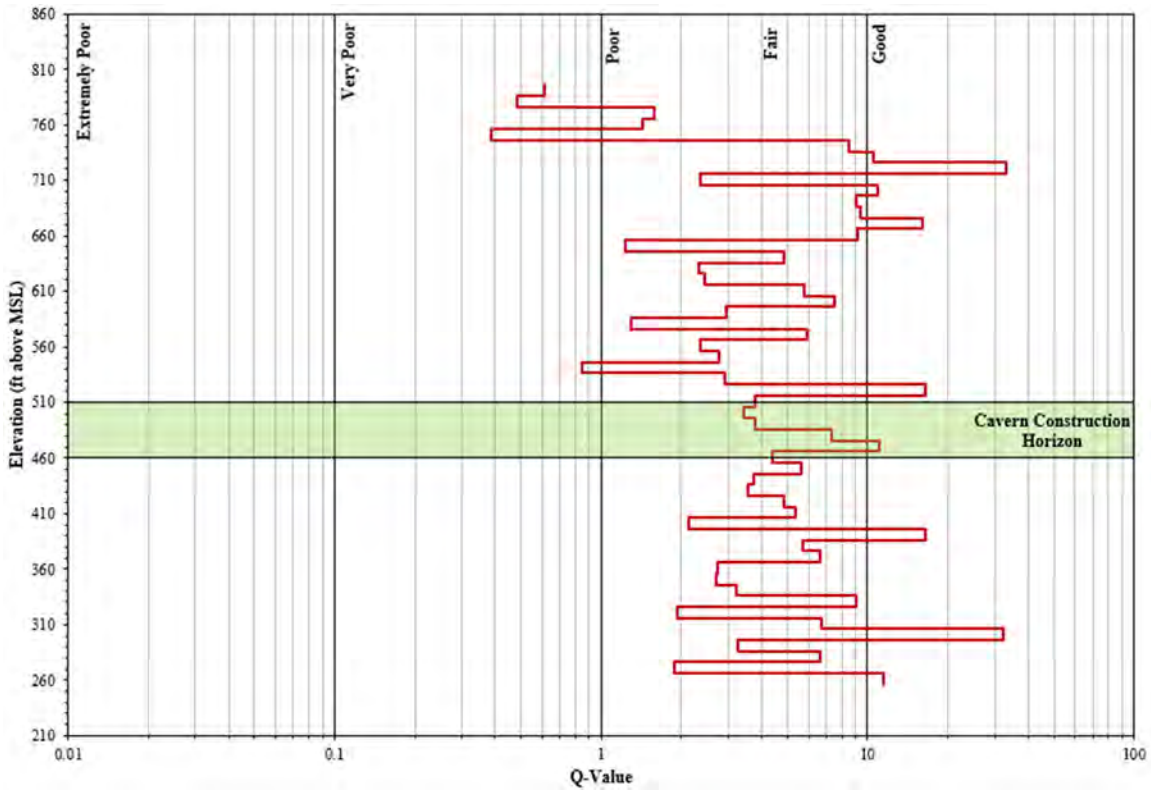


Figure 4-23. Q Ratings for Core Hole ZEV-CH-05-24

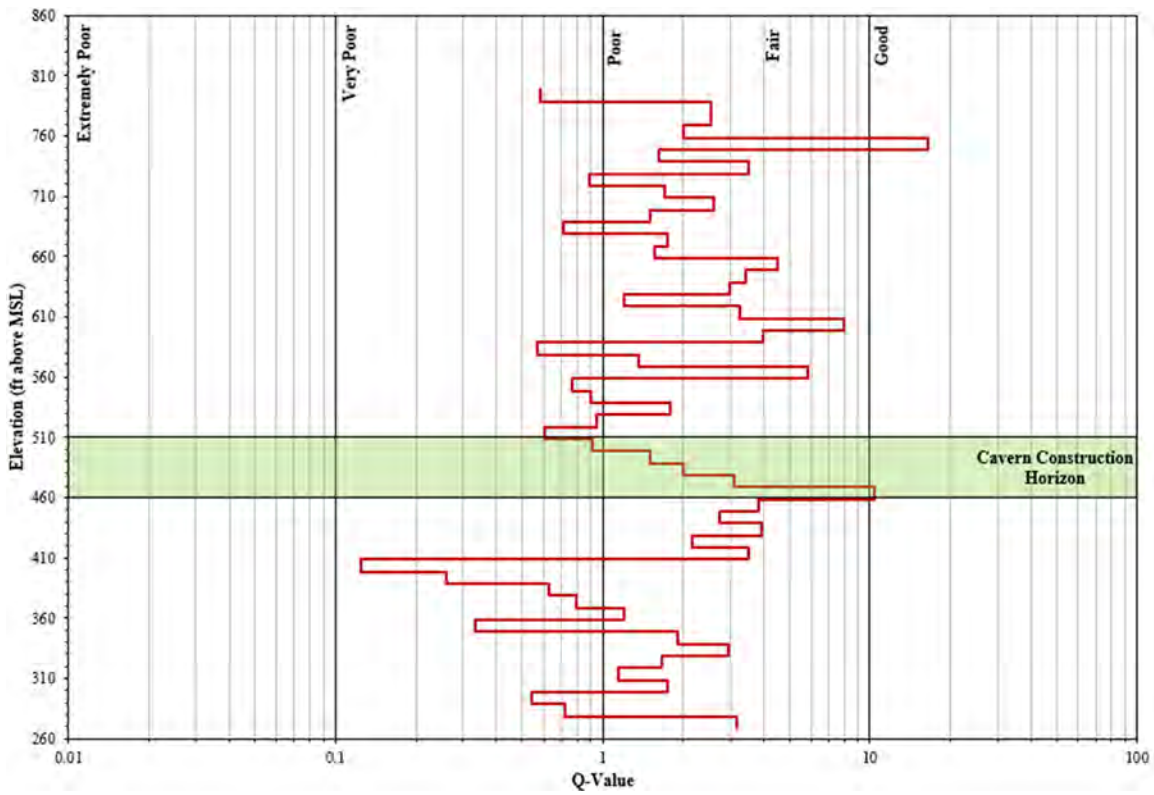


Figure 4-24. Q Ratings for Core Hole ZEV-CH-06-24



## 4.3 In Situ Stress Conditions

### 4.3.1 Regional Stress

The maximum in situ stress ( $\sigma_{hmax}$ ) component near the San Andreas and Garlock Faults is horizontal. McGarr et al. (1982) indicate that  $\sigma_{hmax}$  is aligned in a N20°W direction (Figure 4-25). Numerous measurements have been taken near the San Andreas Fault and other active faults in California. Using regression lines presented by McGarr et al. (1982) at the depths of the potential cavern horizons,  $\sigma_{hmax}$  is estimated between 3,765 and 4,540 psi, the minimum horizontal stress ( $\sigma_{hmin}$ ) between 2,340 and 2,930 psi, and the vertical stress ( $\sigma_v$ ) between 2,305 and 2,880 psi. The ratio between the maximum horizontal stress and vertical stress is termed the K ratio, which in this case is around 1.6.

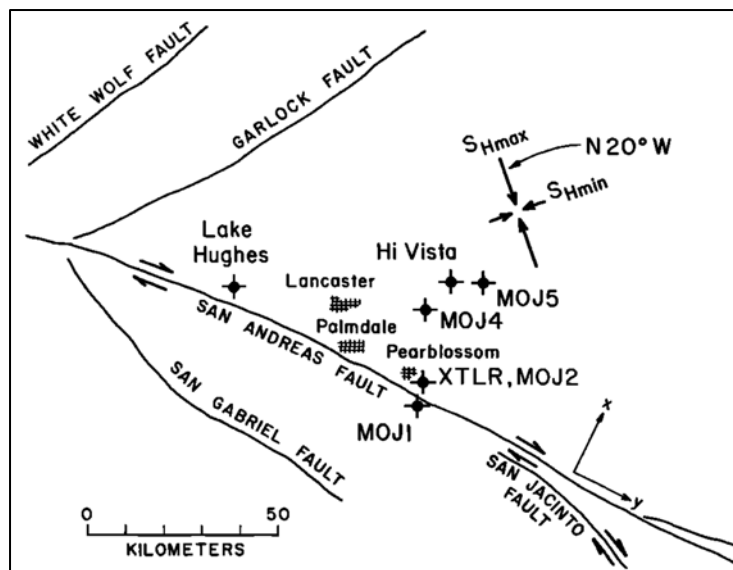


**Figure 4-25. Map Showing the Measured Orientation of the In Situ Horizontal Stresses in the Antelope Valley (McGarr et al. 1982)**

### 4.3.2 Borehole Breakout

Borehole breakout is the stress-induced deformation of a borehole cross section in a preferential direction, which occurs when the stress concentration around the borehole exceeds the rock strength (Ask et al., 2006; Babcock, 1978; Bell and Goug, 1979; Zoback et al., 1985). Breakout is the result of compressive failure along the borehole wall, with borehole spalling in the direction of minimum horizontal stress (Figure 4-26). Maximum principal stress orientations from breakout have been shown to be consistent with the results of other more traditional stress measurement techniques such as hydraulic fracturing and overcoring (Zoback and Zoback, 1980; Plumb and Hickman, 1985; Zajac and Stock, 1997).

Breakout is formed by the spalling of fragments from the borehole wall in the direction of minimum horizontal stress ( $\sigma_h$ ), as shown in Figure 4-26 (Fowler and Wier 2008). In crystalline rocks, such as quartz monzonite, breakout is initially observed as small pits or irregular chips at

the borehole wall (Plumb, 1989). Thus, breakout in crystalline rocks is thought to initiate at the borehole wall.

In core holes ZEV-CH-01-23 and ZEV-CH-02-23, borehole breakout can be seen in the amplitude logs as two 180° opposed dark traces parallel to the borehole wall (Figure 4-27). The breakout is oriented approximately N70°E, which is indicative of a major horizontal stress direction of N20°W. The logs of the six core holes indicate that the location of the breakout and the orientation is similar throughout the potential cavern horizons. This orientation is consistent with the regional major horizontal stress direction measured in Antelope Valley (Figure 4-25).

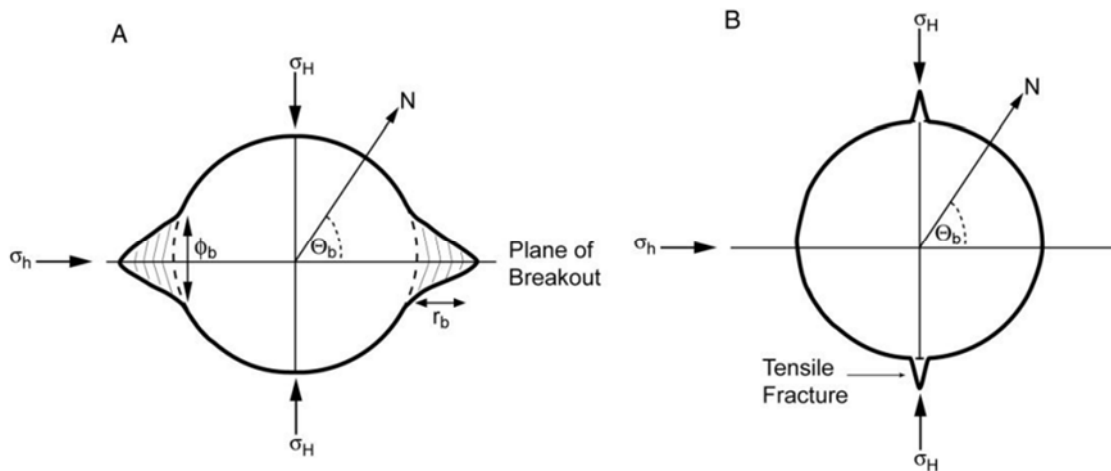


**Figure 4-26. Theoretical Borehole Cross-Section, Showing the Relationship between the Major Principal Horizontal Stress ( $\sigma_H$ ), the Minor Principal Horizontal Stress ( $\sigma_h$ ) for (A) Borehole Breakout, and (B) Tensile Fracture (Fowler and Weir, 2008)**

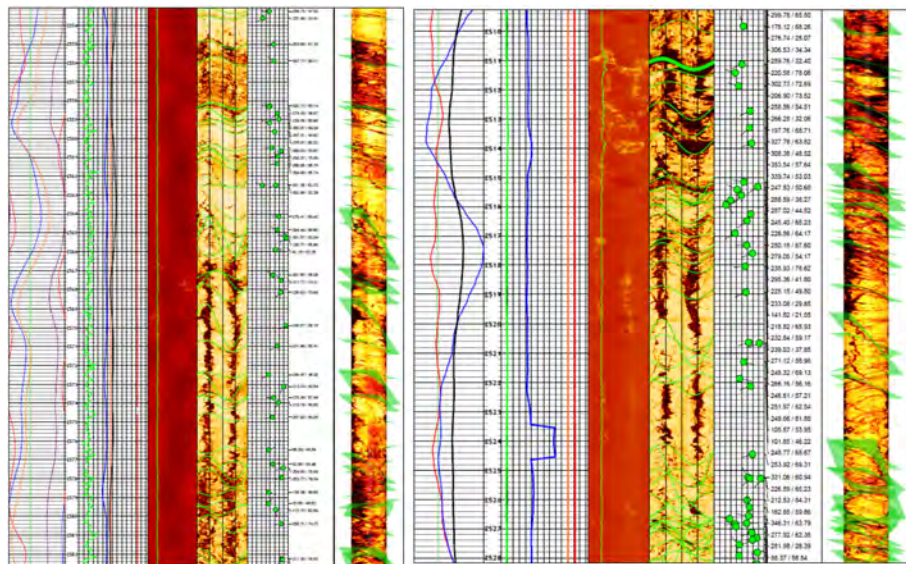


**Figure 4-27. Acoustic Televiwer Logs (ATV) Showing Borehole Breakout in the Amplitude Logs for Core Holes ZEV-CH-01-23 (left) and ZEV-CH-02-23 (right)**

### 4.3.3 Sibra Overcore

The maximum and minimum horizontal stresses within the potential cavern horizons were measured using the overcoring method in core hole ZEV-CH-03-23. The measurements were obtained using the in situ stress measurement tool (IST2D) and downhole technique developed by Sibra, Pty. (Sibra) of Brisbane, Australia (Gray 2000). The IST technique measures the two-dimensional rock stresses in the plane perpendicular to the core hole wall. Because core holes are generally vertical, this technique provides the principal stresses in the horizontal plane at the testing depth.

The IST2D tool is a pilot hole overcoring device that automatically measures the deformation across the diameter of a 25 to 27 mm pilot hole. Six vertical gauges measure deformation as overcoring progresses across the installed tool. The overcored rock samples are then tested to determine the core's mechanical properties relating to Young's Moduli, Poisson's Ratios, and uniaxial compressive strength. The resulting analysis is reported in terms of axisymmetric anisotropic elastic, though not necessarily linearly elastic behavior. The derivation of core properties is described by Gray, Zhao, and Liu (2018).

Two successful measurements were taken at depths of 2,030.0 and 2,033.4 ft in core hole ZEV-CH-03-23. The results are given in Table 4-5, and the details of the testing are provided in Appendix E. Using the axial modulus values derived from the laboratory tests of the overcore samples, the average maximum horizontal stress ( $\sigma_1$ ) is 1.2 times the minimum horizontal stress ( $\sigma_3$ ) and 1.6 times the estimated vertical stress ( $\sigma_v$ ). Thus, the ratio between the major maximum horizontal stress and vertical stress indicates a reasonably high horizontal stress regime, which is almost identical to the regional measurements collected by McGarr et al. (1982). Similarities were also measured in the major horizontal stress orientation, where the direction ranged between N20°W and N54°W. This suggests that the horizontal stresses at the Project site are related to tectonic activity associated with the San Andreas Fault.

**Table 4-5. Summary of IST2D Stress Testing in Core Hole ZEV-CH-03-23**

Hole Name	ZEV-CH-03-23	
Overcore Number	0052-070	0054-070
Date Tested	9/5/2023	9/5/2023
Depth (ft)	2,030.0	2,033.4
Unconfined Compressive Strength (psi)	26,468	12,696
Young's Modulus ( $\times 10^6$ psi)†	10.38	9.31
Poisson's Ratio †	0.32	0.19
Estimated Vertical Stress (psi)	2,368	2,373
Self-loading Horizontal Stress $\sigma_{hsw}$ (psi)	1,114	557
Maximum Horizontal Stress $\sigma_1$ (psi)	4,098.8	3,611
Minimum Horizontal Stress $\sigma_3$ (psi)	3,115.4	3,446
$\sigma_1:\sigma_3$ Ratio	1.3	1.0
True Bearing of Maximum Horizontal Stress	340.38°	303.98°
Maximum Horizontal Strain $\epsilon_1$ (microstrain)	226.8	269.8
Minimum Horizontal Strain $\epsilon_2$ (microstrain)	101.6	248.6
psi = pounds per square inch; ° = degree; E = East		
† Tangent Calculation Method magnetic declination of 11.68° E		

#### 4.4 Seismic Risk

The risk of damage due to earthquakes is primarily restricted to surface or very near-surface structures (Dowding and Rozen 1978). Sharma and Judd (1991) have estimated that little real damage occurs to underground openings at depths greater than 200 to 300 ft, except where a tunnel intersects a fault directly affected by the earthquake. According to Dowding and Rozen (1978) and confirmed by Sharma and Judd (1991) and Jaramillo (2017), no damage occurs in deep rock tunnels for Peak Ground Accelerations (PGAs) less than 19% of the acceleration due to gravity (0.19 grams [g]) and only minor damage occurs for PGAs between 0.19 g and 0.50 g. PGA is by far the most widely accepted index of the ground shaking intensity and damage from earthquakes. Thus, heavy earthquake damage can be sustained by surface buildings, while any deep underground excavations could remain mostly unharmed.

The Project site is located in a region where the likelihood of a damaging earthquake in the next 100 years is one of the highest within the United States (Figure 4-28). Furthermore, the PGA, with a 2% probability of exceedance in 50 years (i.e., occurs once every 2,475 years), was determined to be 0.39 g using Applied Technology Council (ATC) software for the ASCE7-16 Design Standard. This assumes a site amplification factor at PGA of 0.8 for Site Class A material. As per ASCE7-10, Site Class A material includes hard rock with shear waver velocities of > 5,000 ft/s.

Based on the PGA values, earthquake damage to a cavern at the potential target depths is expected to be minor. In this case, minor damage due to shaking includes the fall of stones and the formation of new cracks. Conversely, damage to surface buildings at the site from earthquakes, including cavern access shafts, could be significant as the maximum expected earthquake magnitude within a 50-year period in the area is 7.5. Nevertheless, the risk of landslides and soil liquefaction is small.

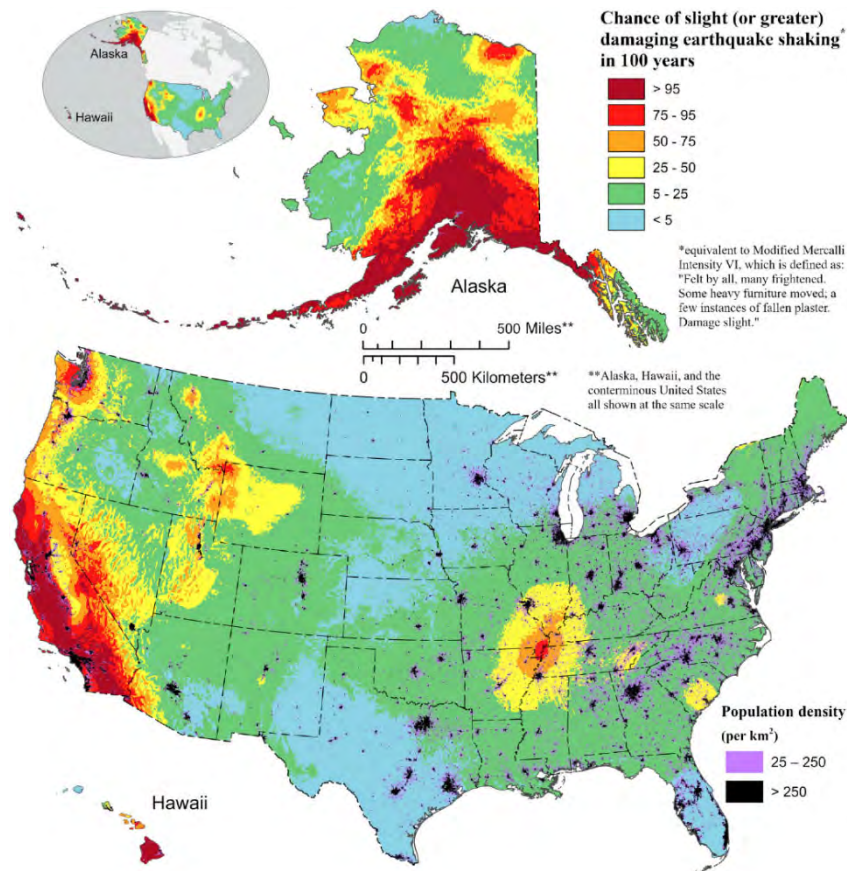


**Figure 4-28. Map Showing the Chance of any Level of Damaging Earthquake Shaking in 100 years from the 2023 50-State National Seismic Hazard Model (US National Seismic Hazard Model 2023)**

## 4.5 Rock Mass Strength and Deformation Properties

### 4.5.1 Geological Strength Index (GSI)

The Geological Strength Index (GSI), first introduced by Hoek (1994), was developed to evaluate parameters for the Hoek-Brown strength criterion for rock masses (Hoek et al. 2002) as well as for estimating deformation modulus of a rock mass. The GSI is a complement to the Hoek-Brown strength criterion and can be used to estimate the parameters  $s$ ,  $a$ , and  $m_b$  in the criterion.

GSI can be determined based on visual assessment of the rock mass and includes consideration of the degree of “blockiness” or mechanical interlock, as well as the discontinuity conditions following a procedure developed by Hoek and Marinos (2000). GSI can also be assessed using correlations with RMR and  $Q$ .

As there are no excavated exposures of the rock mass in the target cavern horizon, the GSI was defined based on correlations with the RMR and  $Q$  values determined from the core logging. RMR and  $Q$  include factors for in situ and groundwater stresses, which are typically determined or defined in the numerical modeling process (Hoek et al. 2000). At this stage, in order to consider only intrinsic rock and joint characteristics, modified  $Q'$  and RMR classifications were applied.

When RMR is used to estimate GSI, the last two parameters are adjusted so that a rating of 15 is assigned to groundwater and a rating of 0 for orientation (Hoek et al. 2000), which is known as the  $RMR_{89}$  term. The rating is then related to GSI using the following relationship when  $RMR_{89} > 23$ :

$$GSI = RMR_{89} - 5 \quad (\text{Eqn. 4-2})$$

For rock masses with  $RMR_{89} < 23$ , the RMR system cannot be used, and the Q-system should be used instead. When using the Q-system to estimate GSI, the joint water reduction factor ( $J_w$ ) and the stress reduction factor (SRF) should both be set to 1 to obtain the modified tunneling quality index  $Q'$ . The following relationship can then be used to determine GSI (Hoek et al. 2000):

$$GSI = 9 \ln Q' + 44 \quad (\text{Eqn. 4-3})$$

Due to the “Fair” to “Good” quality of the rock mass (i.e.,  $RMR > 23$ ), only the RMR correlation was used for determining the respective GSI for each core run. The distribution of the calculated GSI values is provided in Figures 4-29 to 4-34.

The results for core holes ZEV-CH-01-23 and ZEV-CH-02-23 indicate the GSI within the potential cavern horizons ranges between 60 and 78 and the rock mass is anticipated to have a GSI of 66 to 71 on average. For core holes ZEV-CH-03-23 and ZEV-CH-04-24, the GSI ranges between 43 and 60, and averages between 48 to 55. In core hole ZEV-CH-05-24 and ZEV-CH-06-24, the GSI ranges between 50 and 72, and averages between 58 and 64.

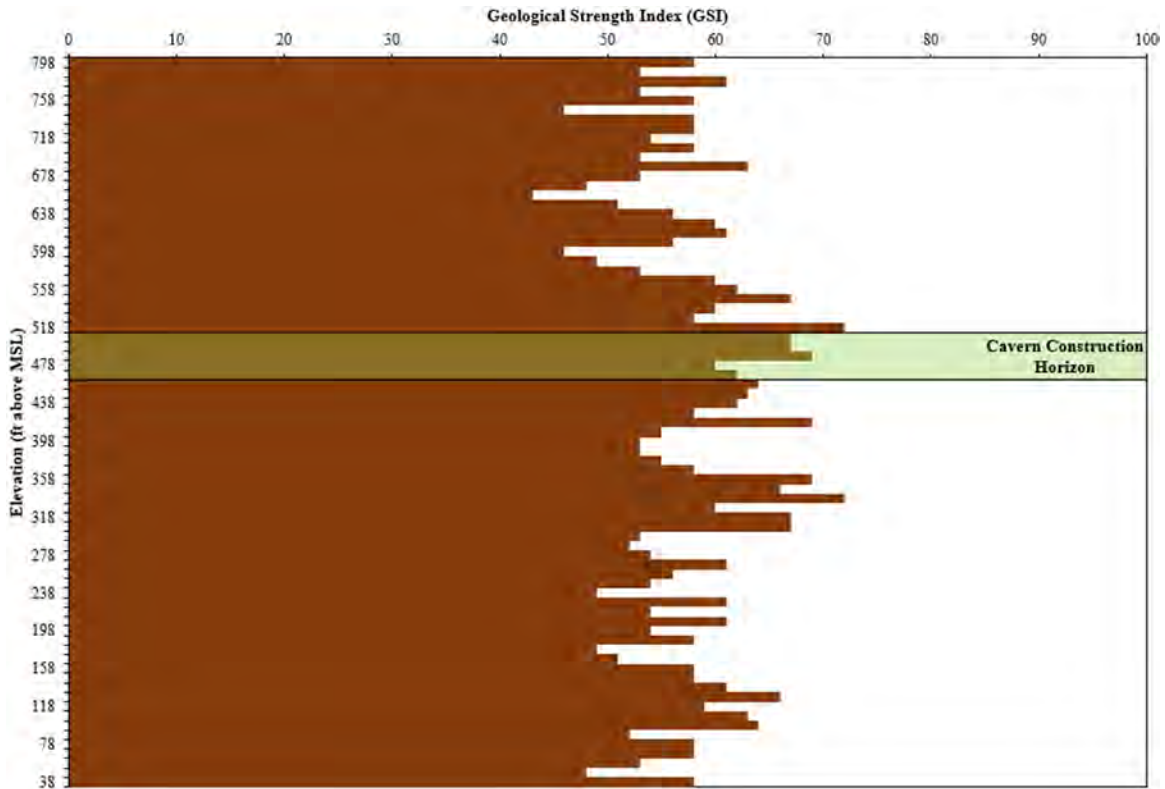


Figure 4-29. GSI Ratings for Core Hole ZEV-CH-01-23

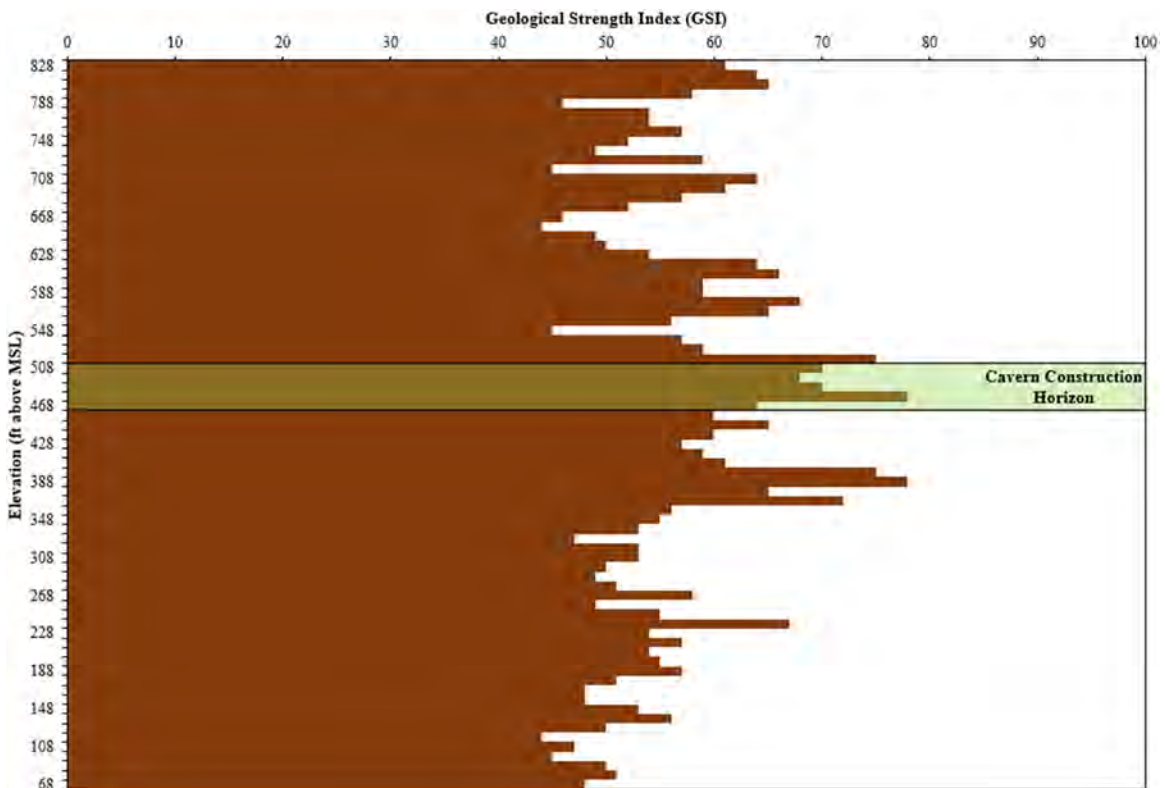


Figure 4-30. GSI Ratings for Core Hole ZEV-CH-02-23

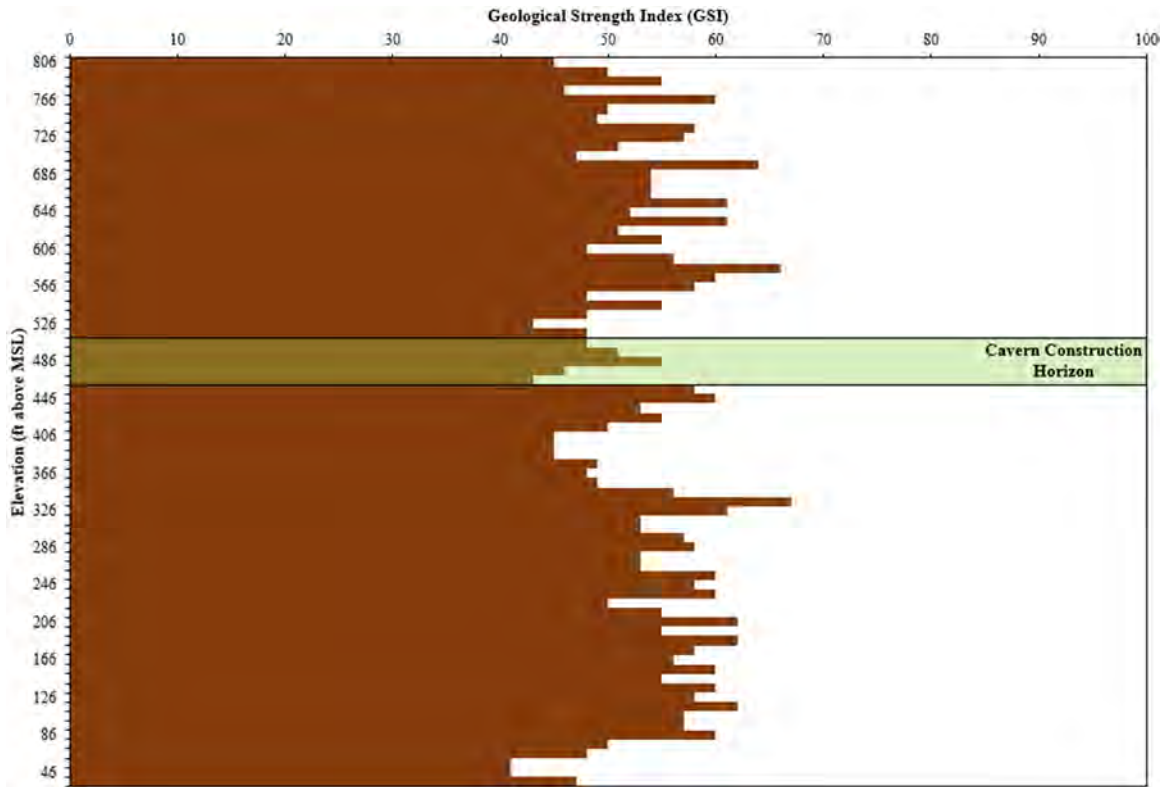


Figure 4-31. GSI Ratings for Core Hole ZEV-CH-03-23

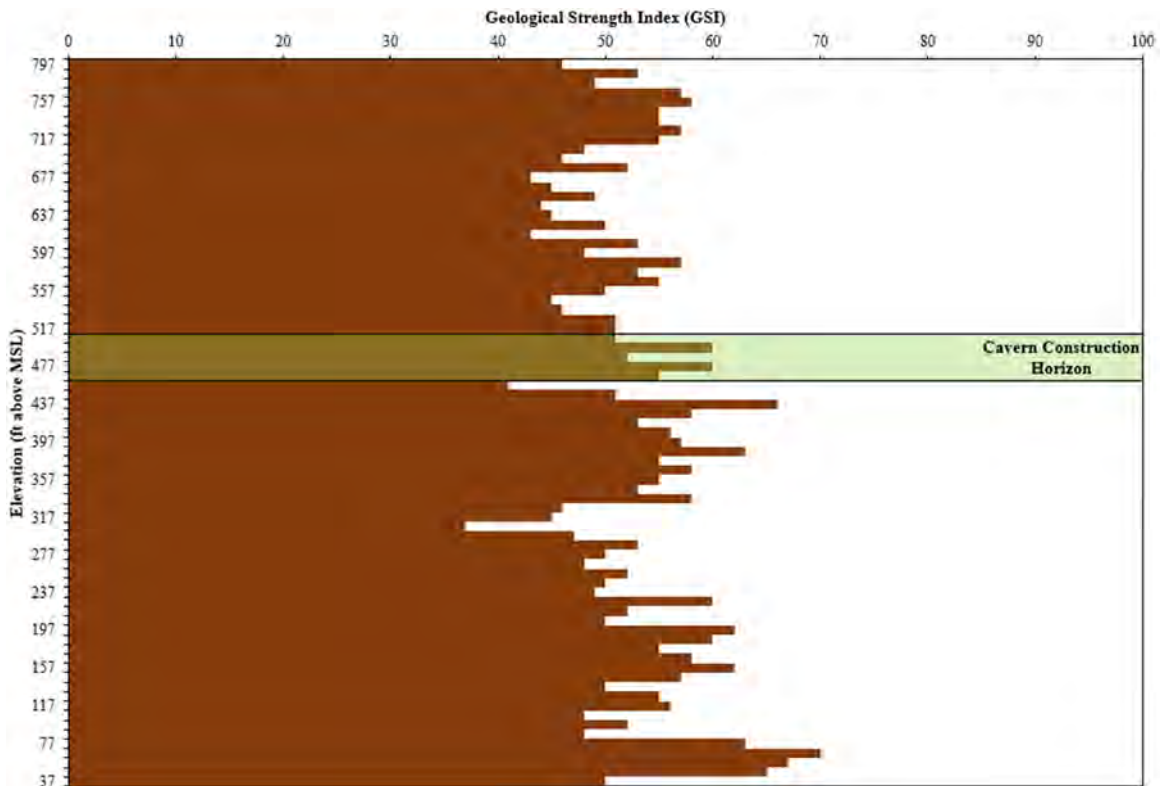


Figure 4-32. GSI Ratings for Core Hole ZEV-CH-04-24



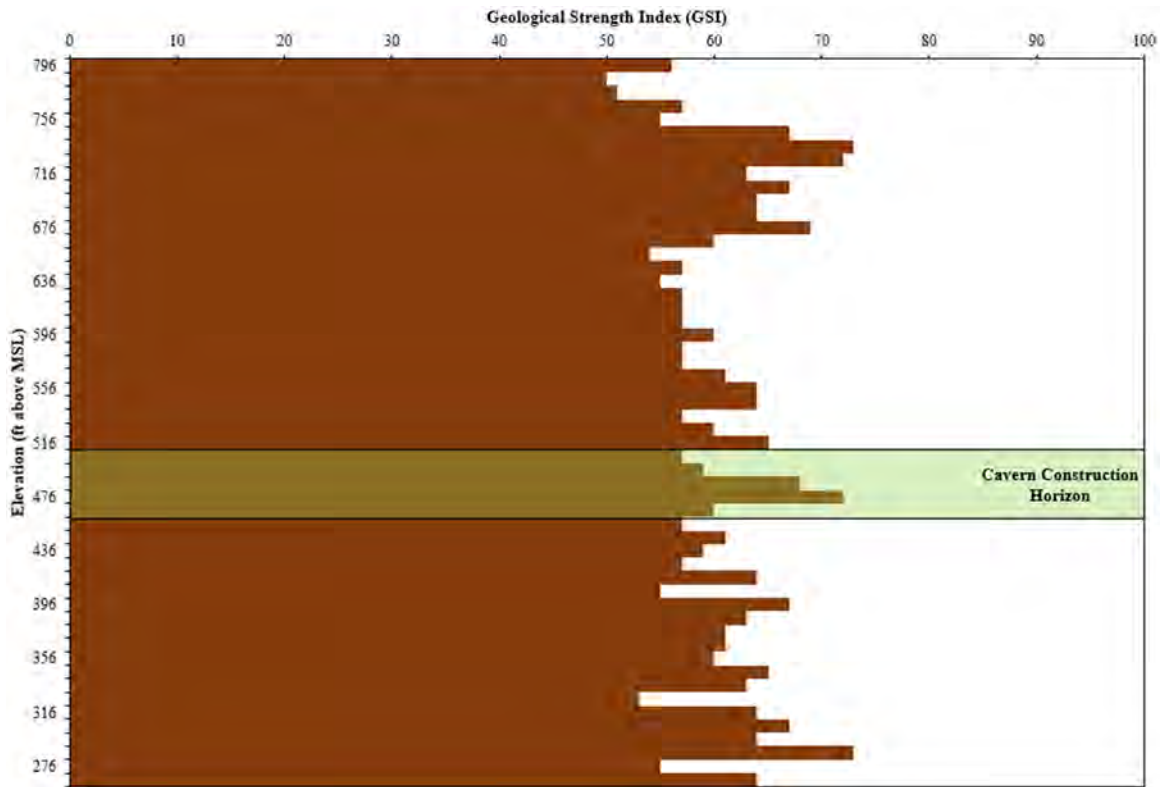


Figure 4-33. GSI Ratings for Core Hole ZEV-CH-05-24

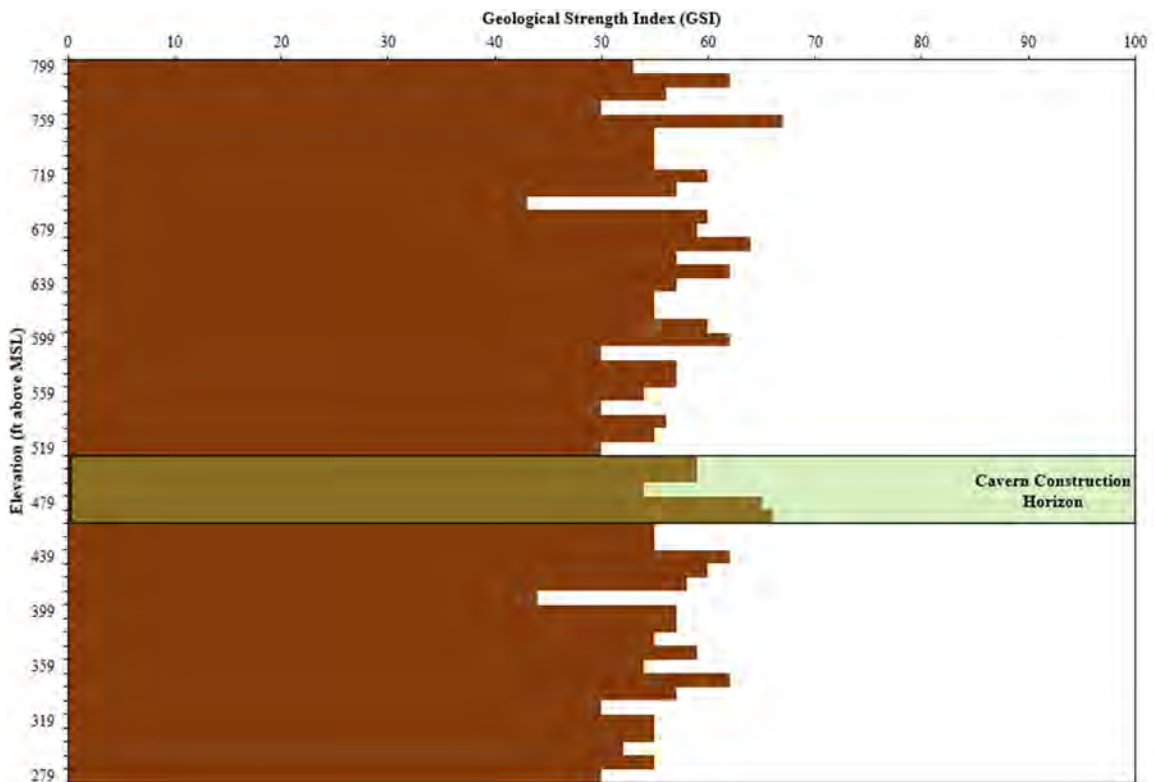


Figure 4-34. GSI Ratings for Core Hole ZEV-CH-05-24

#### 4.5.2 Hoek-Brown Criterion

Hoek et al. (2002) proposed a method for estimating the strength of jointed rock masses based on the assessment of the interlocking of rock blocks and the condition of the surfaces between the blocks. For most rocks of good to reasonable quality, in which the rock mass strength is controlled by tightly interlocking angular rock pieces, the Hoek-Brown failure criterion is defined by the following equation:

$$\sigma_1' = \sigma_3' + \sigma_c \left( m_b \frac{\sigma_3}{\sigma_c} + s \right)^{0.5} \quad (\text{Eqn. 4-4})$$

Where  $\sigma_1$  = maximum effective principal stress  
 $\sigma_3'$  = minimum effective principal stress  
 $\sigma_c$  = UCS of intact rock  
 $m_b$  = value of the constant  $m$  for the rock mass  
 $s$  = constant which depends upon the characteristics of the rock mass

For poor quality rock masses, in which the tight interlocking has been partially destroyed by shearing, weathering, or alteration, the modified Hoek-Brown failure criterion is defined by the following equation:

$$\sigma_1' = \sigma_3' + \sigma_c \left( m_b \frac{\sigma_3}{\sigma_c} \right)^a \quad (\text{Eqn. 4-5})$$

where  $a$  = constant which depends upon the characteristics of the rock mass

The relationships between  $m_b/m_i$ ,  $s$ , and  $a$  and the GSI are as follows:

For GSI > 25 (Undisturbed rock masses)

$$m_b = m_i \exp \left( \frac{GSI-100}{28-14D} \right) \quad (\text{Eqn. 4-6})$$

$$s = \exp \left( \frac{GSI-100}{9-3D} \right) \quad (\text{Eqn. 4-7})$$

For GSI < 25 (Undisturbed rock masses)

$$a = 0.65 - \frac{GSI}{200} \quad (\text{Eqn. 4-8})$$

Based on these relationships, four properties are required to use the Hoek-Brown criterion for estimating the strength and deformability of the rock mass. The four properties include the following:

- Uniaxial compressive strength of the intact rock,  $\sigma_{ci}$
- Value of the Hoek-Brown constant  $m_i$  for the intact rock

- Value of the GSI for the rock mass
- Value of the disturbance factor, D

The uniaxial compressive strength of the intact rock as well as the GSI of the rock mass were previously discussed in the preceding sections; however, the  $m_i$  term and the disturbance factor (D) are discussed below.

**4.5.2.1 Definition of  $m_i$**

The  $m_i$  parameter is considered constant for a specific rock type and does not change with anisotropy direction (Saroglou and Tsiambaos 2008, and Saeidi et al. 2014). Saroglou et al. (2014) suggests that an anisotropic rock is best determined by a set of triaxial compressive strength tests at various confining pressures on core samples. This represents the “true” intact strength with effects of anisotropy being removed, as the sample will not fail structurally but will fail through the intact rock.

The triaxial tests ( $\sigma_3 = 1,500$  and  $2,500$  psi), uniaxial compressive strength tests, and average Brazilian tensile tests were used to define the Hoek-Brown strength envelope for the rock mass in the target cavern horizon (Figure 4-35). The resulting  $m_i$  constant from a best-fit line was determined to be 22.0. This result is consistent with the recommended range for coarse-grained granites ( $20 \pm 5$ ) based on published values of  $m_i$  provided by Hoek and Marinos (2000).

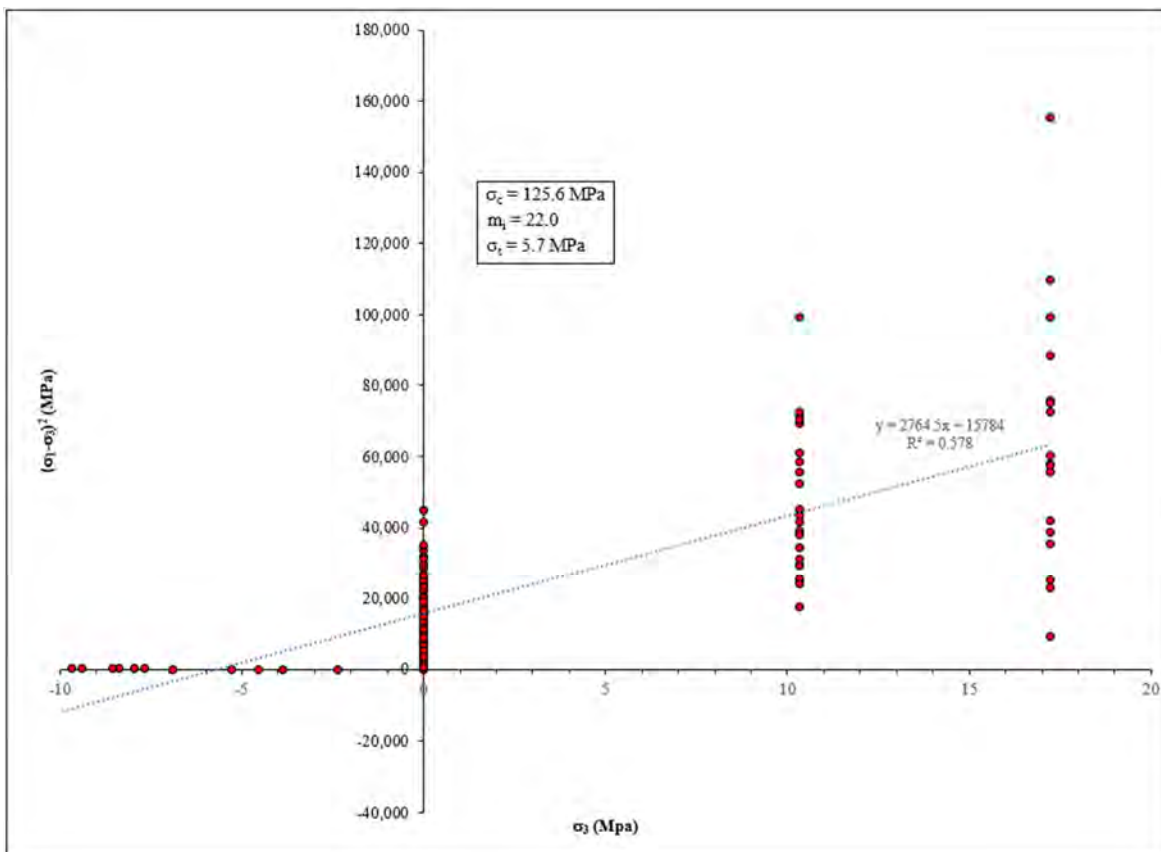







**Figure 4-35. Linear Regression Analysis for the Input and Derivation of  $m_i$  Constant**

**4.5.2.2 Disturbance Factor (D)**

The disturbance factor, D, is a factor that depends on the degree of disturbance to the rock due to blast damage and stress relaxation around the excavation. The disturbance factor varies from 0 for undisturbed rock masses to 1 for very disturbed rock masses. It is important to note that the disturbance factor should only be applied to the blast damaged zone and not to the entire rock mass. Applying the blast damage to the entire rock mass is inappropriate and results in overly conservative results.

Guidelines for estimating disturbance factor are provided by Hoek et al (2002) and are provided in Figure 4-36. For the purpose of this assessment, a disturbance factor of 0 has been assumed, which represents excellent quality-controlled blasting that results in minimal disturbance to the confined rock mass surrounding the excavation.

Appearance of rock mass	Description of rock mass	Suggested value of D
	Excellent quality controlled blasting or excavation by Tunnel Boring Machine results in minimal disturbance to the confined rock mass surrounding a tunnel.	D = 0
	Mechanical or hand excavation in poor quality rock masses (no blasting) results in minimal disturbance to the surrounding rock mass. Where squeezing problems result in significant floor heave, disturbance can be severe unless a temporary invert, as shown in the photograph, is placed.	D = 0  D = 0.5 No invert
	Very poor quality blasting in a hard rock tunnel results in severe local damage, extending 2 or 3 m, in the surrounding rock mass.	D = 0.8
	Small scale blasting in civil engineering slopes results in modest rock mass damage, particularly if controlled blasting is used as shown on the left hand side of the photograph. However, stress relief results in some disturbance.	D = 0.7 Good blasting  D = 1.0 Poor blasting
	Very large open pit mine slopes suffer significant disturbance due to heavy production blasting and also due to stress relief from overburden removal. In some softer rocks excavation can be carried out by ripping and dozing and the degree of damage to the slopes is less.	D = 1.0 Production blasting  D = 0.7 Mechanical excavation

**Figure 4-36. Guidelines for Estimating Disturbance Factor (D) (Hoek et al. 2002)**

**4.5.2.3 Summary of Hoek-Brown Parameters**

The Hoek-Brown parameters for the rock mass anticipated in the target cavern horizon were determined using the following values:

- GSI Range: 49 to 64 (one standard deviation)
- Uniaxial Compressive Strength of Intact Rock Range: 10,000 to 22,000 psi (one standard deviation)
- $m_i$  Parameter: 22.0
- Disturbance Factor, D: 0

The resulting Hoek-Brown parameters are summarized in Table 4-6.

**Table 4-6. Hoek-Brown Parameters**

Hoek-Brown Parameter	Typical Range	Representative Value
$m_b$	3.559 - 6.082	4.570
$s$	0.003 - 0.018	0.008
$a$	0.5	0.5

**4.5.2.4 Hoek-Brown Global Rock Mass Strength**

The following relationship between the global rock mass strength,  $\sigma_{cm}$ , and the Hoek-Brown parameters is given by:

$$\sigma_{cm} = \sigma_{ci} \left( \frac{(m_b + 4s - a(m_b - 8s)) \left(\frac{m_b}{4+s}\right)^{a-1}}{2(1+a)(2+a)} \right) \tag{Eqn. 4-9}$$

Table 4-7 provides a summary of the global rock mass strength for the various alteration conditions of the quartz monzonite within the potential cavern horizons.

**Table 4-7 Global Rock Mass Strength for Various Rock Conditions**

Rock Type	Rock Mass Strength ( $\sigma_{cm}$ ) Typical Range (psi)	Rock Mass Strength ( $\sigma_{cm}$ ) Representative Value (psi)
Quartz Monzonite (all)	2,515 - 7,579	4,453
Quartz Monzonite (Fr-SA)	2,808 - 7,579	4,777
Quartz Monzonite (MA-HA)	349 - 5,691	2,655

### 4.5.3 Mohr-Coulomb Criterion

Many geotechnical software programs are written in terms of the Mohr-Coulomb failure criterion, so it is necessary to determine equivalent angles of friction and cohesive strengths for each rock mass and stress range. Mohr-Coulomb parameters for the rock mass can be determined by using the following equations (Hoek, Carranza-Torres, and Corkum, 2002):

$$\phi' = \sin^{-1} \left( \frac{6am_b(s+m_b\sigma'_{3n})^{a-1}}{2(1+a)(2+a)+6am_b(s+m_b\sigma'_{3n})^{a-1}} \right) \quad (\text{Eqn. 4-10})$$

$$c' = \frac{\sigma_{ci}[(1+2a)s+(1-a)m_b\sigma'_{3n}](s+m_b\sigma'_{3n})^{a-1}}{(1+a)(2+a) \sqrt{1 + \left( \frac{6am_b(s+m_b\sigma'_{3n})^{a-1}}{(1+a)(2+a)} \right)^2}} \quad (\text{Eqn. 4-11})$$

where  $\sigma'_{3n} = \sigma'_{3max}/\sigma_{ci}$

The critical aspect of developing appropriate Mohr-Coulomb parameters is selecting the appropriate value of  $\sigma'_{3max}$  that is anticipated in the rock mass. Hoek-Brown suggests the following relationship for deep tunnels:

$$\frac{\sigma'_{3max}}{\sigma'_{cm}} = 0.47 \left( \frac{\sigma'_{cm}}{\gamma H} \right)^{-0.94} \quad (\text{Eqn. 4-12})$$

where  $\sigma'_{cm}$  is the rock mass strength determined by the Hoek-Brown failure criterion,  $\gamma$  is the unit weight of the rock mass and  $H$  is the depth of the tunnel below the surface.

For the potential cavern horizons, this relationship results in a  $\sigma'_{3max}$  range of between 1,085 and 1,430 psi for the nominal rock mass strengths determined at a unit weight of 166 pcf. This stress is considerably lower than the major horizontal stress measured through the in situ stress testing. Hoek and Brown (2002) state that where the horizontal stress is higher than the vertical stress, the horizontal stress value should be used in place of  $\gamma H$ . On this basis, a range of stresses between 1,790 psi and 2,360 psi was assumed for determining Mohr-Coulomb parameters.

#### 4.5.3.1 Intact Mohr-Coulomb Parameters

The intact Mohr-Coulomb Parameters were calculated for the assumed stress range for intact rock (i.e. GSI = 100,  $m_b = m_i$ ,  $a = 0.5$ , and  $s = 1$ ). Table 4-8 provides a summary of the Mohr-Coulomb parameters for intact rock for the various stresses.

**Table 4-8. Intact Mohr-Coulomb Properties for Various Stresses**

Depth (ft)	$\sigma_{3\max}$ (psi)	Range of Anticipated Values		Representative Values	
		Cohesion, C' (psi)	Friction Angle, f' (°)	Cohesion, C' (psi)	Friction Angle, f' (°)
2,000	2,016	1,715 - 3,166	52.4 - 56.5	2,339	54.7
2,100	2,110	1,739 - 3,191	52.1 - 56.3	2,364	54.4
2,200	2,205	1,764 - 3,216	51.8 - 56.1	2,389	54.2
2,300	2,299	1,789 - 3,241	51.5 - 55.9	2,415	54.0
2,400	2,393	1,813 - 3,266	51.3 - 55.7	2,440	53.7
2,500	2,486	1,838 - 3,291	51.0 - 55.5	2,465	53.5

#### 4.5.3.2 Rock Mass Mohr-Coulomb Parameters

The Mohr-Coulomb properties were calculated for the assumed stress range for the rock mass in the potential cavern horizons. Table 4-9 provides a summary of the Mohr-Coulomb parameters for an isotropic rock mass (i.e. GSI = 49 to 64, UCS = 10,000 psi to 22,000 psi,  $m_i = 22$ , and  $D = 0$ ).

**Table 4-9. Rock Mass Mohr-Coulomb Properties for Various Stresses**

Depth (ft)	$\sigma_{3\max}$ (psi)	Range of Anticipated Values		Representative Values	
		Cohesion, C' (psi)	Friction Angle, f' (°)	Cohesion, C' (psi)	Friction Angle, f' (°)
2,000	2,016	544 - 909	39.9 - 50.1	691	45.2
2,100	2,110	562 - 936	39.5 - 49.8	713	44.8
2,200	2,205	580 - 962	39.1 - 49.4	735	44.4
2,300	2,299	598 - 988	38.8 - 49.1	757	44.1
2,400	2,393	616 - 1,013	38.4 - 48.8	778	43.7
2,500	2,486	632 - 1,039	38.1 - 48.5	799	43.4

#### 4.5.4 Rock Mass Elastic Modulus

The elastic modulus ( $E_{rm}$ ) of the rock mass within the target cavern horizon was determined based on the following relationship (Hoek and Diederichs, 2006) using laboratory test results for intact elastic modulus:

- GSI Range: 49 to 64
- Uniaxial Compressive Strength of Intact Rock Range: 10,000 to 22,000 psi
- Modulus Ratio (MR): 515
- Disturbance Factor, D: 0

The resulting rock mass modulus for a GSI range of 49 to 64 with a D value of 0 are summarized in Table 4-10.

**Table 4-10. Rock Mass Modulus**

Rock Mass Modulus	Typical Range (psi)	Representative Value (psi)
$E_m$	1,137 - 3,999	2,095

#### 4.5.5 Joint Stiffness

The normal and shear stiffness of the joints in the potential cavern horizons can be estimated from the rock mass modulus, the intact rock modulus, and the mean joint spacing (Ingrad and Kraushaar 1960). It is assumed that the deformability of the overall mass is due to both elastic deformation of the intact rock mass and joint deformation. The following equation simplifies the rock mass into a system, best illustrated as two springs aligned in a series:

$$\frac{1}{E_{rm}} = \frac{1}{E_i} + \frac{1}{k_n L} \quad (\text{Eqn. 4-15})$$

where  $E_{rm}$  is the rock mass modulus,  $E_i$  is the intact rock modulus,  $k_n$  is the joint normal stiffness, and  $L$  is the mean joint spacing. It is assumed that there is only one joint set oriented normal to the applied loading.

The same methodology can be followed to estimate the shear stiffness of the joints using the following equation:

$$\frac{1}{G_m} = \frac{1}{G_i} + \frac{1}{k_s L} \quad (\text{Eqn. 4-16})$$

where  $G$  is the shear modulus and  $k_s$  is the joint shear stiffness.

The following relationship is used to relate E to G:

$$E = 2(1 + \nu)G \quad (\text{Eqn. 4-17})$$

Based on (1) the Young's modulus determined for the intact rock tested within the potential cavern horizons, (2) the Young's modulus of the rock mass determined through the rock mass characterization, and (3) an assumed mean joint spacing ranging between 0.3 and 1.3 ft, the joint normal and shear stiffnesses were calculated. A summary of the joint normal and shear stiffness values is provided in Table 4-11.

**Table 4-11. Summary of Joint Normal Stiffness and Joint Shear Stiffness**

Parameter	Range of Anticipated Values (ksf/ft)	Representative Value (ksf/ft)
$k_n$	$4.89 \times 10^4 - 7.56 \times 10^5$	$2.97 \times 10^5$
$k_s$	$1.94 \times 10^4 - 3.00 \times 10^5$	$1.18 \times 10^5$



#### *4.5.6 Rock Mass Dilation*

The rock mass dilation angle was not directly measured during laboratory testing, however, recommendations from Hoek (2001) can be used to estimate the dilation angle. For average quality rock masses, the dilation angle can be estimated by dividing the friction angle of the rock mass by eight. Based on the Mohr-Coulomb parameters determined above for various cavern depths, the rock mass dilation angle is estimated to range between 6.4 and 7.1 degrees.

## 5 CONCLUSIONS

Geological and geotechnical data were collected from six deep subsurface core holes at the Willow Rock Project site. The rock core in all holes was logged, and samples were selected for a full suite of geomechanical laboratory testing. Packer testing was carried out at key intervals to determine hydraulic conductivity, and each hole was surveyed with downhole geophysical tools. In one of the core holes, both falling head and rising head testing were carried out at intervals above and within the targeted cavern horizon to determine water inflow and outflow rates. In another core hole, IST2D overcore testing was carried out to measure horizontal stress directions and magnitudes in the potential cavern horizon. This data was used to develop a preliminary geotechnical model for the proposed A-CAES cavern construction.

The geotechnical design parameters were developed and presented within this report to support the Front-End Engineering Design (FEED) study for cavern construction. Consistent with the information outlined in this report, it is Agapito's assessment that the geotechnical conditions anticipated in the target cavern horizon are conducive for cavern construction using the room and pillar method of development. Although not the focus of this report, it is nonetheless of note that the vertical shafts required for construction and operation of the cavern can likely be constructed using the blind bore method.

---

## 6 REFERENCES

- Ask, M.V.S., Ask, D. and Christiansson, R. (2006) Detection of borehole breakouts at Forsmark site, Sweden. In-situ Rock Stress - Measurement, Interpretation and Application, Lu, Li, Kjølholt and Dhale (editors), Taylor & Francis, London, pp. 79–86.
- Babcock, E.A. (1978) Measurement of subsurface fractures from dipmeter logs: AAPG Bulletin, 62(7), pp. 111–1126. Reprinted 1990 in Foster, N.H. and Beaumont, E.A. (editors) Formation evaluation II – log interpretation: AAPG Treatise of Petroleum Geology Reprint Series 17, pp. 457–472.
- Barton, N., Lien, R., and Lunde, J. (1974). “Engineering classification of rock masses for the design of tunnel support”. *Rock Mech.* 6. pp. 189-236.
- Bieniawski, Z.T. (1976). ”Rock mass classifications in rock engineering”. *Proc. of Symposium on Exploration for Rock Engineering*, Belkema, Rotterdam, Vol. 1, pp 97-106.
- Bieniawski, Z. T. (1989). *Engineering Rock Mass Classifications*. J.W. Wiley & Sons. New York.
- Bell, J.S. and Gough, D.I. (1979) Northeast-southwest compressive stress in Alberta: Evidence from oil wells. *Earth and Planetary Science Letters* 45(2), pp. 475–482.
- Deere D.U. 1968. Chapter 1: Geological considerations. In *Rock Mechanics in Engineering Practice* (eds. Stagg K.G. and Zienkiewicz, O.C.), 1-20. London: John Wiley and Sons.
- Deere, D. U., and D. W. Deere (1988), “The Rock Quality Designation (RQD) Index in Practice,” *Rock Classification Systems for Engineering Purposes, ASTM STP 984*, Louis Kirkaldie Ed., American Society for Testing and Materials, Philadelphia, 1988, pp. 91-101.
- Dibblee, Jr., T. W. (1963), *Geology of the Willow Springs and Rosamond Quadrangles*, Geological Survey Bulletin 1089-C, Washington, DC: US Government Printing Office, 117 pp.
- Dibblee, Jr., T. W. (1967), *Areal Geology of the Western Mojave Desert, Plate 1 (West-Half)*, Geological Survey Professional Paper 522, Washington, DC: US Government Printing Office, 1 sheet.
- Dowding, C. H. and A. Rozen (1978), “Damage to Rock Tunnels from Earthquake Shaking,” *J. Geotech. Eng. Div.*, 104(GT2):175–191.
- Fowler, MJ & Weir, FM 2008, 'The Use of Borehole Breakout for Geotechnical Investigation of an Open Pit Mine', in Y Potvin, J Carter, A Dyskin & R Jeffrey (eds), *SHIRMS 2008: Proceedings of the First Southern Hemisphere International Rock Mechanics Symposium*, Australian Centre for Geomechanics, Perth, pp. 541-550.
- Gray, I. (2000), “The Measurement and Interpretation of Stress,” *Bowen Basin Symposium on Seam Gas*, pp. 321–324.

- 
- Gray, I., Zhao, X., and Liu, L. (2018) Mechanical Properties of Coal Measure Rocks Containing Fluids at Pressure, Proceedings of the 18th Coal Operators' Conference, Mining Engineering, University of Wollongong, 195-204.
- Hoek, E. (1994). "Strength of rock and rock masses". *ISRM News Journal*. 2 (2). Pp. 4-16.
- Hoek, E., Carranza-Torres C., Corkum B. (2002), "Hoek-Brown criterion – 2002 Edition", Proc. NARMS-TAC Conference, Toronto, 2002, 1, 267-273.
- Hoek, E. and Marinos, P. (2000) "Predicting Tunnel Squeezing". *Tunnels and Tunneling International*. Part 1 – November 2000, Part 2 – December 2000.
- Hoek, E., Kaiser, P.K., and Bawden, W.F. (2000). Support of Underground Excavations in Hard Rock. A.A. Balkema. Rotterdam.
- Hoek, E. (2001) "Rock mass properties for underground mines". *Underground Mining Methods: Engineering Fundamentals and International Case Studies*. (Edited by W. A. Hustrulid and R.L. Bullock), Littleton, Colorado: Society for Mining, Metallurgy, and Exploration (SME) 2001.
- Hoek, E. and Diederichs, M.S. (2006). "Empirical estimation of rock mass modulus". *International Journal of Rock Mechanics and Mining Sciences*. 43. Pp. 2013-215.
- Ingard, U and Kraushaar, W.L. (1960), *Introduction to Mechanics, Matter, and Waves*. Addison Wesley, London p76.
- ISRM (2007), The Complete ISRM Suggested Methods for Rock Classification, Testing and Monitoring: 1974-2006 (eds R Ulusay & JA Hudson). ISRM Turkish National Group, Ankara, Turkey.
- Jaramillo, C. A. (2017), "Impact of Seismic Design on Tunnels in Rock – Case Histories," *Underground Space*, Vol. 2, pp. 106–114.
- Marinos. P., and Hoek, E. (2000) "GSI: A geologically friendly tool for rock mass strength estimation". *Proc. GeoEng 2000 Conference*, Melbourne. 1422-1442.
- McGarr, A., M. D. Zoback, and T. C. Hanks (1982), "Implications of an Elastic Analysis of In Situ Stress Measurements near the San Andreas Fault," *J. Geophys. Res.*, 87(B9):7797–7806.
- Plumb, R.A. (1989) Fracture patterns associated with incipient borehole breakouts. *Rock at Great Depth*, V. Maury and D. Fourmantaux (editors), 2, Balkema, Rotterdam, pp. 761–768.
- Plumb, R.A. and Hickman, S.H. (1985) Stress-induced borehole elongation: A comparison between the four-arm dipmeter and the borehole televiewer in the Auburn Geothermal well. *Journal of Geophysical Research* 90(B7), pp. 5513–5522.

- 
- Quiñones-Rozo, C., (2010), Lugeon test interpretation, revisited, in: Collaborative Management of Integrated Watersheds, US Society of Dams, 30th Annual Conference, 2010, pp. 405–414.
- Saeidi, O., Rasouli, V., Vaneghi, R.G., Gholami, R., and Torabi, S.R. (2014). “A modified failure criterion for transversely isotropic rocks”. *Geoscience Frontiers*. 5. Pp. 215-225.
- Saraglou, H. and Tsiambaos, G. (2008). “Modified Hoek-Brown failure criterion for anisotropic intact rock” *International Journal of Rock Mechanics and Mining Sciences*. 45. Pp. 223-234.
- Sharma, S. and W. R. Judd (1991), “Underground Opening Damage from Earthquakes,” *Engineering Geology*, Vol. 30, pp. 263-276.
- Yeh and Associates, Inc (2023). Geotechnical Data Report. Zevsar Energy Storage Project Seirra Highway and Dawn Road, Kern County, California. Yeh Project No.: 223-202. November 17, 2023.
- Zajac, B.J. and Stock, J.M. (1997) Using borehole breakouts to constrain the complete stress tensor: Results from the Sijan Deep Drilling Project and offshore Santa Maria Basin, California. *Journal of Geophysical Research* 102(B5), pp. 10083–10100.
- Zoback, M.L. and Zoback, M.D. (1980) State of stress in the conterminous United States. *Journal of Geophysical Research* 85(B11), pp. 6113–6156.
- Zoback, M.D., Moos, D., Mastin, L. and Anderson, R.N. (1985) Well bore breakouts and in situ stress. *Journal of Geophysical Research* 90, pp. 5523–5530

## **APPENDIX A**

### **GEOTECHNICAL LOGS**

## **APPENDIX B**

### **ACOUSTIC TELEVIEWER (ATV) LOGS**

## **APPENDIX C**

### **LABORATORY TESTING REPORTS**



## **APPENDIX D**

### **ROCK MASS RATINGS**

## **APPENDIX E**

### **IST2D STRESS MEASUREMENTS**